INVESTIGATIONS IN SOUTHEAST TEXAS PRECIPITATING STORMS: MODELED AND OBSERVED CHARACTERISTICS, MODEL SENSITIVITIES, AND EDUCATIONAL BENEFITS

A Dissertation

by

LARRY JOHN HOPPER, JR.

Submitted to the Office of Graduate Studies of
Texas A&M University
in partial fulfillment of the requirements for the degree of

DOCTOR OF PHILOSOPHY

December 2011

Major Subject: Atmospheric Sciences

INVESTIGATIONS IN SOUTHEAST TEXAS PRECIPITATING STORMS: MODELED AND OBSERVED CHARACTERISTICS, MODEL SENSITIVITIES, AND EDUCATIONAL BENEFITS

A Dissertation

by

LARRY JOHN HOPPER, JR.

Submitted to the Office of Graduate Studies of
Texas A&M University
in partial fulfillment of the requirements for the degree of

DOCTOR OF PHILOSOPHY

Approved by:

Chair of Committee,	Courtney Schumacher
Committee Members,	Craig Epifanio
	Jeffrey Liew
	Russ Schumacher
Head of Department,	Kenneth P. Bowman

December 2011

Major Subject: Atmospheric Sciences

ABSTRACT

Investigations in Southeast Texas Precipitating Storms: Modeled and Observed Characteristics, Model Sensitivities, and Educational Benefits. (December 2011)

Larry John Hopper, Jr., B.S., University of Oklahoma; M.S., Texas A&M University

Chair of Advisory Committee: Dr. Courtney Schumacher

This dissertation establishes a precipitation climatology for common storm types and structures in southeast Texas, investigating diurnal, seasonal, and interannual rainfall variations in addition to climatological differences in raindrop size distributions and storm divergence profiles. Divergence profiles observed by an S-band, Doppler radar are compared to ensemble simulations of ten precipitating systems occurring in warm season, weakly baroclinic, and strongly baroclinic environments. Eight triply-nested mesoscale model simulations are conducted for each case using single- and double-moment microphysics with four convective treatments (i.e., two convective parameterizations and explicit vs. parameterized convection at 9 km). Observed and simulated radar reflectivities are objectively separated into convective, stratiform, and non-precipitating anvil columns and comparisons are made between ensemble mean echo coverages and levels of non-divergence (LNDs). In both the model and observations, storms occurring in less baroclinic environments have more convective rain area, less stratiform rain area, and more elevated divergence profiles.

The model and observations agree best for well-organized, leading-line trailing stratiform systems. Excessive convective rain area and elevated LNDs are simulated for several less organized cases. Simulations parameterizing convection on the intermediate grid produced less elevated divergence profiles with smaller magnitudes compared to their explicit counterparts. In one warm season case, double-moment microphysics generated lower LNDs associated with variations in convective intensity and depth, detraining less ice to anvil and stratiform regions at midlevels relative to a single-moment scheme. Similarly, mesoscale convective vortex simulations employing an ensemble-based versus a single-closure convective parameterization produced the least elevated heating structures (closer to observed) resulting in the weakest midlevel vortices.

Finally, this dissertation is unique in that some of the data collection and a portion of the analysis involved 95 undergraduates in a five-year research and education program, the Student Operational ADRAD Project (SOAP). In addition to documenting the program's structure and implementation, student-reported experiences, confidence, and interest in performing SOAP tasks are also analyzed. Students participating in SOAP for multiple years were significantly more confident in performing SOAP tasks, more likely to obtain science or meteorology-related employment upon graduation, and more likely to matriculate to graduate programs, suggesting programs like SOAP have a strong influence on students' career outcomes and self-efficacy.

DEDICATION

To my closest friends and family

that have supported and motivated me over the years,

particularly my grandparents Irene and Henry Ashworth.

ACKNOWLEDGEMENTS

I would like to thank family, particularly my grandparents to whom I dedicate this dissertation, for their unwavering support and encouragement and for respecting my decision to leave Oklahoma back in July 2005 when I had the opportunity to stay. Many friends have also been very supportive, especially Dr. Don Conlee, Kyle Bucher, Ryan Machala, Julia O'Hern, Ruth Mullins-Perry, and Emily Riley, who has listened to my scientific struggles more than anyone else. I have also thoroughly enjoyed working with my fellow A-Team members and seven undergraduate researchers I mentored.

I would like to thank my committee chair, Dr. Courtney Schumacher, and my committee members, Drs. Craig Epifanio, Jeffrey Liew, and Russ Schumacher (who also provided computing resources), for their guidance and support throughout the course of this research. Dr. Schumacher recognized my desire to stay back in 2007-2008 when I could not and has been an invaluable source of advice throughout my graduate career, helping me develop into the best educator, scientist, and person I can be.

Thanks also go to Kaycee Bevers for calibrating the ADRAD data and Cameron Homeyer for implementing Drs. Brian Mapes and Jialin Lin's CYLBIN code and analysis software at Texas A&M. Jerry Guynes and Neil Smith provided valuable technical support that allowed our SOAP undergraduate students to collect some of the data used in this study. Comments from three anonymous reviewers and discussions with Drs. Fuqing Zhang, Hugh Morrison, Gretchen Mullendore, and Sandra Yuter have also shaped parts of this work, which was supported by NSF Grant ATM-0449782.

TABLE OF CONTENTS

Page

ABSTRACT iii

DEDICATION v

ACKNOWLEDGEMENTS vi

TABLE OF CONTENTS vii

CHAPTER

I INTRODUCTION 1

II SOUTHEAST TEXAS PRECIPITATION CLIMATOLOGY 6

1. Storm types and structures 6
2. Precipitation distributions and characteristics by storm type 9
3. Diagnosing the summertime midday precipitation peak 13
4. Storm type raindrop size distributions and divergence profiles 17

III MODEL AND OBSERVATIONAL COMPARISONS OF DIVERGENCE AND STRATIFORM RAIN PRODUCTION 23

1. Methods 24
2. WRF-ARW and observational comparisons by storm type 31
3. MM5 and observational comparisons by storm type 41

IV MODEL SENSITIVITIES 44

1. Variations in echo coverage 44
2. Divergence variations and possible implications 51

V UNDERGRADUATE EXPERIENCES IN SOAP: A RESEARCH AND EDUCATION PROGRAM 56

1. SOAP program description 57
2. Survey methods and correlations 61
3. Results and career outcomes 64
4. Additional lessons learned 66

CHAPTER Page

VI CONCLUSIONS 69

REFERENCES 74

APPENDIX A FIGURES 83

APPENDIX B TABLES 120

APPENDIX C LIST OF FALL SOAP PROJECTS 132

VITA 133

CHAPTER I

INTRODUCTION

Evaluating a model's ability to simulate precipitating cloud systems and their potential upscale feedbacks is a challenging yet important task. An observable quantity with broad ramifications that is analogous to a simulated quantity should be used a basis for comparison. Horizontal wind divergence is a good comparative candidate at many temporal and spatial scales because it can be calculated from a variety of direct wind observations. Divergence is also linked to vertical motions through mass continuity, providing insights into diabatic heating variations that cannot be measured directly. In the tropics, diabatic heating within convective systems has been linked to important large-scale circulation anomalies (Houze 1982; Hartmann et al. 1984; Mapes and Houze 1995; Schumacher et al. 2004). Some extratropical mesoscale convective systems (MCSs) can also induce additional convection by creating diabatically-maintained warm core anticyclones that intensify upper-level divergence and lower-level convergence (Ninomiya 1971a,b; Maddox et al. 1981; Stensrud 1996), but extratropical diabatic convective feedbacks are still poorly understood otherwise. Assessing how well models simulate divergence structures for extratropical MCSs using Doppler radar observations may help bridge this gap.

Both observed and modeled divergence profiles across a range of common extratropical storm types and background environments must be investigated before

---

This dissertation follows the style of *Monthly Weather Review*.

studying their large-scale feedbacks. Unlike storms caused by synoptic-scale baroclinic systems common in the midlatitudes, storms forming in more barotropic, tropical-like environments depend more strongly on local processes imposed by the convection itself and are thought to have a more active large-scale feedback (Fritsch and Forbes 2001). Hopper and Schumacher (2009: hereafter HS09) have shown that warm season upper-level disturbances occurring in southeast Texas generate more elevated levels of non-divergence (LNDs) than their more strongly baroclinic, cold season counterparts. However, HS09 only utilized one set of parameterizations within an older model framework, did not investigate frontal storms, and presented a cold season MCS caused by an upper-level disturbance that produced divergence structures that were as elevated as the warm season cases. Therefore, the first objective of this study is to expand upon HS09 in evaluating how well horizontal wind divergence is simulated for different model configurations across a wide spectrum of storm types and environments, identifying where large deviations from observations occur and their possible implications.

Separating precipitating systems into their convective and stratiform components helps place divergence variations in context because both regions contain different kinematic and thermodynamic processes that affect divergence and heating profiles (Houze 1982, 1989, 1997). Deep convection associated with most tropical and warm season midlatitude precipitation systems has strong vertical velocities throughout the depth of the troposphere, whereas stratiform rain forming from the convection has weaker mesoscale updrafts and downdrafts above and below the 0°C level, respectively.

Extratropical stratiform precipitation caused by synoptic-scale (~10^3 km) lifting without a deep convective source exhibits similar characteristics to stratiform rain forming from deep convection, although several studies (e.g., HS09) show that the vertical extent of nonconvective stratiform echo is lower than that forming from deep convection.

Strong low-level convergence and upper-level divergence occurs within convective regions, where condensation in intense updrafts results in net latent heat release throughout the troposphere. The atmosphere adjusts to active convection through compensating adiabatic subsidence (Yanai et al. 1973) represented by fast-moving gravity waves (Mapes and Houze 1995). Alternatively, stratiform regions contain moderate convergence near the 0^oC level associated with net latent heating in weak updrafts above the 0^oC level and net latent cooling induced by evaporation and melting in weak downdrafts below the 0^oC level. In response, adiabatically driven slower-moving gravity waves that warm the upper troposphere and cool the lower troposphere are caused by tropical (Mapes 1993; Mapes and Houze 1995) and midlatitude (Stensrud 1996) MCSs in weakly forced environments, destabilizing the environment and encouraging additional convection to develop nearby. However, these characteristics may be less applicable to frontal MCSs and non-deep convective extratropical systems, the latter of which generated lower stratiform LNDs than in embedded regions of elevated convection (HS09).

Doppler radars can measure the divergence associated with convective and stratiform rain regions. Radar divergence measurements also include non-precipitating anvil regions even though the latent heating processes and vertical velocities observed

within these regions may be small. Frederick and Schumacher (2008; hereafter FS08) used a ground-based C-band radar during the Tropical Warm Pool International Cloud Experiment (TWP-ICE) to show that non-precipitating anvil covered 10-20% of the radar grid on several occasions during mature phases of MCSs and >30% during their dissipating phases. Other tropical studies suggest that cloud- resolving models produce too much non-precipitating anvil (Jakob et al. 2004; May and Lane 2009). Quantifying how much excess non-precipitating anvil is simulated in mature extratropical MCSs may help explain variations in divergence and heating profiles and partially explain why stratiform rain areas modeled in squall lines are often underestimated (e.g., Tao et al. 1993; Yang and Houze 1995; Done et al. 2004). Therefore, a second objective of this study is to show how simulated convective, stratiform, and anvil regions compare to observations and any implications these deviations may have for the variety of storms and model parameterizations investigated.

Finally, a third objective investigates whether cumulus (CPs) and microphysics (MPs) parameterizations *systematically affect divergence profiles and stratiform rain production* across a range of storm types and environments. Instead of determining which schemes are most valid or delving into details of the parameterizations, general sensitivities relevant to this study are presented for a few sets of extensively used schemes. These results should apply to mesoscale and climate models with regional nests using parameterizations that contain similar assumptions to those used in this study. Quantifying variations in simulated divergence structures and echo coverages relative to radar observations and identifying possible implications for diabatically

maintained midlevel circulations associated with these sensitivities should motivate several avenues for future work.

This dissertation presents a storm climatology for southeast Texas in Chapter II that quantifies climatological variations in rainfall, raindrop-size distributions, and radar-estimated divergence structures. Chapter III outlines the methods used to compare modeled and observed variations in storm divergence and convective, stratiform, and non-precipitating anvil area echo coverage, presenting results for ten disparate precipitating systems occurring in warm season, weakly baroclinic, and strongly baroclinic environments in southeast Texas. Variations in divergence profiles and echo coverage between ensemble members utilizing different combinations of microphysics schemes and convective parameterization treatments are investigated in Chapter IV.

Finally, this dissertation is unique in that some of the data collection and a portion of the analysis involved 95 undergraduates in a five-year research and education program, the Student Operational ADRAD Project (SOAP). Although empirical analyses of undergraduate research programs are essential for improving such experiences and advancing undergraduate science education (Sadler and McKinney 2010), very few have evaluated undergraduate research experiences in the atmospheric sciences (Gonzales-Espada and LaDue 2006). Therefore, one final objective of this dissertation is to evaluate individual student experiences, confidence, and interests while participating in SOAP activities. The educational experience reported by undergraduates participating in SOAP and its effects on these students' career interests and outcomes are evaluated in Chapter V before conclusions are presented in Chapter VI.

CHAPTER II

SOUTHEAST TEXAS PRECIPITATION CLIMATOLOGY

Southeast Texas experiences a diverse spectrum of precipitating systems and background environments common in both the tropics and midlatitudes, making this subtropical region ideal for quantifying rainfall variations from these influences in addition to investigating variations in storm divergence and areal echo coverages. This chapter defines the storm type and structure classifications used in this dissertation, presenting characteristics of each that highlight the diversity of precipitating storms in southeast Texas and provide context for the storms investigated further in subsequent chapters. The annual storm climatology for College Station, TX and a summertime rainfall climatology based on these storm types are presented before applying these classifications to variations in climatological raindrop size distributions (DSD) observed by a Joss-Waldvogel (JW) disdrometer and climatological storm divergence profiles observed by the Aggie Doppler Radar (ADRAD). Collaborations with two graduate students and with SOAP undergraduate researchers supervised by the author have helped shape some of the work presented in this chapter.

1. Storm types and structures

Each storm utilized in the rain gauge-based climatologies, DSD analysis, and climatological storm divergence profiles is categorized by its *primary* dynamical forcing and precipitation structure. Surface and upper-air maps, satellite images, and Next-

Generation Radar (NEXRAD) images from the online image archive maintained by the Precipitation Diagnostics Group (PDG) in the Mesoscale and Microscale Meteorology Division of NCAR (http://locust.mmm.ucar.edu/imagearchive) are matched and analyzed to determine each storm's classification. In addition, archives of mesoscale discussions and mesoanalyses from the Storm Prediction Center were used in classifying some storms. The methods used for defining storm periods and splitting storms are discussed at the beginning of each section in this chapter.

Five dynamical forcing mechanisms are used to categorize each storm depending on the mechanism most responsible for initiating precipitation. Storms are classified as a(n):

- **cold front (CF) or trof** if precipitation initiates along a surface cold front, dryline (Schaefer 1974), pre-frontal trough or wind shift (Schultz 2004), baroclinic surface trough (Sanders 2005), or a convectively-induced outflow boundary.
- **warm front** (**WF)** if precipitation initiates along a surface warm front or on the cool side of an advancing warm front associated with a midlatitude cyclone.
- **upper-level disturbance (ULD)** if precipitation initiates in the presence of a stationary or propagating midlevel circulation (700-500 hPa closed low or trough) or upper-level jet streak that is not collocated with a cold or warm front.
- **tropical cyclone (TC)** if precipitation initiates within a named tropical cyclone.
- **weakly forced storm (WK)** if precipitation initiates from a forcing not described above (e.g., sea breeze convection and daytime air-mass thunderstorms).

Stationary frontal storms are classified as either warm or cold frontal depending on whether the storm's more convective elements propagate away from the cold front into the warm sector (cold frontal) or move parallel to the front or into the cool sector (warm frontal). Splitting stationary frontal storms and merging several types of surface boundaries into the cold frontal category simplifies the climatology while combining storm types that appear to have similar microphysical and dynamical properties as indicated by their DSD and divergence structures, respectively.

Three categories of precipitation structures are also used to characterize each storm in addition to the dynamical forcings outlined above. Storms are classified as:

- **predominantly convective (c)** if a convective line or cells form with little or no stratiform rain present (Figs. A.1 a and b). This designation also includes shallow and deep convection that does not merge into MCSs or stratiform rain regions.
- **deep-convective stratiform (dcs)** if stratiform rain originates from a deep (> 6 km), vertically-oriented convective source (Figs. A.1 c and d). This classification also includes cellular storms that merge into MCSs.
- **non-deep convective stratiform (ncs)** if stratiform precipitation originates from synoptic-scale lifting without a deep convective source (Figs. A.1 e and f). This category also includes cases with slantwise, elevated, or weak shallow convection that merges into larger stratiform regions.

The WFc category has not been used in this dissertation because southeast Texas warm frontal storms typically produce widespread, non-convective precipitation primarily ahead of the frontal boundary (Matejka et al. 1980) or convection along the boundary

that produces stratiform rain. The TCncs and WKncs classifications are also not used in this study because stratiform rain originates from deep convection in tropical cyclones and conditionally unstable, weakly forced storms. Although most of the classifications for each storm are consistent for each analysis in this section, a small fraction of the storms are classified differently for the rain gauge and DSD analyses, which are point observations, compared to the divergence analyses, which require more holistic categorizations for the larger radar domain.

2. Precipitation distributions and characteristics by storm type

a. Annual mean

Eight years (March 2002-February 2010) of hourly rain gauge data from Easterwood Airport (KCLL) in College Station, TX, is matched with NEXRAD images and data archives in determining each storm's precipitation amount and dynamical forcing to quantify each storm type's contribution to annual rainfall. Gauge-identified storms are included in this analysis if at least 0.05 mm (0.02 in) of rain occurs in a 1-hr period. Storms are separated if measurable precipitation is not recorded for 6 hr or if a distinct shift in the storm's dynamical forcing occurs (e.g., warm to cold frontal). A few storms have been excluded because hourly rain totals did not match radar observations.

Each storm type's count and precipitation contribution during the eight-year analysis period is presented in Table B.1. Statistics for each of the storm types are also broken down by structure, with storms whose stratiform rain is caused by deep convection generally producing more precipitation than their non-deep convective and

predominantly convective counterparts. Although cold fronts contributed the most to annual rainfall (44%) and occurred most frequently (43%), upper-level disturbances (ULDs) and warm fronts also accounted for a large portion of precipitation. ULDs were three times more frequent than warm fronts; however, warm fronts generate the most precipitation per storm, particularly throughout the interquartile range and above the 95th percentile of warm frontal storms sampled (Fig. A.2). Landfalling TCs and weakly-forced storms produced small amounts of precipitation, with weakly-forced storms (TCs) causing the least rain per storm above (below) the 60th percentile. Due to the small sample size of TCs during the analysis period, results for TCs will only be presented where necessary for completion and are likely not representative of a longer time period.

b. Interannual and seasonal variations

Large interannual variations in precipitation amounts and relative contribution by storm type occurred in College Station during the analysis period (Fig. A.3a). However, the analysis period mean of 1036 mm was near the 1971-2000 climatological mean of 1008 mm (NWS Houston-Galveston). Precipitation was 33% above normal during 2004-05 when 92 storms were identified and more than 33% below normal during 2005-06 and 2008-09 when 52 storms were identified. Each storm type's contribution to the annual rainfall did not deviate significantly from the mean during the wettest (2004-05) and driest (2005-06) years, but did during 2008-09 when ~60% of precipitation was cold frontal and TCs produced more rain than warm fronts or ULDs. In addition, although cold frontal storms usually accounted for the most precipitation and occurred most

frequently each year (Fig. A.3b), ULDs were the most prevalent storm type during 2007-08 and 2009-10 while warm fronts and ULDs produced the most precipitation during 2002-03 and 2007-08, respectively.

Substantial shifts in each storm type's contribution to rainfall also occur during each season in College Station. These general trends should be applicable to longer time periods even though large year-to-year fluctuations in seasonal precipitation totals occurred during the analysis period, whose mean spring and summer rainfall were 17% below and 19% above their 1971-2000 climatological means, respectively (NWS, Houston-Galveston). Over three-fourths of precipitation during fall, winter, and spring is frontal, with cold fronts producing the most during spring (60%) and fall (43%) as opposed to winter when warm and cold frontal contributions are equal (39%; Table B.2). Although ULDs only cause ~20% of precipitation during these seasons, they generate the majority of summertime rainfall, the season when warm frontal precipitation does not occur. Weakly forced storms and TCs produce a small fraction of rainfall during summer and fall, but do not contribute to winter or springtime precipitation.

Finally, interannual precipitation variations in College Station appear to be strongly modulated by the El Niño-Southern Oscillation (ENSO), particularly during October-March. The four El Niño events and one neutral episode with a positive Oceanic Niño Index (ONI) generated the greatest annual (Fig. A.3a) and October-March (Table B.3) precipitation totals in agreement with longer-term studies performed by Ropelewski and Halbert (1996) and Gershunov and Barnett (1998). Warm fronts and ULDs accounted for more October-March precipitation during the five positive ONI

episodes compared to the single La Niña event and two neutral episodes with negative ONIs. This difference is likely associated with the equatorward shift in storm tracks during El Niño events noted by Chang et al. (2002) and Eicher and Higgins (2006), who also found an increase in the frequency of storms over the Gulf of Mexico and southeast Texas. Indeed, warm frontal storms were most frequent during the two strongest El Niños in 2002-03 and 2009-10 (Fig. A.3b) and ULDs typically occurred more often during the warm episodes as well. One notable exception to this occurred during 2007-08, when ULDs caused persistent rainfall for several weeks during the summer of 2007 (Figs. A.3a and b). Future research utilizing additional sites in the southeast United States over longer time periods should be performed to determine how consistent and significant any trends between storm types and ENSO are.

c. Diurnal variations

Each storm type also exhibits unique diurnal characteristics that contribute to College Station's midday peak (12-1pm LT for single hour totals) in annual rainfall during the analysis period. Cold frontal storms (Fig. A.4a) are bimodal, peaking during the overnight and morning hours due to afternoon convection forming upstream in northwest flow with a secondary peak in early evening from convection initiating off nearby boundaries. Warm fronts (Fig. A.4b) and ULDs (Fig. A.4c) both display midday maxima, although warm fronts peak during late morning as opposed to ULDs that have a more amplified peak during early afternoon. Weakly forced storms (Fig. A.4d) favor late afternoon and early evening convection coincident with maximum daytime heating.

Previous studies of precipitation in southeast Texas (Winkler et al. 1988) and in the Gulf of Mexico (Yang and Slingo 2001, cf. Figs. 3c and 3d) have also identified a late morning to early afternoon peak in annual rainfall. Seven years (March 2002-February 2009) of rain gauge data from five stations in southeast Texas show that this maximum is most amplified during summer (Fig. A.5) when ULDs cause the majority of rainfall. The following section verifies that ULDs contribute most to this summer peak and attempts to place these results in the context of Winkler et al.'s (1988) hypothesis, which asserts that the earlier peak is caused by the inland progression of storms that form overnight due the convergence of the land breeze with southerly regional flow. In addition, variations in thermodynamic instability during the morning are also investigated as an alternative explanation for why convection occurs earlier in the day prior to the time of maximum daytime heating.

3. Diagnosing the summertime midday precipitation peak

Hourly rain gauge data from five locations in southeast Texas during seven summers (2002-2008) are matched with map archives to determine how each storm type affects the midday summertime rainfall peak. Two inland locations in College Station, TX (CLL) and Lufkin, TX (LFK) are compared to three coastal sites in Beaumont, TX (BPT) and the northern (IAH) and southern (HOU) parts of Houston, TX (Fig. A.6). Four hundred nineteen gauge-identified storms are included in this analysis, each of which produced > 0.05 mm (0.02 in) of rain in a 1-hr period and were separated if measurable precipitation was not recorded for 6 hr. Only one storm included in this

analysis (which is discussed further in section 3b) has a 12-hr rain total that exceeds its 5-yr recurrence interval amount (Hershfield 1961).

a. Summer diurnal characteristics by storm type

Each storm type's summertime diurnal cycle was investigated for the multiple sites, verifying that ULDs exhibit a pronounced midday maximum (Fig. A.7a). Cold frontal (Fig. A.7b) and weakly forced (Fig. A.7c) storms produce amplified precipitation peaks during late afternoon and early evening that coincide with maximum daytime heating. Cold frontal storms also exhibit a secondary peak attributed to nocturnal MCSs that is more pronounced in its annual diurnal cycle (cf. Fig. A.4a). Weakly forced convection peaks during early afternoon along the coast and early evening inland, likely due to the inland progression of sea breeze convection or outflow boundaries from this convection. Although TCs (Fig. A.7d) produced more rainfall in the morning during the summers analyzed, a longer record is needed to discern the validity of these trends.

Differences between the diurnal cycle and relative contribution of each storm type between coastal and inland stations are highlighted in Fig. A.8. Coastal precipitation (Fig. A.8a) peaks at midday, whereas it is shifted later inland (Fig. A.8b) to coincide with maximum daytime heating. ULDs account for over two-thirds of coastal rainfall from 3am-12pm LT, whereas they only produce over two-thirds of precipitation from 9am-12pm inland where cold frontal storms cause the majority of rainfall between 3-9am LT. In general, cold frontal storms account for a larger fraction of rainfall inland (37%) compared to the coast (24%) where weakly forced storms and TCs cause a higher

fraction of rainfall relative to the inland locations. Nevertheless, the midday peak in coastal and inland summertime rainfall is attributed most to ULDs, justifying their isolation for further investigation.

b. Dynamic and thermodynamic explanations of the summertime midday peak

Winkler et al. (1988) hypothesized that the late morning convective maxima over southeast Texas is caused by nocturnal convective activity that initiates off the Gulf Coast where the land breeze circulation and southerly regional airflow converge. A case study illustrating this *idealized* hypothesis in the context of precipitation caused by ULDs is presented in Fig. A.9. As convection begins to dissipate and surface temperatures cool during early evening (Fig. A.9a), a land breeze forms with a stationary cutoff upper-level low to the west that generates vorticity and enhances southerly regional flow. Nocturnal convection initiates and intensifies in this convergence zone (Fig. A.9b), with weak southerly shear encouraging a leading stratiform MCS (Parker and Johnson 2000) to form (Fig. A.9c). Stratiform rain continues to expand north of the stationary convergence zone during the morning (Fig. A.9d) as the land breeze weakens. As this MCS begins dissipating by early afternoon, outflow boundaries or gravity waves originating from the MCS initiate new convective cells further inland (Fig. A.9e) that propagate to the north throughout the afternoon (Fig. A.9f).

In order to test Winkler et al.'s (1988) hypothesis, ULD rainfall was separated by whether it was caused by a disturbance located to the west of the station or centered over or east of the site. Although a large fraction of the ULDs analyzed are propagating

shortwave troughs, separating these from cutoff lows does not change the results. Precipitation caused by ULDs located to the west of each station peaks at midday and decreases dramatically after 3pm LT, except in LFK whose maximum rainfall occurs during late afternoon (Fig. A.10a). Convection peaks later with daytime heating at CLL, IAH, and LFK when ULDs are not located to the west (Fig. A.10b), whereas BPT and HOU exhibit nocturnal rainfall maxima. However, excluding one 236 mm rain event at HOU from 0300-1300 UTC on 19 June 2006 whose 12-h rain total exceeds its 25-yr recurrence interval (Hershfield 1961) removes this nocturnal peak (dashed lines in Fig. A.10b). Although this backbuilding-quasi stationary MCS (Schumacher and Johnson 2005) associated with an MCV also caused 117 mm of rain in BPT, excluding this case does not eliminate BPT's nocturnal maximum because several storms > 25.4 mm (1 in) contribute to its peak. Nevertheless, the diurnal characteristics of ULDs appear to be affected by the location of disturbances causing precipitation at all other locations.

Pre-existing thermodynamic instability was also investigated to provide another possible explanation for what causes the earlier onset of convection in ULD storms during summer. For this analysis, only storms at BPT are compared to 1200 UTC (7 am LT) sounding data from Lake Charles, LA (LCH) because none of the other stations are located within 100 km of an upper-air observation site. ULDs at BPT whose heaviest precipitation totals occurred between 9am-3pm LT typically had higher amounts of pre-existing convective available potential energy (CAPE; Fig. A.11a) and lower values of convective inhibition (CINS; Fig. A.11b) at sunrise compared to ULDs whose most intense rainfall occurred later. Conversely, the lowest CAPE and highest CINS values at

1200 UTC were associated with ULDs whose heaviest rainfall occurred between 3-6 pm LT, with over half of these cases containing > 50 J kg^{-1} of CINS. Therefore, thermodynamic instability appears to play an important role in modulating the diurnal cycle of summertime rainfall at BPT. Future research linking these thermodynamic and dynamic justifications together and investigating ULDs situated to the west that do not exhibit a midday rainfall peak would likely be beneficial. In addition, the late onset of convection in simulations of a ULD case presented in Chapter III suggests models may struggle to initiate late morning convection and should be investigated in future work.

4. Storm type raindrop size distributions and divergence profiles

Microphysical variations in climatological DSDs and dynamical variations in climatological divergence profiles are presented for southeast Texas storm types and structures. The storm classifications outlined in section 1 are used in both of these analyses, but some of methods used to classify and identify storms differ. Each *hour* of data from Texas A&M University's S-band Aggie Doppler Radar (ADRAD) located in College Station, TX (30.6^{o}N, 96.3^{o}W) that is included in the divergence analysis is assigned a storm type and structure, giving consideration to the entire radar domain as opposed a single point. Most consecutive hours of radar data have the same classification, but changes during storms are more frequent in this analysis due to the radar domain's size. Ground-based observations of raindrop spectra from the JW RD-80 disdrometer located 5 km northeast of ADRAD are included in the DSD analysis if a storm's total rainfall accumulation exceeds 2.5 mm (0.1 in). In addition, a minimum rain

rate of 0.1 mm hr^{-1} is used to identify the beginning and end of storms in the analysis, which are separated if measurable rainfall (> 0.1 mm hr^{-1}) is not recorded for > 5 hr.

a. Climatological DSDs by storm type

Raindrop size distributions from 160 storms between December 2004-September 2008 are used to verify expected microphysical variations between non-convective stratiform and predominantly deep convective storms while displaying other differences between storm types. JW disdrometers (Joss and Waldvogel 1967) convert mechanical drop impacts on a sensor with an area of 50 cm^2 into electronic pulses as a function of drop diameter. A signal processor applied to these pulses generates DSDs in 10-s intervals by placing the data into 20 bins ranging from 0.3-5.5 mm. All data have been rebinned into 1-min intervals for this analysis, only using DSD samples exceeding 100 drops to minimize the standard errors of rain rates and reflectivity factors as suggested by Joss and Waldvogel (1969) and Steiner and Smith (2000).

The normalized climatological DSD for all storms included in this analysis is shown in Fig. A.12, whose tick marks on the x-axis represent the preset JW disdrometer bins as opposed to being strictly linear. Preferred peaks in drop diameters occur at 1.116 (bin 6) and 1.912 mm (bin 10) in agreement with many studies of JW disdrometer data beginning with Steiner and Waldvogel (1987), but no peak is observed between 0.6-0.7 mm (bin 4) in contrast to these studies. This may be caused by errors in undersampling very small drops that occur when 1) the magnitude of background noise exceeds the impacts of these very small drops (Tokay et al. 2003), 2) larger drops in heavy rain rates

prevent smaller drops (< 1.0 mm) from being recorded simultaneously (Tokay and Short 1996), and 3) windy conditions cause small drops' fall velocities to vary from their assumed terminal fall velocities. However, McFarquhar and List (1993) showed that these multiple peaks are due to instrumental errors arising from using a smooth curve fit to the calibration data instead of a linear curve fit that removes these peaks.

The normalized climatological DSD (Fig. A.12) is subtracted from the mean DSD for each storm type shown in Fig. A.13, analyzing their anomalies from the mean distribution to minimize the effects of calibration errors discussed above. Warm fronts contribute the most to the small drop mode with a smaller contribution from ULDs. Cold frontal and weakly forced storms dominate the medium and large drop modes because most storms contain stronger convection with accompanying stratiform rain relative to warm fronts and ULDs, which produce non-convective stratiform precipitation more than one-third of the time (cf. Table B.1).

Subdividing each storm type by structure provides additional insight into how each influences the climatological DSD (Fig. A.14). Predominantly convective weakly forced storms (WKc; Fig. A.14a) generate pronounced positive anomalies for large and medium drop modes and negative anomalies for smaller raindrop sizes. Weakly forced storms containing stratiform rain from deep convection (WKdcs) exhibit similar, less pronounced trends. Predominantly convective cold frontal storms (CFc; Fig. A.14b) generate the greatest positive anomalies for large and medium drops and negative anomalies for small raindrop sizes, although some of this signal may be an artifact caused by small raindrop sizes being underestimated in heavy rain rates. Nevertheless,

deep convection from CFc storms and their CFdcs counterparts that display similar trends with smaller magnitudes both likely generate large amounts of graupel and small hail capable of producing large raindrops when they melt before reaching the ground.

Precipitation caused by warm fronts (Fig. A.14c), ULDs (Fig. A.14d), and CFncs storms contribute most to the small raindrop maxima evident in the climatological DSD (cf. Fig. A.12). Non-deep convective precipitating systems across all storm types produce the largest positive anomalies for small raindrop sizes while being deficient in medium and large raindrops, with WFncs storms peaking at slightly smaller raindrop sizes than their CFncs and ULDncs counterparts. Warm frontal storms containing pockets of deep convection (WKdcs) are also weighted towards smaller drops, but their DSD anomalies are less pronounced than in WFncs storms. Although ULDs producing deep convection are deficient in small drops, ULDc and ULDdcs storms both exhibit bimodal DSD anomalies with peaks in medium and very small raindrop sizes between 0.6-0.7 mm, the latter of which has been shown by previous studies like Steiner and Waldvogel (1987) despite not appearing in the climatological DSD. Although the cause of this bimodal DSD anomaly is unknown, it suggests convective updrafts in ULDs may be weak or strong. Therefore, the microphysical processes producing raindrops in convective cells and their resulting stratiform rain regions in ULD systems differ climatologically from WF storms predisposed towards smaller drops and CF and WK storms dominated by medium and larger raindrop sizes, justifying the need for separating these storm types.

b. Climatological divergence profiles by storm type

Mean storm divergence profiles for precipitating systems occurring between June 2006-July 2010 were collated to present dynamical variations between storm types and structures containing enough data. Hourly horizontal wind divergence profiles from an S-band radar (ADRAD) were generated using Mapes and Lin's (2005) technique that incorporates velocity-azimuth display (VAD; Browning and Wexler 1968) analysis. The radar data and VAD divergence methods employed in this analysis are similar to those described further in Chapter III except that only hourly divergence profiles generated from radar data 16-56 km in range with concentric echo coverage are utilized in this analysis. Although these constraints significantly reduce the amount of radar data used to 275 hours, they minimize the bias associated with averaging together hourly divergence profiles from several different storms to generate robust estimates of climatological divergence profiles for several storm types. In addition, results from WKdcs and CFncs storms are not presented because of insufficient echo coverage.

Climatological mean divergence profiles are presented for the remaining storm types and structures in Fig. A.15, each of which contains at least 29 hrs of radar data from more than five distinct storms. Upper-level disturbances producing stratiform rain from deep convection (Fig. A.15a) generate the most elevated climatological divergence profiles (that also include the deep convective regions) and have the least amount of variability between cases as indicated by the relatively narrow standard deviation. Warm fronts (Fig. A.15b) and cold fronts (Fig. A.15c) with deep-convective stratiform rain produce climatological divergence profiles that are similar to each other, but exhibit

greater variability between cases and have levels of non-divergence (LNDs) that are 0.6-0.8 km lower than their ULDdcs counterparts. Although there is not enough data to perform a reliable seasonal decomposition of each storm type, these differences may be caused by the higher proportion of ULD precipitating systems during summer. However, the only non-warm season storm presented in Chapter III that produces an observed LND above 6.5 km is caused by a ULD, implying ULDs may be more capable of generating more elevated divergence profiles than frontal storms.

In contrast, divergence profiles in storms whose stratiform precipitation does not originate from a deep convective source are much less elevated than those containing deep-convective stratiform rain. ULD cases lacking deep convection (Fig. A.15d) have much smaller divergence magnitudes and a mean LND that is 2 km lower than their deep convective counterparts, whereas non-convective warm frontal precipitation (Fig. A.15e) generates an incoherent divergence profile with weak magnitudes. However, large case-to-case variability for ULDncs storms still exists, as some cases like one shown in Chapter III generate LNDs approaching 5.5 km. Nevertheless, these results indicate that deep convective precipitating systems typically produce a more elevated divergence signal with stronger magnitudes that are much more capable of dynamically modifying their environment than non-deep convective systems. Therefore, most of the cases investigated in the next chapter contain stratiform rain originating from deep convection that should exhibit large case-to-case variability and may display sensitivities to the choice of microphysics and convective parameterizations used in simulating them.

CHAPTER III

MODEL AND OBSERVATIONAL COMPARISONS OF DIVERGENCE AND STRATIFORM RAIN PRODUCTION

Investigating variations in storm divergence for a wide variety of precipitating systems is possible in southeast Texas because it experiences several disparate storm types in a variety of background environments. Using a scale analysis, Mapes and Houze (1995) showed that the diabatic component of divergence nearly equals the total horizontal divergence in tropical MCSs whose temperature perturbations are much smaller than their tropospheric latent heating rates. Although the diabatic and adiabatic components of divergence are not formally separated in this dissertation, the warm season cases and a few weakly baroclinic systems presented herein satisfy this scaling argument. However, larger temperature perturbations associated with the large frontal MCSs and other strongly baroclinic cases investigated in this study likely render their adiabatic contributions to the total divergence non-negligible, albeit secondary, to the diabatic component. This chapter presents modeled and observed variations in storm divergence for both types of cases occurring across a wide spectrum of storm types and environments in addition to comparing their convective, stratiform, and non-precipitating anvil echo coverage.

1. Methods

a. Radar observations and VAD divergence

Radar observations for the storms presented in this study are from Texas A&M University's S-band Aggie Doppler Radar (ADRAD) located in College Station, TX (30.6^{o}N, 96.3^{o}W; Fig. A.16). ADRAD's volume scan strategy was run every 10 minutes using 16 tilts ranging from 0.5^{o} to 33^{o} between June 2006 and January 2008. After January 2008, an interleaved set of 24 tilts ranging from 0.4^{o} to 29.5^{o} was run in succession every 12 minutes. The interleaved scans were merged before the following processing steps were completed.

Using a simple area-matching method developed by Schumacher and Houze (2000), ADRAD echo area coverage from over 30 storms was compared to the Tropical Rainfall Measuring Mission Precipitation Radar (TRMM PR) 2A25 attenuation-corrected reflectivity product (Iguchi et al. 2000) and a +6 dB calibration correction was applied to the ADRAD polar coordinate data from July 2006-June 2009. Ground clutter return was used to assess the stability of the calibration shift (Silberstein et al. 2008). The data was further vetted by the University of Washington (UW) quality control (QC) algorithm (Houze et al. 2004). The UW QC algorithm removes a majority of ADRAD's pervasive ground clutter in the lower 2 km, but anomalous propagation and second trip echo can also be removed. ADRAD data was then interpolated to a 2-km Cartesian grid with 0.5 km vertical resolution using National Center for Atmospheric Research (NCAR) Reorder software. After interpolation, a velocity mask that removes echo with $|V_r| < 0.25$ m s^{-1} was used to filter out false echo not flagged by the UW QC algorithm.

Mean horizontal wind divergence profiles from ADRAD were generated using Mapes and Lin's (2005) technique that incorporates velocity-azimuth display (VAD; Browning and Wexler 1968) analysis (as in HS09). This technique uses a space-time binning algorithm named CYLBIN to separate hourly-averaged radar data into a cylindrical grid consisting of 500-m vertical layers with twenty-four 15^{o} bins in azimuth and twelve 8-km bins in range. All data are repooled into 50-hPa pressure layers in the vertical and five-range pooled 40-km wide annulus segments in range centered about 20, 28, 36, 44, 52, 60, 68, and 76 km (using the four closest adjacent sets of 8-km annuli) to increase the number of measurements in sparse echo regions. Annulus segments including 8-km annuli that cannot observe upper levels near ADRAD and low levels ($\leq$ 1 km) at farther ranges are excluded from the analysis at those altitudes. Histograms and floating-point sums of radial velocities for each pooled grid cell are retained and folded values are dealiased before calculating hourly mean divergence profiles through VAD analysis.

b. Model simulations

Ensemble simulations of each storm were conducted using version 3.1.1 of the Advanced Weather Research and Forecasting Model (WRF-ARW; Skamarock et al. 2008). Two domains with 9-km (D2) and 3-km (D3) grid spacing were nested inside a 27-km coarse grid (D1; Fig. A.16) with 27 vertical sigma levels containing greater resolution in the boundary layer. Although higher resolution simulations may be preferred, "convection-resolving" ~100-m grid spacings (Bryan et al. 2003) are not

computationally feasible in this study, which seeks to adequately resolve the organization of convective *systems* to an acceptable degree using "convection-permitting" grid spacings $\leq$10 km (Zhang et al. 2007). Initial and lateral boundary conditions were created using the National Centers for Environmental Prediction (NCEP) Global Final Tropospheric Analysis with 1^{o} horizontal and 6-h temporal resolution. Two-way nesting was used for the two inner domains' lateral boundary conditions. Table B.4 summarizes the configurations used in every model run while Table B.5 outlines the eight-member ensemble simulations created for each case by alternating between two microphysics parameterizations (MPs) on each grid, two cumulus parameterizations (CPs) on D1, and turning the CP on and off on D2.

Two mass-flux convective schemes designed for mesoscale models were used: Kain-Fritsch (Kain 2004) and the Grell-Devenyi (2002) ensemble scheme. The Kain-Fritsch CP removes CAPE over a prescribed time period for an entraining parcel (Fritsch and Chappell 1980), permitting a two-way exchange of mass between clouds and the environment at all sigma levels (described in Kain and Fritsch 1990). The Grell-Devenyi CP uses the CAPE removal closure with three other closures [i.e., quasi-equilibrium (Arakawa and Schubert 1974), low-level vertical velocity (Brown 1979), and moisture convergence (Krishnamurti et al. 1983)] while changing several parameters (e.g., entrainment and detrainment rates, precipitation efficiencies, cloud radii) to generate an ensemble of 144 members weighted equally in this study.

The Goddard one-moment (Tao et al. 1989; Tao and Simpson 1993) and Morrison two-moment (Morrison et al. 2009) MPs were used to parameterize explicit

microphysics. Both bulk MPs assume inverse-exponential size distributions for each precipitating hydrometeor species and predict the mixing ratios of cloud ice, snow, graupel, and raindrops, assuming the latter three species are spheres with constant densities of 0.1, 0.4, and 1.0 g cm^{-3}, respectively. The most distinct difference between them is that the Goddard MP uses fixed intercept parameters for rain ($N_{o,r}$ = 8x10^6 m^{-4}), graupel ($N_{o,g}$ = 4x10^6 m^{-4}), and snow ($N_{o,s}$ = 1.6 x10^7 m^{-4}), whereas Morrison's two-moment MP derives intercept parameters from the predicted number concentrations and mixing ratios of each species. As a result, the two-moment scheme better captures "N_o jumps," or $N_{o,r}$ decreases when transitioning from convective (~10^7 m^{-4}) to stratiform (~10^6 m^{-4}) rain regions. This decrease is associated with a shift from small to large raindrops (Waldvogel 1974), which in turn reduces (increases) rain evaporation rates in stratiform (convective) regions relative to one-moment MPs in simulated squall lines (Morrison et al. 2009).

c. Objective model and observational analysis

Convective and stratiform rain regions at 2 km MSL were identified for radar reflectivity observations and simulated equivalent reflectivities (dBZ_e) using an algorithm described in Steiner et al. (1995; hereafter SHY95). WRF reflectivities were calculated following Stoelinga (2005) for the Goddard MP and substituting in for N_o following Morrison et al. (2009) for the Morrison MP. The convective-stratiform separation uses horizontal gradients to classify reflectivity maxima as convective and the remainder of the precipitation field as stratiform. Although Lang et al. (2003) note that

the convective-stratiform rain separation can be performed using other model parameters, SHY95's reflectivity-based approach has been used by recent modeling studies (e.g., May and Lane 2009; HS09) and allows for more direct comparison between radar observations and model results.

SHY95's criteria used in determining convective centers was tuned for southeast Texas convection using ADRAD observations. First, grid points whose reflectivities exceed 46 dBZ were classified as convective centers instead of 40 dBZ as originally used by SHY95 and HS09. This change ensures that heavy stratiform rain exceeding 40 dBZ is not classified as convective, a concern also noted by Biggerstaff and Listemaa (2000) for southeast Texas MCSs. Second, pixels below 46 dBZ were still identified as convective centers if their reflectivity exceeded the mean background value taken over an 11-km radius (Z_{bg}; dBZ) by at least the difference (ΔZ; dB) given by Yuter and Houze's (1997) cosine function [Eq. (1)].

$$\Delta Z = 10\cos(\pi Z_{bg}/100) \qquad 0 \leq Z_{bg} < 46.0. \tag{1}$$

This peakedness criteria curve was adjusted slightly from HS09 to constrain the number of local reflectivity maxima falsely classified as convective within broad stratiform regions, a problem also noted in Biggerstaff and Listemaa (2000). Although model reflectivities are overpredicted above the 0^{o}C level, their distributions are typically within 3 dB of those observed below the 0^{o}C level, thus having little effect on SHY95's separation and the anvil echo base criteria discussed next.

Non-precipitating echo columns were identified as anvil if they satisfied FS08's definition of echo with bases > 2.5 km and tops $\geq$ 6 km. One limitation of this definition

is that it cannot identify anvil located over shallow convection reaching 2.5 km, although such occurrences are relatively infrequent. Similarly, some anvil columns include shallow convection with echo tops below 2 km, causing some contamination in simulated anvil divergence profiles at low levels. ADRAD has a beamwidth of 1.5^{o} and a minimum detectable reflectivity of -16 dBZ at 10 km and +4 dBZ at 100 km. Therefore, a minimum reflectivity of 5 dBZ is used in this study, excluding echoes outside 96 km in range to mitigate beam spreading issues and to match the VAD divergence profiles. Although smaller frozen hydrometeors at cloud top are excluded, the reflectivity threshold selected best satisfies the limitations of the radar data and captures "thick" anvil (especially its base) associated with deep convection

Observed convective, stratiform, and anvil reflectivity structures for leading-line, trailing stratiform MCSs forming in disparate environments (i.e., warm season and strongly baroclinic cold season) are shown in Fig. A.17. Convective reflectivities for the 18 June 2006 warm season MCS (Fig. A.17a) are similar to West African convection shown by Schumacher and Houze (2006), but have larger (smaller) values below (above) 8 km indicative of enhanced warm rain processes. Although near-surface reflectivities are similar to the warm season case, the 20 March 2010 strongly baroclinic MCS (Fig. A.17b) produces a narrower distribution of generally weaker convective echoes with lower echo tops that decrease toward the surface below the 0^{o}C level, implying stronger rain evaporation rates. Both cases' stratiform structures exhibit broad reflectivities below the 0^{o}C level, but the strongly baroclinic MCS (Fig. A.17d) has a narrower distribution above the 0^{o}C level and intense fallstreaks that result in near-surface reflectivties that are

3-4 dB higher than in the warm season case (Fig. A.17c). Anvil reflectivities in the warm season MCS (Fig. A.17e) are weaker than their stratiform counterparts (Fig. A.17c) except just above 7 km, similar to observed in Schumacher and Houze (2006). The strongly baroclinic anvil reflectivities hug the minimum reflectivity threshold and do not exhibit an upper-level peak (Fig. A.17f). This strongly baroclinic case contains the lowest 0^{o}C level (2.7 km) observed in this study and would likely benefit from lowering the SHY95 separation level to 1.5 km and the echo base and top requirements for identifying anvil; however, the methods still produce reasonable reflectivity distributions for this case and best satisfy all storms investigated.

Detectable precipitation must be present in all radar quadrants to calculate robust estimates of mean divergence profiles using ADRAD. Therefore, observed divergence profiles for each case were calculated by averaging hourly profiles when ADRAD's mean echo coverage exceeded 75%. In order to match the time duration of the mature phase of each storm captured by ADRAD and account for variability in timing between model runs, WRF divergence profiles were calculated for each ensemble member by averaging half-hourly profiles from the times having the greatest precipitating areal coverage over the same number of hours used to calculate divergence from ADRAD. Model-predicted horizontal velocities on D3 within 96 km of ADRAD were used to calculate divergence, excluding data within unclassified columns because ADRAD cannot estimate radial velocities in areas without radar echo. Using all grid points within 96 km of ADRAD produces negligible differences in WRF divergence profiles.

Although most of the ten storms analyzed in this study use observed and modeled data at similar times, Table B.6 shows that a few storms include data for time periods offset by several hours or with wide ranges of time durations. Figure A.18 displays observed and simulated snapshots of each case. Storms with similar structures (e.g., leading-line, trailing-stratiform MCSs) and forcing mechanisms (e.g., upper-level disturbances) are grouped together. Cases are additionally classified as warm season, weakly baroclinic, and strongly baroclinic relative to each other to highlight differences between these environments for similar storm types.

2. WRF-ARW and observational comparisons by storm type

a. Leading-line, trailing-stratiform MCSs (LLTS-MCSs)

MCSs initiated along surface boundaries (e.g., fronts, troughs, outflows) often take the form of a leading line of convection followed by a trailing stratiform region. LLTS-MCSs are characterized by strong line-perpendicular midlevel shear with front-to-rear storm relative winds that decrease with height (Parker and Johnson 2000), advecting hydrometeors rearward into the stratiform region (Rutledge and Houze 1987). These storms occur in a wide variety of vertical wind shears and temperature gradients, ranging from weakly forced to strongly baroclinic. Three LLTS-MCSs with disparate degrees of baroclinicity are discussed in this section.

The warm season LLTS-MCS began as a cluster of storms on 17 June 2006 that formed around Wichita Falls, TX along a convective outflow boundary near a dissipating surface front. Several convective cells merged together into a squall line that

moved southeast with a midlevel trough, developing a mature stratiform rain region behind it (Fig. A.18a). Anvil area decreased as the leading convective line approached ADRAD's domain while stratiform and convective rain areas increased, peaking above 60% and 20%, respectively, around 0930 UTC (Fig. A.19a). Stratiform and convective areal coverages simulated by WRF progress similarly (Fig. A.19b) and have identical ensemble means (Table B.7) to those observed even though all ensemble members simulate MCSs that were delayed by 1-2 hr. The ensemble mean (14%) and observed (9%) anvil area fractions were also similar during their analysis periods, but WRF simulated more trailing anvil and missed most of the elevated echo and forward anvil observed prior to the passage of the MCS.

Although temperature gradients were still weak, stronger vertical wind shears associated with a midlevel trough cutoff over western Kansas (not shown) were present for the 25 April 2007 weakly baroclinic LLTS-MCS. Convection initiated along a pre-frontal trough and wind shift (Schultz 2004) near the Texas-Mexico border around 2100 UTC 24 April 2007, evolving into a tornadic supercell near Eagle Pass, TX (SPC Storm Reports). Several convective cells formed in the outflow behind this supercell and merged together to form the squall line (Fig. A.18b) that moved over ADRAD between 0700-1000 UTC 25 April. The observed (Fig. A.19c) convective peak (16% at 0730 UTC) occurs before the stratiform maximum (82% at 0830 UTC), after which trailing anvil echo increases from 10-20% (the false convective peak observed at 1045 UTC is caused by anomalous propagation not flagged by QC procedures). In general, the

observed and simulated (Fig. A.19d) evolution of echo coverages are similar, both displaying less convection than in the warm season case (Table B.7).

In contrast to the first two cases, the strongly baroclinic case formed along a cold front with a large temperature gradient downstream from a midlevel trough (not shown). Convection formed near Big Bend on 20 March 2010 and evolved into an LLTS-MCS that moved east over ADRAD between 1400-1600 UTC (Fig. A.18c). The observed stratiform peak (80% at 1500 UTC; Fig. A.19e) once again occurs after the convective peak (> 10%; data is unavailable before 1413 UTC). All model runs are delayed by 1-2 hr and generate more stratiform rain and less anvil echo than observed following their respective analysis periods (Fig. A.19f), but ensemble mean echo coverages are once again close to observed and indicate less convection and more stratiform rain than their less baroclinic counterparts during the times analyzed (Table B.7).

Divergence profiles for each mature LLTS-MCS (Figs. A.20a, c, and e) show that the ensemble profiles (thin red) have structures and magnitudes similar to those observed (thick black). The +/-1 standard deviation of the range-pooled mean VAD estimates (light gray shading) is plotted to display uncertainties in the observed divergence profiles. Although ensemble spread exists for each case, each ensemble mean LND falls within the sampling variability in the observed profiles. The greatest uncertainties in the observed divergence profiles occur at upper-levels in each case, particularly where echo is sparse or peak magnitudes of upper-level divergence are large. Both of these sampling issues are mentioned by Mapes and Lin (2005) and become more significant if errors in unfolding Doppler velocities that exceed the Nyquist velocity

(V_{nyq} = 25 m s^{-1} for ADRAD) also contribute, as in the two more baroclinic cases. In addition, the weakly baroclinic case's observed divergence maximum at 2.5 km (Fig. A.20c) is caused by intense divergence during the last hour (0900-1000 UTC), suggesting that distinct features in the hourly profiles may affect the mean results. Although this narrow peak may be caused by poor observational data, a strong descending rear-inflow jet that was located exclusively on the east side of ADRAD during the entire hour may also be the culprit. Removing this hour's estimate at 2.5 km results in a smoother profile that appears to be interpolated between the estimates above and below it.

Figures A.20b, d, and f show the ensemble mean profiles separated by echo type with a horizontal line indicating the 0°C level. Ensemble mean LNDs decrease in height as the degree of baroclinicity increases in agreement with HS09, and are within 0.4 km of those observed in each case (Table B.7). Although the LND appears to be related to deeper tropospheres with higher melting levels, subsequent cases presented and previous tropical studies do not necessarily support this assertion. Each storm's LND is higher than observed in an east Atlantic tropical squall line (Gamache and Houze 1982) despite having lower 0°C levels, but generally lower than most of the tropical west Pacific MCSs shown in Mapes and Houze (1995). The warm season LLTS-MCS (Fig. A.20b) generates the highest LND observed in this study, eclipsing a few of the tropical MCS LNDs. This storm's elevated heating, which is associated with the strongest stratiform midlevel convergence simulated in this study, likely helped initiate the mesoscale convective vortex (MCV; Bartels and Maddox 1991) that developed the next day,

causing flash flooding in Houston, TX. Magnitudes of low-level convergence and upper level divergence are greatest in the weakly baroclinic case (Fig. A.20d), which WRF suggests is due to intense stratiform convergence near the 0^{o}C level and large corresponding convective profile peaks. The strongly baroclinic case's mean divergence profile (Fig. A.20f) is similar to its stratiform profile except just above the 0^{o}C level where divergence from shallow convection may cause deviations.

b. Large frontal MCSs

This section describes a warm frontal system and two cold frontal MCSs, one in a weakly baroclinic and one in a strongly baroclinic environment. On 3 October 2009, precipitation formed along and north of a warm front in south Texas (Fig. A.18d) as moisture from a tropical depression near Baja California approached from the west, increasing as a 700 hPa shortwave propagated through the region (not shown). Stratiform rain covered > 80% of ADRAD's grid while < 5% of anvil echo coverage was observed from 2030-0200 UTC (Fig. A.21a), causing this storm to have the greatest (least) mean stratiform (anvil) echo observed in this study (Table B.7). Convective rain area is oversimulated in the warm frontal case (Fig. A.21b), but is modeled more accurately for the cold frontal weakly baroclinic MCS that produced three times more convective echo (Table B.7). On 18 September 2006, convective cells ahead of the weakly baroclinic cold front merged to form an MCS (Fig. A.18e) whose stratiform area peaked at 1000 UTC in observations (85%; Fig. A.21c) and the model ensemble (65%;

Fig. A.21d). As in the warm frontal case, stratiform area is undersimulated while anvil area generated by WRF doubled that observed.

In contrast to the LLTS-MCSs, divergence profiles simulated for these less organized weakly baroclinic frontal storms exhibit distinct variations from their radar-observed structures. Although simulated magnitudes of low-level convergence are similar to observed in the warm frontal case (Fig. A.22a), midlevel magnitudes of divergence are greater than observed between 5-7 km because WRF overpredicts convective echo containing intense divergence (Fig. A.22b). Weak magnitudes of stratiform convergence peaking at the 0^{o}C level cannot compensate. Simulated divergence profiles for the weakly baroclinic cold frontal case (Fig. A.22c) exhibit a larger ensemble spread and are more elevated than in the warm frontal case, producing weaker magnitudes and a higher LND than observed. Observed profiles in both cases exhibit large uncertainties above 8 km, while the cold frontal case has high sampling error in the region of maximum low-level convergence. Deeper convection, a thicker, stronger layer of stratiform convergence peaking at the 0^{o}C level, and a more elevated anvil divergence structure (Fig. A.22d) are responsible for elevating this simulated cold frontal profile above the warm frontal case.

These weakly baroclinic frontal cases are compared to a strongly baroclinic cold frontal storm containing stronger temperature gradients and wind shears that produced several hours of rain over southeast Texas on 9 October 2009 (Fig. A.18f). Precipitation developed on 8 October between a cold front extending from Ontario and an advancing warm front to the south in the right-entrance region of a jet streak as convection formed

in west Texas along the cold front and a pre-frontal trough (not shown). The southern edge of this synoptic system extending over 2000 km had a similar observed (Fig. A.21e) and modeled (Fig. A.21f) evolution, but more convective and less stratiform rain area is simulated behind the surface-based convective line than observed. Non-precipitating anvil area increased above 45% of WRF and ADRAD's grid by 2200 UTC, greater than observed at any point by FS08. However, this anvil differs from the deep tropical convection they studied because this case's anvil is at least partially caused by elevated echo forming well behind the surface front.

The divergence profile observed in this case (Fig. A.22e) is similar to the strongly baroclinic LLTS-MCS (Fig. A.20e) and weakly baroclinic cold frontal storm (Fig. A.22c) except that it has smaller magnitudes of low-level convergence that peak ~1 km higher. These differences between the cases are likely caused by the relatively high occurrence of stratiform and anvil echo that produces midlevel convergence peaking at the 0^{o}C level and 1 km above, respectively (Fig. A.22f). Uncertainties in the observed structures are very high above 9 km where sparse echoes and strong winds associated with a jet streak introduce large errors (Fig. A.22e), but are relatively small elsewhere. The structures and magnitudes of the ensemble members and observed divergence profiles are similar except between 6-8 km where the model produces weaker divergence than observed. This difference and other causes of ensemble spread are discussed in Chapter IV.

c. Upper-level disturbances

1) WARM SEASON MCV

Although fronts produce most southeast Texas precipitation, upper-level disturbances also account for a large amount of annual rainfall, particularly during summer. A fraction of these storms are associated with diabatically maintained MCVs, or deep midlevel circulations 100-300 km in diameter, that typically develop within the stratiform regions of mature, nocturnal MCSs and can occasionally persist for days (Davis and Trier 2007). On 8 June 2010, convection initiated near a cutoff 500 hPa low in south Texas and persisted overnight in the presence of a ~15 m s^{-1} southerly low-level jet and weaker midlevel flow favoring back-building convection (Corfidi et al. 1996, not shown). An MCV developed in the stratiform region of this back-building, quasi-stationary MCS (Schumacher and Johnson 2005, 2009; Fig. A.18j) that caused flash flooding and one fatality after producing > 287 mm of rain between 0300-1400 UTC 9 June near New Braunfels, TX (based on three overtopped Community Collaborative Rain Hail and Snow Network, or CoCoRAHS, gauges). The observed (Fig. A.23a) and modeled (Fig. A.23b) echo coverage time series shows that convective and anvil area gradually decrease while stratiform rain area increases, with WRF simulating more convective rain area than observed (Table B.7).

Ensemble simulations of this mature MCV generate one of the most elevated divergence structures in this study, despite the observed LND being 1-3 km lower than all of the ensemble members, which are well outside of the uncertainty of the observed profile (Fig. A.24a). In contrast to the other cases presented, large magnitudes of

stratiform convergence peak 1.5 km above the 0°C level with an equally intense anvil convergence peak at ~9 km (Fig. A.24b). Precipitating and anvil components simulated by this MCV also generate large magnitudes of cyclonic (anticyclonic) relative vorticity below (above) 10 km (Fig. A.24c), with the stratiform region producing the largest magnitudes of midlevel relative vorticity in agreement with Bosart's (1986) analysis of the July 1977 Johnstown, PA MCV (Bosart's profiles are an order of magnitude smaller due to his use of coarser radiosonde data). In addition, relative vorticity magnitudes peak near the 0°C level in the stratiform region and at 2 km in the convective region, matching the maxima in MCV potential vorticity anomalies shown by Davis and Trier (2002).

2) SHORTWAVE DISTURBANCES

Three storms triggered by 700-500 hPa shortwaves with varying baroclinicities are also presented for comparison. Descriptions of the cases and MM5 results of the warm season and weakly baroclinic cases are given in HS09; therefore, there is only a brief treatment of cases in this section focusing on interesting features that differ from the previous cases.

A shortwave embedded within an inverted trough initiated convection (Fig. A.18g) in an otherwise barotropic environment on 20 July 2007, whereas a shortwave propagating ahead of a closed low produced convection in an environment with stronger wind shears on 13 March 2007. This storm evolved into a training line-adjoining stratiform MCS (Schumacher and Johnson 2005; Fig. A.18h) as cells moved along a storm-induced outflow boundary. On 13 March 2009, positive differential vorticity

advection ahead of a shortwave provided the primary forcing for the strongly baroclinic case (Fig. A.18i) along with isentropic lifting north and west of a surface front in the Gulf. Mean echo coverages simulated by the WRF ensemble for this predominantly stratiform case are similar, whereas WRF generates more anvil for the two less baroclinic cases, double the convective area for the 20 July storm, and less stratiform rain area than observed by ADRAD for the 13 March case (Table B.7).

Mean divergence profiles simulated for these three shortwave disturbances exhibit similar structures and magnitudes to those observed except the warm season case, whose divergence profiles are most variable and have a mean LND that is ~2 km higher than observed (Fig. A.25a; Table B.7). Although the uncertainly in the observed LND is fairly large in this case, most of the ensemble members produce much stronger magnitudes of convergence between 6-9 km that is evaluated further in Chapter IV. The weakly baroclinic case's (Fig. A.25b) observed divergence profile has an LND similar to the warm season case despite occurring during March and having a 0^{o}C level over 1 km lower, suggesting that elevated heating patterns can occur during the cold season in the subtropics. Although the predominantly non-convective, strongly baroclinic case (Fig. A.25c) has a lower LND and generates much weaker magnitudes of convergence with a smaller ensemble spread than its weakly baroclinic counterpart, its observed and simulated magnitudes of convergence below the LND are similar to the deep-convective warm season case.

3. MM5 and observational comparisons by storm type

a. Model simulations

Ensemble simulations of each storm were also conducted using version 3.7 of the fifth-generation Pennsylvania State University-NCAR nonhydrostatic Mesoscale Model (MM5; Dudhia 1993). Initial and lateral boundary conditions and the triple-nested domain setup matched that used in WRF-ARW (cf. Fig. A.16) except that the innermost analysis domain (D3) with 3-km grid spacing contained 100x100 grid points as opposed to 130x130. All simulations utilized a high-resolution Blackadar (1979) planetary boundary layer scheme (Zhang and Anthes 1982; Zhang and Fritsch 1986) that accounts for moist vertical diffusion in clouds and a radiation scheme that parameterizes longwave and shortwave interactions in clouds and the clear atmosphere (Dudhia 1989).

As in the WRF-ARW analysis described earlier in this chapter, eight-member ensemble simulations were created for each case in MM5 by alternating between two MPs on each grid, two CPs on D1, and turning this CP on and off on D2. Two mass-flux convective schemes were used: Grell (1993) and Kain-Fritsch-2 (Kain 2004), which share similarities with the CPs used in WRF-ARW. The Grell CP only allows detrainment at cloud top, as opposed to Kain-Fritsch-2 that allows clouds and the environment to exchange mass at all levels. In addition, the Grell CP's quasi-equilibrium closure (Arakawa and Schubert 1974) assumes convection eliminates CAPE created by large-scale processes, whereas Kain-Fritsch-2 removes CAPE over a prescribed time period for an entraining parcel.

Two bulk one-moment MPs including cloud ice, snow, and graupel processes were also used to parameterize explicit microphysics: Reisner-2 (Reisner et al. 1998) and Goddard (Tao et al. 1989; Tao and Simpson 1993), the latter of which is similar to the Goddard scheme used in the WRF-ARW analysis. Unlike the Goddard MP, which uses the fixed intercept parameters for rain ($N_{o,r}$), graupel ($N_{o,g}$), and snow ($N_{o,s}$) given in Table B.8, the Reisner-2 MP N_o for each species varies as a function of predicted thermodynamic or cloud variables given in Thompson et al. (2004). The biggest limitation of both one-moment MPs is that neither predicts number concentrations for each species or accounts for $N_{o,r}$ decreases (or "N_o jumps"; Waldvogel 1974) observed when transitioning from convective (~10^7 m^{-4}) to stratiform (~10^6 m^{-4}) captured by two-moment schemes like the Morrison MP in WRF-ARW. In the MM5 experiments, the Goddard MP specifies a more balanced Marshall and Palmer (1948) DSD ($N_{o,r} = 8 \times 10^6$ m^{-4}) compared to the Reisner-2 MP's more convective DSD ($N_{o,r} \sim 2 \times 10^7$ m^{-4} except for drizzle drops with low mixing ratios).

b. Summary of MM5 results

Aside from their differing model platforms and configurations, the methods used to generate ensemble mean divergence profiles and echo coverages in MM5 match those used for WRF-ARW described earlier in this chapter. Instead of presenting the ensemble mean divergence profiles for each case again, the mean LNDs and echo coverages simulated by MM5 are presented in Table B.9. Although the MM5 and WRF-ARW (cf. Table B.7) ensemble mean LNDs are within 0.4 km of each other in nine of the ten

cases, WRF-ARW's mean area echo coverages are typically much closer to observed than those generated by MM5, whose simulations generally produce deficient stratiform and excessive convective and non-precipitating anvil echo relative to observations. Therefore, echo coverage variations associated with using different parameterization treatments in MM5 are further discussed in Chapter IV.

CHAPTER IV

MODEL SENSITIVITIES

This chapter investigates variations in echo area and divergence structures from the ensemble means presented in Chapter III associated with utilizing different combinations of parameterization treatments in WRF-ARW and MM5, analyzing both models' most significant sensitivities in greater detail. The reflectivity structures simulated in MM5 by the Goddard and Reisner-2 MPs are also presented to partially explain their significant differences in stratiform rain and non-precipitating anvil area. Although these echo coverage variations are not associated with significant differences in MM5 divergence structures, areal echo coverages exhibit significant sensitivities to whether or not a CP is employed on the intermediate grid in WRF-ARW that partially explains some of the ensemble spread in divergence profiles noted in Chapter III. Therefore, variations in divergence structures simulated by WRF-ARW are analyzed in greater detail, utilizing relevant MM5 results to supplement the discussion.

1. Variations in echo coverage

Table B.10 summarizes the cases discussed so far and highlights that as the degree of baroclinicity increases, convective area decreases and stratiform area increases in both models and observations. The observed warm season stratiform to convective area ratio (~4:1) is similar to the ~3:1 tropics-wide (Schumacher and Houze 2003) and TWP-ICE (FS08) ratios, implying the results in this dissertation may extend to more

barotropic tropical conditions. Non-precipitating thick anvil area remains steady during the mature precipitating phases of the systems studied (except in the MM5 runs), but time series shown by FS08 and in many of the cases in this study indicate that anvil may persist several hours after the initial convective rain area peak and these time periods are not reflected in Table B.10. Although strong case-to-case variability has been noted, convective rain and anvil echo is typically overpredicted and stratiform rain area is underpredicted in both models, particularly in MM5.

a. MM5 variations in echo coverage and reflectivity structures

Table B.11 shows that although variations in convective area fractions are typically small, stratiform and anvil area fractions exhibit their largest sensitivities to MPs, with Goddard producing more stratiform and less anvil echo than Reisner-2 across all storm environments. Although results from individual cases are not shown, these MP effects occur in every case except the strongly baroclinic LLTS-MCS and are significant in half of the cases at the 95% confidence level using Lenth's method for unreplicated factorial experiments (Lenth 1989; Ye and Hamada 2000). One statistically significant exception to this trend is the 20 March 2010 strongly baroclinic LLTS-MCS that is discussed further in this section. Explicitly resolving convection at 9 km also appears to produce more stratiform echo on the inner 3 km grid than parameterizing convection on D2. Although every storm exhibits this trend except the warm frontal case, this effect is only significant in one case and is not associated with consistent changes in anvil echo.

The 18 June 2006 and 20 March 2010 LLTS-MCSs are used to highlight the Goddard and Reisner-2 differences. Both MPs simulate a similar time evolution of convective coverage in the warm season 18 June case (Figs. A.26a and b), but anvil (stratiform rain) increases (decreases) more rapidly in the Reisner-2 runs. In contrast, Goddard runs (Fig. A.26c) of the strongly baroclinic LLTS-MCS on 20 March produce more trailing anvil and a smaller stratiform rain region than their Reisner-2 counterparts (Fig. A.26d) that is closer to that observed (cf. Fig. A.19e).

Representative cross sections of the LLTS-MCSs observed by ADRAD and simulated by both MPs (using the Kain-Fritsch 2 CP with explicit convection on D2) are shown in Fig. A.27. Precipitating regions of the warm season MCS simulated by both MPs are similar in size to that observed (Figs. A.27a-c), but the model convection is more intense and zonally oriented towards the southern edge. In addition to lacking a transition region and generating multiple convective cores, the simulations display excessive trailing anvil echo and simulated reflectivities above the 0^{o}C level (4.6 km) relative to observations (Figs. A.27d-f). Echo tops simulated by the Goddard MP decrease behind the convective line in agreement with observations, but are higher and more variable in the Reisner-2 run, possibly due to this run's greater specified $N_{o,r}$ values that are more appropriate for convective than stratiform rain regions. Convective cells are not simulated in the strongly baroclinic MCS's stratiform region (Figs. A.27g-i), but the Reisner-2 stratiform region is wider than observed in agreement with Fig. A.26d. Although vertical cross sections simulated by both MPs better match observations, reflectivities are still greater than observed above the 2.7 km melting layer. Furthermore,

the Goddard echo tops are lower than observed despite simulating more anvil echo, whereas the Reisner-2 echo tops are more still variable (Figs. A.27j-l).

Figures A.28-A.30 display the convective, stratiform, and anvil vertical reflectivity distributions, respectively, observed by ADRAD (as in Fig. A.17) for both MCSs and show how selected quantiles of model reflectivities simulated by the four Goddard and Reisner-2 MP runs (using all CP combinations) differ from observations. These figures also illustrate simulated mixing ratio profiles. Although the magnitudes of reflectivity differences may be sensitive to how reflectivity is calculated from model variables, the qualitative differences between both MPs should not change.

Observed convective reflectivities for the warm season MCS (Fig. A.28a) are similar to West African convection shown by Schumacher and Houze (2006), but have larger (smaller) values below (above) 8 km indicative of enhanced warm rain processes. Although most near-surface reflectivities are only overpredicted by 1-2 dB (Fig. A.28b), both MPs simulate a much wider distribution of convective reflectivities than observed above the 0^{o}C level. The majority of echoes between 6-8 km are overpredicted by at least 10 dB in the Goddard runs, whereas the Reisner-2 runs are 5-8 dB greater than observed. This difference is associated with the Goddard MP's greater production of graupel aloft relative to the Reisner-2 MP, which preferentially simulates more snow mass above 8.5 km (Fig. A.28c). These results also apply to most of the MM5 ensemble simulations in this dissertation. A narrower distribution of generally weaker convective reflectivities is observed in the strongly baroclinic MCS (Fig. A.28d) except at the surface where values are similar to the warm season case. Goddard reflectivities (Fig.

A.28e) and graupel mixing ratios (Fig. A.28f) aloft are still greater than those simulated by Reisner-2, but more snow mass is produced by the Goddard MP aloft, a feature that is unique to this case.

Both cases exhibit similar stratiform reflectivity distributions below the 0^{o}C level, but the strongly baroclinic MCS (Fig. A.29d) has a narrower distribution above the 0^{o}C level and intense fallstreaks that result in near-surface reflectivties that are 3-4 dB higher than in the warm season case (Fig. A.29a). Near-surface stratiform reflectivities predicted by the Goddard MP for the warm season MCS are similar to those observed, but are overpredicted by 4-6 dB in the Reisner-2 runs (Fig. A.29b) whose rain mixing ratios are greater (Fig. A.29c). This difference is partially attributed to enhanced evaporation rates associated with the Reisner-2 MP's higher $N_{o,r}$ values (Morrison et al. 2009) that cause more cloud droplets and small raindrops to evaporate than in the Goddard runs that simulate more stratiform echo (41% vs. 30% coverage). Both MPs' stratiform distributions are similar above the 0^{o}C level, but the Goddard median reflectivity is lower above 8 km where it produces less snow mass compared to Reinser-2. Graupel mass also unrealistically exceeds snow mass between 3.5-5 km in both MPs, which Lang et al. (2007) corrected by eliminating the dry growth of graupel (but producing excessive snow in its absence). Both MPs produce a lower ratio of graupel to snow mass for the strongly baroclinic MCS, with the Goddard simulations producing higher reflectivities (Fig. A.29e) and snow mixing ratios between 3-6 km (Fig. A.29f).

Anvil reflectivities observed in the warm season MCS are lower than their stratiform counterparts except just above 7 km, similar to those observed in Schumacher

and Houze (2006) (Fig. A.30a). Anvil reflectivities are weaker and do not exhibit an upper-level peak in the strongly baroclinic case (Fig. A.30d). Both MPs' reflectivities are within 5 dB of those observed in the warm season case above 6 km, but most Reisner-2 echoes are overpredicted below that because hydrometeors that should fall as stratiform rain evaporate above 2.5 km and are classified as anvil instead (Fig. A.30b). This is verified by the rapid decrease in Reisner-2's rain mixing ratios from 4.0-2.5 km (Fig. A.30c). Overprediction of snow mass aloft also likely accounts for much of the excessive anvil echo both MPs produce, which may be reduced some by decreasing the collection efficiency of cloud water by snow following Lang et al. (2007). The Goddard MP's ability to produce less snow mass relative to Reisner-2 suggests that stratiform rain area may be increased in models by reducing the presence of low-density ice hydrometeors that may remain lofted in anvil instead of precipitating in models. This assertion is supported even when the trends between both MPs are reversed as indicated by the reflectivities (Fig. A.30e) and snow mixing ratios (Fig. A.30f) simulated in the strongly baroclinic case.

b. WRF-ARW echo coverage variations

Table B.12 presents differences in mean echo coverage simulated by ensemble members employing different parameterization treatments in WRF-ARW. More convective and less stratiform rain area is produced by the Morrison two-moment MP compared to the Goddard one-moment MP in most weakly and strongly baroclinic storms, a result that is statistically significant for four of the seven cases at the 95%

confidence level. One might expect reduced stratiform evaporation rates (and thus higher stratiform rain areas) using two-moment MPs (Morrison et al. 2009), but this is only the case during the warm season when area differences are smaller and only statistically significant for one case. The Morrison MP typically simulates convective and stratiform rain area fractions closer to observed in cases whose domain-averaged time series exhibit distinct convective and subsequent stratiform peaks (e.g., LLTS-MCSs). However, lower stratiform areas than those observed are simulated with the Morrison MP in storms that likely do not exhibit pronounced intrastorm DSD changes (e.g., weakly baroclinic warm frontal and upper-level disturbance cases). These results suggest that capturing N_o jumps in DSD spectra is important, but its applicability to storms whose convection is embedded within stratiform regions should be investigated further.

Stratiform and anvil areas exhibit more significant and consistent sensitivities to whether or not a CP is used on the 9-km grid (D2) in WRF, with runs parameterizing convection simulating less stratiform rain area than their explicit counterparts, a result that is statistically significant for seven storms including all three warm season cases. These changes are coupled with significant reductions in anvil echo in the baroclinic cases. Warner and Hsu (2000) showed that using a CP on a 10 km intermediate grid (similar to our D2) induced stabilization and drying between 500-700 hPa that reduced rainfall on the inner-grid, potentially explaining why less stratiform rain area is generated in our parameterized runs. Further investigation of this is left to future work.

2. Divergence variations and possible implications

Table B.13 displays differences in LNDs from each environment's mean value simulated by specific parameterizations and combinations of parameterizations in MM5. The warm season LNDs exhibit the largest sensitivities to the model configuration, but differences between employing the Goddard and Reisner-2 MPs are small despite the variations in stratiform rain and anvil area noted in the previous section. The largest LND variations are associated with utilizing different CPs and for two-factor interactions between explicit and parameterized convection on D2 depending on which CP is used. However, these warm season LND variations are generally not significant for each case, with only the 9 June 2010 MCV (results of which are presented later in this section) exhibiting marginally significant ($p < 0.1$) variations.

Table B.14 lists the five cases simulated in WRF-ARW whose divergence profiles in Chapter III exhibited the largest ensemble spread along with variations in LNDs associated with employing different parameterization treatments. For example, not parameterizing convection on D2 partially accounts for statistically significant increases in LNDs that may be caused by their increased stratiform rain fractions, variations in convective intensity (discussed below), or a combination of both. Significant variations in LNDs are also found for two-factor interactions between the choice of parameterized or explicit convection on the 9 km intermediate grid depending on the MP and CP used.

Divergence, vertical velocity and mixing ratio variations caused by explicit and parameterized convection on D2 when using the Morrison and Goddard MPs are

presented for the 20-21 July 2007 warm season case in Figs. A.31 and A.32. Many of the storms in Table B.14 also exhibit similar, albeit less significant trends, to the results shown in this case. Figure A.31a shows that the two Morrison MP runs that parameterize convection on D2 (MORcp) produce weaker and less elevated divergence profiles than those observed, whereas all other members produce more elevated profiles with stronger magnitudes. The uncertainty in the observed divergence profile (cf. Fig. A.25a) suggests that the ideal simulation likely lies between these groups.

Figure A.32a shows that the Morrison runs (red lines) contain one distinct peak in convective updrafts between 4-6 km, whereas the Goddard runs (green lines) produce stronger updrafts above 8 km. Convective magnitudes of divergence peak at higher levels for the Goddard runs (Fig. A.31b), detraining greater quantities of ice-phase hydrometeors to the stratiform region than in the Morrison runs (Figs. A.32d and e), in agreement with Luo et al.'s (2010) comparisons to other one-moment MPs. Although none of the members exhibit pronounced mesoscale downdrafts below the 0^{o}C level (as in HS09), weaker stratiform (Fig. A.32b) and anvil (Fig. A.32c) vertical velocities are also associated with weaker convective vertical motions above 7 km for the Morrison runs. The Goddard MP also produces a higher proportion of dense graupel in the stratiform region relative to the Morrison MP that generates more snow (not shown), allowing the Morrison MP ice-phase anvil hydrometeors to be concentrated higher aloft and distinct from the stratiform region (Fig. A.32f). Greater quantities of ice-phase mixing ratios are also simulated above 12 km by the MORexp runs producing more stratiform rain area than observed, potentially explaining why their stratiform (Fig.

A.31c) and mean LNDs are more elevated than the Goddard runs. Although stratiform area plays a strong role, this case's divergence structures are clearly sensitive to both the intensity of convection dictated by whether a CP is used on D2 and where its horizontal divergence is focused based on the MP employed.

The ensemble spread in LNDs for the three baroclinic cases in Table B.14 are most sensitive to whether or not convection is parameterized on the 9 km intermediate grid and which CP is used. Although many active factors make discerning the primary cause of divergence variations in the 18 September 2006 case difficult, variations in stratiform and anvil coverage appear to cause divergence variations in the 13-14 March 2007 upper-level disturbance and the 9 October 2009 cold frontal case. Representative results are shown for the 9 October 2009 case in Fig. A.33 whose two-factor interactions in echo coverage variations are significant, with the GDEcp runs producing significantly lower stratiform rain (42%) and higher anvil (25%) fractions compared to all other members, including the KFcp runs (60% and 16%, respectively). Simulations not parameterizing convection on D2 produce LNDs ~1 km higher than observed (Fig. A.33a), whereas those that do simulate more reasonable LNDs. Although the GDEcp members' LNDs are closer to those observed, their magnitudes of convergence below the LND are weaker than observed compared to other runs containing larger magnitudes of stratiform (Fig. A.33b) and anvil (Fig. A.33c) convergence at midlevels, the latter of which is more elevated in the explicit runs. These results suggest that LNDs deviations should be considered with other factors (e.g., divergence profile magnitudes and echo coverages) in determining which simulation(s) best match observations.

Finally, divergence variations for the 9 June 2010 MCV are strongest between explicit and parameterized convection on D2 depending on which CP is used (Table B.14). Although all of the WRF members simulate much more elevated divergence profiles than observed, the structure and magnitudes of the divergence profiles simulated by the GDEcp members are much closer to those observed (Fig. A.34a). In addition, the GDEcp runs producing the least elevated heating structures also generate the smallest magnitudes of mean relative vorticity throughout the depth of the troposphere (Fig. A.34b). Differences are most pronounced between 3-6 km where stratiform positive vorticity magnitudes in the GDEcp members are 30-45% smaller than the other sets of simulations (Fig. A.34c), yielding less intense midlevel vortices and weaker anticyclones aloft.

Compared to the other ensemble members whose divergence profiles deviate more from observations, the GDEcp runs exhibit stronger convective horizontal divergence between 5-11 km (Fig. A.35a) associated with their more intense convective updrafts over a similar or shallower (as for the median) depth of the troposphere (Fig. A.35b). The GDEcp runs also produce the most intense mesoscale updraft-downdraft couplet within the stratiform region between 2-10 km (Fig. A.35c) and strongest anvil downdrafts between 3-11 km (Fig. A.35d) that concentrate larger magnitudes of stratiform convergence between 6-8 km (not shown). Despite simulating stratiform and anvil coverages similar to the GDEcp runs, the KFcp members generate the most elevated divergence profiles (Fig. A.34a) and a stratiform LND that is ~1 km higher than in the other members (not shown).

Considering that the CAPE removal closure used in the KFcp runs is one of four closures used in the GDEcp members, at least some (if not all) of the other individual closures likely simulate less elevated divergence profiles closer to observed. Divergence profiles simulated by MM5 support this assertion by showing that ensemble members employing the Grell CP on both outer grids (GRLcp; Fig. A.36a) simulate LNDs that are lower than observed and magnitudes of convergence that are weaker than observed between 2-6 km. Although the quasi-equilibrium closure (Arakawa and Schubert 1974) may not necessarily produce the same results for the Grell-Devenyi CP in WRF-ARW, this CP's ensemble members that utilize this assumption likely produce lower LNDs relative to those using the CAPE removal closure employed by the Kain-Fritsch CPs in WRF-ARW and MM5. Once again, the GRLcp runs' less elevated heating structures that generate the smallest magnitudes of mean relative vorticity below 9 km (Fig. A.36b) are associated with differences in convective intensity that result in stronger (weaker) magnitudes of divergence in convective rain regions at midlevels (upper levels) relative to the other model runs (Fig. A.36c). Thus, an ensemble-based CP that utilizes numerous closures and variations in parameters (e.g., changing the convective time scale for the CAPE removal closure) may better represent convective spectra (and possibly their stratiform byproducts) in certain cases, particularly when using these parameterizations on outer domains whose grid spacings are on the order of ~10 km.

CHAPTER V

UNDERGRADUATE EXPERIENCES IN SOAP: A RESEARCH AND EDUCATION PROGRAM

Some of the data collection and preliminary research for the results presented in this dissertation involved undergraduate participants in the Student Operational ADRAD Project (SOAP) over its five-year duration. Undergraduate research continues to be increasingly regarded as a critical component of science education (Halstead 1997), something that over half (53%) of all science, technology, education, and mathematics (STEM) undergraduates participate in during their college careers (Russell 2006). Sadler and McKinney (2010) emphasize that empirical analyses of undergraduate research programs are essential for improving such experiences and advancing undergraduate science education. Evaluating SOAP is particularly important for the atmospheric sciences because most empirical studies of undergraduate research programs come from other STEM fields (Gonzales-Espada and LaDue 2006) and focus more on the program's goals and its students' educational achievement than on evaluating its participants' experiences. Furthermore, SOAP appears to be unique because its primary component focused on data collection, education, and peer interactions involving many undergraduates instead of primarily mentoring undergraduates through individual research projects. Therefore, this chapter documents students' educational experiences in SOAP, evaluating how they affect student confidence, interests, and career outcomes.

1. SOAP program description

Ninety-five Texas A&M undergraduates participated in SOAP, a spring semester "field" research and education program between 2006-2010 that provided 25-30 students each year with hands-on experience outside the traditional classroom. SOAP participants gained forecasting and research experience by predicting, observing, and analyzing a variety of precipitating systems, while also collecting data and providing useful results towards this dissertation and the broader NSF CAREER grant's research goals. SOAP students were placed into daily groups of 5-6 students that were primarily responsible for producing a precipitation forecast and operating ADRAD if precipitation was in the radar domain on their day. Each group was led by a senior-level undergraduate with SOAP experience (excluding 2006) who was directly mentored by one of three graduate students and a faculty advisor in charge of the program (Fig. A.37). Monthly meetings with the group leaders, graduate students, and faculty advisor were also held between December-April for training, brainstorming, and feedback. In addition, the graduate students and faculty advisor also made a conscientious effort to interact with SOAP participants regularly, with the majority of students reporting eight or more interactions out of 11 weeks (Table B.15) with these mentors during the last three years of SOAP.

Students were expected to perform several tasks on their day, many of which were part of SOAP every year. Training and organizational meetings were held during the first three weeks of the semester, followed by 11 weeks of operations and a wrap-up meeting during the last week. Groups met at least once in the morning and once in the afternoon for 1-2 h to perform their daily responsibilities in a lab space designed for

SOAP on the twelfth floor of the O&M Building, meeting more if precipitation was in the area. Daily tasks that were incorporated during each year of SOAP included:

- **Forecasting and writing the daily forecast discussion** for precipitation during the morning with an afternoon update. Each shift analyzed national satellite and radar imagery and upper-air maps before focusing on southeast Texas. Students then posted a forecast discussion on the SOAP website (soap.tamu.edu), indicating the likelihood precipitation would occur before 8 am the next day and over the next three days.
- **Identifying cloud types** according to the World Meteorological Organization's (WMO's) synoptic code (WMO 1974) using the ten classifications (including no cloud) for low (cloud bases > 800 hPa), middle (cloud bases 800-400 hPa), and high (cloud bases < 400 hPa) clouds. Students took eight panoramic snapshots of the sky during the morning and afternoon from the fifteenth floor observatory in the O&M Building, posting these images on the SOAP website in real-time.
- **Operating the radar** when precipitation was within ADRAD's domain between 8am-10pm LT. Students chose appropriate scan strategies and monitored the radar to ensure data was being collected continuously. Group leaders organized their group members in covering the radar and coordinated with their graduate student mentor and the next day's group leader if overnight operations were necessary.
- **Analyzing radar data** in real-time and from old cases using Sigmet's Interactive Radar Information System (IRIS). Each group also posted representative cross-

sections with a precipitation summary on the SOAP website for each event that occurred on their day, presenting one case study in detail at the wrap-up meeting.

In addition to these daily tasks, several additional activities were implemented into the program permanently or for a few years. These tasks include:

- **Analyzing online archives for the radar climatology (2007-2008)** to classify storms by their dynamical forcing and structure for the climatology presented in Chapter II. Advanced undergraduates supervised by the author vetted all storm classifications before additional analyses were performed.
- **Using FX-Net software to forecast (2008-2010)** in addition to the web-based resources used during the first two years of SOAP. FX-net imitates the National Weather Service's (NWS) Advanced Weather Interactive Processing System (AWIPS) Graphics User Interface (GUI), permitting students to create their own analysis products in addition to default products specifically created for SOAP.
- **Learning modules for FX-Net and ADRAD (2008-2010)** to learn how to perform specific tasks or new analysis methods for forecasting using FX-Net or analyzing radar data in IRIS. Groups typically completed 4-6 learning modules a semester on relatively slow days when precipitation was not in the area.
- **Recording and submitting rain gauge data (2009-2010)** daily between 7-9 am LT on the CoCoRAHS website (www.cocorahs.org) for gauges sited by each student, typically at their residence.

- **Creating a quantitative precipitation forecast (2009-2010)** based on past rainfall totals for their predicted storm type and structure, WRF model output, and the Storm Prediction Center's short-range ensemble forecasts. Students forecast the timing of precipitation and a mean, minimum, and maximum QPF that they verified the next week using data from ~30 SOAP CoCoRAHS gauges.
- **Performing sounding launches (2008 and 2010)** from the 17th green of the Texas A&M University Golf Course. All groups released two radiosondes at 0000 UTC during the last two weeks of April 2008, whereas each group was given three radiosondes to release at 0000, 1200, or 1800 UTC on days of their choice during the last five weeks of SOAP in 2010. Sounding observations were sent to nearby NWS WFOs when needed for forecasting severe weather events.

In addition, 13 of the 95 SOAP participants also performed advanced research projects in pairs under the direction of the faculty advisor or a graduate student mentor during Fall 2007, 2008, and 2009, presenting their work at the AMS Annual Meeting Student Conference and TAMU Student Research Week. Appendix C lists the eight projects completed during "Fall SOAP," many of which incorporated data collected or research performed by SOAP students during the spring. Some of these projects also influenced the research and data collection objectives of Spring SOAP between 2008-2010 when many of the group leaders were Fall SOAP participants. Nevertheless, this chapter focuses on the spring component of SOAP for which participant feedback was obtained.

2. Survey methods and correlations

a. Survey instrument

Anonymous student surveys that were approved by the Institutional Review Board (IRB) were administered at the end of Spring SOAP during the last four years of the program (2007-2010). Each question on the survey was optional, ensuring participant privacy by only having students identify their classification (upper or lower), years of SOAP experience, and shift they participated in (morning or afternoon). Students also indicated which career goals they were considering upon graduation, including research, forecasting, and broadcast meteorology. Qualitative responses were solicited through open-ended questions that allowed students to evaluate their SOAP experience more holistically and suggest how specific elements of the program could be improved, the original intent of the surveys. Students also quantified how often they completed many of the SOAP tasks discussed in the previous section (i.e., "experience") in addition to rating their confidence and interest in performing each task using Likert-type items rated on a discrete five-point scale. The exact wording of the question, items, and response scale descriptors used for each scale in the survey is provided in Table B.16.

Although some studies (e.g, Norman 2010) defend the use of parametric statistical measures for Likert (1931) scales, utilizing non-parametric statistical measures for ordinal data are less objectionable and must be used when analyzing the individual Likert-type items. Therefore, non-parametric statistics are generally utilized in this chapter, beginning with Table B.16, which presents median and mode student responses for confidence, interest, and experience for individual SOAP tasks. Students generally

exhibited high confidence and interest in performing most program tasks each year except for creating quantitative precipitation forecasts and completing learning modules when they were first implemented in 2008. In addition, SOAP participants were least confident in operating ADRAD and analyzing radar data during 2008 when ADRAD was inoperable for several weeks due to building renovations. Aside from increased participation in sounding launches during 2010 than 2008, median experience responses for each task were similar each year. However, the lower reliability of the experience scale relative to the interest and confidence scales (Table B.17, described further in the next section) suggests the numeric ranges used discretize experience for each task may be unreliable, thus possibly indicating constant participation levels inaccurately.

b. Instrument reliability and validity

Internal consistency of the confidence, interest, and experience scales were measured using the Cronbach alpha estimate of the reliability coefficient, or the squared correlation between the observed and true values of a variable (Table B.17). Cronbach alpha values indirectly indicate the degree to which a set of items measures a single underlying construct, ranging from 0-1.0 with 1.0 expressing perfect reliability. Alpha values exceeding 0.7 are generally regarded as acceptable, whereas values below 0.5 are unacceptable (George and Mallory 2003). Three SOAP tasks (identifying cloud types, recording and submitting rain gauge data, and analyzing online archives for the radar climatology) were removed from the analysis due to having poor statistical relationships with multiple overall scales as indicated by a low factor loading. Removing these tasks

increased the reliability estimate of the scales most affected by including these tasks without changing the reliability of the other scales appreciably. Results are presented for an overall SOAP Likert scale created by summing together the seven tasks in Table B.16 along with a radar subscale including responses for operating ADRAD and analyzing its radar data. In general, the confidence and interest scales are more reliable than experience responses, with all scales and radar subscales exceeding the unacceptable threshold except interest responses during 2007. Conclusions from scales exhibiting poor (0.5-0.6) or questionable (0.6-0.7) reliabilities should be considered carefully, but are still typically presented in this dissertation.

Empirical analysis of these quantitative survey elements centers on analyzing student confidence, or self-efficacy, in performing SOAP tasks. Self efficacy, the "belief in one's *capabilities* to organize and execute the courses of action required to manage prospective situations (Bandura 1995)," has been shown to affect student interests, career choices, and performance in educational and career pursuits (Lent et al. 1994). Although the lack of a longitudinal set of surveys precludes direct investigation of the latter two assertions, a construct validity for the survey is established by correlating student-reported self-efficacy with their breadth of experience and interest in performing SOAP tasks as shown in Table B.18. Confidence correlations are not presented for 2007 because the interest and experience scales both demonstrate poor or unacceptable reliability.

In agreement with Lent et al. (1994), confidence and interest exhibit statistically significant positive correlations for all SOAP tasks except analyzing radar data during

2008 and 2009. Correlations between confidence and experience are typically less significant, particularly for forecasting, operating ADRAD, and analyzing radar data, the latter of which demonstrates a negative correlation during 2009. However, drawing conclusions from the 2009 data is difficult due to the confidence scale's poor reliability (cf. Table B.16). Nevertheless, the high correlations between confidence and interest for most SOAP tasks each year suggest the surveys are valid and imply that confidence is more strongly related to interest than experience.

3. Results and career outcomes

Previous studies indicate that undergraduates participating in research over multiple semesters report greater perceived benefits, stronger career outcomes, and higher levels of self-efficacy (Bauer and Bennett 2003, Russell 2006, Berkes 2007). Therefore, statistical comparisons between students who participated in SOAP during previous semesters ("veterans") and students participating in SOAP for the first time ("rookies") were performed. Figure A.38 shows that veteran participants' confidence in performing SOAP tasks was significantly higher than rookie participants during each year of the program, increasing 19% on average. These variations in confidence were not associated with significant differences between the experience and interest reported by both groups for each year (not shown). Although these confidence variations were not statistically significant for each individual task, Fig. A.39 shows that veteran students were always significantly more confident in operating ADRAD and analyzing radar data than rookie students, increasing 23% on average. Interestingly, these differences were

most exaggerated during 2008 when all students garnered less experience operating ADRAD due to technical issues, causing veteran students to have much greater cumulative levels of radar experience that were not measured but likely result in their much higher confidence levels.

Students also indicated their career goals after participating in SOAP, with two-thirds expressing interest in forecasting positions compared to one third for research and broadcast meteorology professions (Table B.19). Although the career goals of first and second-year participants' were similar, half of the students associated with SOAP for 3-4 years were interested in research careers compared to 36% otherwise. Participants interested in research careers were typically more confident and interested in performing SOAP tasks than those not interested in research careers. However, these trends were only statistically significant for confidence during 2010 (Fig. A.40a), with research-oriented students indicating higher interest in program tasks (Fig. A.40b) and similar levels of involvement (Fig. A.40c) compared to other participants. Although research-oriented students indicated higher, albeit typically insignificant, levels of confidence and interest in performing most individual tasks, non-research-oriented students were significantly more confident in writing forecast discussions and enjoyed doing so more during 2008 and 2009 (not shown). Most of these non-research oriented students were interested in forecast careers, providing support for Lent et al.'s (1994) finding that self-efficacy affects career goals while also suggesting that not all program tasks were strictly geared towards satisfying students interested in research.

Finally, career outcomes for 59 SOAP graduates between 2007-2010 were tracked by staying in contact with former students through social networking sites (e.g., Facebook, LinkedIn). Similar to national career statistics presented by Knox (2008) for 624 bachelor's degree recipients between 2003-2005, 37% of SOAP graduates obtained forecasting careers (40% including broadcast meteorologists) and 29% matriculated to graduate programs in meteorology or the atmospheric sciences (Table B.20). Students that participated in SOAP 3-4 years were twice as likely to pursue graduate degrees and research careers than those that only were involved for one year, in agreement with Bauer and Bennett (2003) and Russell (2006). In addition, 97% of graduates that participated in SOAP for 2-4 years obtained meteorology or science-related employment compared to 63% of students that only participated in SOAP for one year, differences that are statistically significant ($p < 0.001$; Z-Test for comparing two proportions). Although these results may simply reflect that the most engaged students sign up for more active learning, they also suggest that applied education and research experiences outside the traditional classroom may increase the likelihood that students will remain in science after graduation, a retention issue that should be considered to be as important as graduation and university retention rates.

4. Additional lessons learned

Implementing a research and education program like SOAP provided many lessons and experiences that investigators proposing similar programs may want to consider. First and foremost, allowing advanced undergraduates to direct younger or less

experienced students enabled the senior students to claim some ownership of the program. Students coined their own mascot (a rubber chicken named “Rossby”), developed the SOAP logo and website, and often volunteered for extra responsibilities (e.g., meeting at 5 am to launch special radiosondes, overnight radar operations, etc). In addition, many students reported peer interactions as being as beneficial as those with the faculty and graduate student mentors. All of these factors likely contributed to SOAP’s 66% retention rate of non-graduating students and numerous graduating students declaring SOAP as one of or the most important experience(s) they had at Texas A&M on their departmental exit surveys.

Second, involving many undergraduates in a field-like research experience outside the traditional classroom has several caveats. In agreement with White et al. (2008), implementing and running SOAP was initially very time consuming for the faculty advisor and would have been difficult to maintain without two full-time graduate students that typically spent 10-20 h each week on SOAP during the spring. Group leaders, graduate student mentors, and the faculty advisor had to be mindful of their participants’ capabilities, figuring out how to teach meteorological concepts without pedagogical training. Contingency plans also had to be developed when things did not go as planned like when ADRAD was inoperable during several weeks in 2008, requiring flexibility, patience, and innovation from everyone involved in SOAP. Proactively planning for such events by having possible contingency plans on the shelf (e.g., launching soundings in 2008) contributed to the success of SOAP by benefitting students educationally while also providing useful research data.

Finally, although we had the foresight to assess student-reported experiences in SOAP, these surveys were primarily administered for evaluating and improving SOAP. Investigating educational research questions and measuring SOAP's impacts on students was more of an afterthought than a deliberate enterprise, the latter of which would have likely resulted in more robust assessment results. Libarkin and Kurdziel (2001) outline methods for carrying out educational research more deliberately similar to the scientific method, with special emphasis on considering how assessments or surveys will be administered (including when and to whom) and analyzed. Charlevoix (2008) suggests that higher education may be required to provide evidence of student learning in the near future, for which a strong base of scholarly research on teaching and learning is a prerequisite. Indeed, she notes that Texas has already considered legislation to mandate testing requirements for graduating college seniors that undoubtedly would originate within individual departments, many of which are not prepared and ill-equipped for providing evidence of student learning and achievement. In addition, some grant agencies that already mandate an educational component for some proposals may call for more rigorous and deliberate educational research plans in the future. Therefore, sharing *and* properly assessing teaching and learning in traditional courses and informal learning experiences (e.g., authentic undergraduate research) would help universities proactively prepare for such changes while also building up a knowledge base of teaching and learning in the atmospheric sciences that is relatively sparse.

CHAPTER VI

CONCLUSIONS

Large seasonal and interannual variations in precipitation occur in southeast Texas, a precipitating subtropical region affected by midlatitude and tropical influences. This dissertation establishes a storm climatology for the region, classifying storms by their primary forcing (i.e., cold frontal, warm frontal, upper-level disturbance, and weak forcing) and precipitation structure (i.e., predominantly convective, deep-convective stratiform, and non-deep convective stratiform). Investigating rainfall variations and microphysical differences in climatological raindrop size distributions between these storm types supports the following conclusions:

- Cold (44%) and warm (23%) fronts account for two-thirds of precipitation in southeast Texas, whose annual diurnal cycle in rainfall exhibits a late morning to early afternoon peak. However, this peak is most amplified during summer when the majority of rainfall is caused by upper-level disturbances, the only storm type that exhibits a midday precipitation maximum.
- Upper-level disturbances situated west of southeast Texas exhibit a pronounced summertime midday rainfall peak that is likely caused by the inland progression of coastal nocturnal convection that forms where the land breeze and southerly synoptic flow (generated by disturbances west of the region) collide. In addition, upper-level disturbance rain events that peak at midday are also associated with more thermodynamically unstable, weakly capped morning environments.

- Cold frontal and weakly forced storms yield climatological DSDs that are weighted towards larger drops, particularly for predominantly convective storms. Conversely, DSDs are weighted towards small drops for non-deep convective systems (regardless of storm type), warm fronts, and upper-level disturbances whose weaker convection likely results in smaller amounts of graupel and hail capable of producing large raindrops when they melt before reaching the surface.

This dissertation also compares radar-observed mean divergence profiles and convective, stratiform, and non-precipitating anvil area fractions to ensemble simulations of ten precipitating systems occurring across the spectrum of common storm types and environments in southeast Texas. Although WRF-ARW and MM5 simulated similar ensemble mean LNDs for each case, mean echo coverages simulated by WRF-ARW were much closer to observations than in MM5, whose simulations typically produced excessive convective and non-precipitating anvil and deficient stratiform area relative to observations. The stratiform and anvil area deviations in MM5 were primarily caused by the Reisner-2 MP's excessive rain evaporation rates (due to specifying a convective-like $N_{o,r}$) and overproduction of snow mass aloft relative to the Goddard single-moment (used in MM5 and WRF) and Morrison double-moment (used in WRF) MPs. Analysis of ten case studies in WRF-ARW supports the following conclusions:

- Observed and modeled mean divergence profiles are most elevated for the warm season cases, whereas the warm frontal and strongly baroclinic cases with the smallest amount of deep convection generate the least elevated divergence

structures with the smallest ensemble spread. Therefore, mean LNDs generally decrease as the degree of baroclinicity and/or stratiform area fractions increase, in agreement with HS09.

- Divergence structures and areal echo coverage simulated by the model ensemble for mature LLTS-MCSs are similar to those observed, likely due to their shorter durations, more organized wind shears, and distinct precipitation structures relative to other cases.
- Ensemble mean divergence profiles were ~1-2 km more elevated than observed in two cold frontal MCSs and two warm season upper-level disturbances whose simulations produced excessive convective area fractions in every ensemble member. Simulations not parameterizing convection on the intermediate 9 km grid produced more elevated divergence profiles with larger magnitudes than those that used a CP associated with the explicit runs' 1) greater stratiform area fractions in each case and 2) more elevated mass divergence due to changes in convective intensity and depth for the warm season cases.
- In one warm season case whose model runs parameterized convection on D2, using a double-moment MP generated lower LNDs associated with variations in convective intensity and depth, detraining less ice to anvil and stratiform regions at midlevels relative to a single-moment MP. Similarly, mesoscale convective vortex simulations employing an ensemble-based (single-closure) CP produced the least (most) elevated heating structures closer to observed, resulting in the weakest midlevel vortices.

In addition to providing a climatology of divergence profiles and areal echo coverage for a wide variety of precipitating systems, this study also motivates future work. Only a handful of predominantly tropical studies have identified the prevalence of non-precipitating anvil and its role on tropospheric latent and radiative heating processes. Although extratropical deep convection is less "gregarious" (Mapes 1993) than in the tropics, this work suggests that extratropical MCSs also produce large amounts of anvil that may have short-term radiative and dynamical implications and longer-lived effects on the larger-scale circulation. This study also indicates that although the Morrison two-moment MP simulated convective and stratiform areas closer to those observed in several cases exhibiting distinct stratiform and convective regions, it degenerated areal coverages for precipitating systems whose convection was embedded within larger stratiform rain regions. Therefore, an observation-model comparison of several two-moment MPs investigating the relative importance of capturing N_o jumps in DSD spectra for a variety of storms would likely be beneficial. Furthermore, convective parameterizations recently implemented into WRF-ARW that utilize different closure assumptions should also be evaluated to determine which produce more accurate divergence and heating profiles for a *variety* of storms, particularly diabatically-maintained midlevel circulations like MCVs that can produce extreme rainfall.

Finally, some of the data collection and a portion of this dissertation's analysis involved 95 undergraduate participants in a research and education program (SOAP) each spring between 2006-2010. Thirteen of the students also presented advanced research projects at the AMS Annual Meeting Student Conference and TAMU Student

Research Week. Groups of 5-6 students led by a senior-level undergraduate performed several daily tasks including producing precipitation forecasts, archiving observations, and operating and analyzing data from an S-band Doppler radar (ADRAD) for precipitation events on their day. Anonymous surveys given to SOAP students at the end of each semester indicated that student confidence in performing most SOAP tasks exhibited statistically significant positive correlations with their interest and (to a lesser degree) experience in doing them. In addition, students participating in SOAP for multiple years were significantly more confident in performing program tasks than rookie participants (increasing 19% on average) and were more likely to obtain science or meteorology-related employment upon graduation (97% vs. 63%). Students were also more likely to consider research careers and matriculate to graduate programs the longer they participated in SOAP, suggesting research and education programs have a strong influence on student's career outcomes in addition to fostering positive self-efficacy.

REFERENCES

Arakawa, A., and W. H. Schubert, 1974: Interaction of a cumulus cloud ensemble with the large scale environment. Part I. *J. Atmos. Sci.*, **31,** 674-701.

Bandura, A. (Ed.), 1995: *Self-efficacy in Changing Societies*. Cambridge University Press, 334 pp.

Bartels, D. L., and R. A. Maddox, 1991: Midlevel cyclonic vortices generated by mesoscale convective systems. *Mon. Wea. Rev.*, **119,** 104-118.

Bauer, K. W., and J. A. Bennett, 2003: Alumni perceptions used to assess undergraduate research experience. *J. of Higher Educ.*, **74(2),** 210-230.

Berkes, E, 2007: Practicing biology: Undergraduate laboratory research, persistence in science, and the impact of self-efficacy beliefs. Ph.D. Dissertation, Washington University, 244 pp.

Biggerstaff, M. I., and S. A. Listemaa, 2000: An improved scheme for convective/ stratiform echo classification using radar reflectivity. *J. Appl. Meteor.*, **39,** 2129-2150.

Blackadar, A. K., 1979: High resolution models of the planetary boundary layer. In *Advances in Environmental Science and Engineering,* J. Pfafflin and E. Ziegler, Eds., Vol. 1, Gordon and Breach, 50-85.

Bosart, L. F., 1986: Kinematic vertical motion and relative vorticity profiles in a long-lived convective system. *J. Atmos. Sci.,* **43,** 1297-1300.

Brown, J. M., 1979: Mesoscale unsaturated downdrafts driven by rainfall evaporation: A numerical study. *J. Atmos. Sci.*, **36,** 313-338.

Browning, K. A., and R. Wexler, 1968: The determination of kinematic properties of a wind field using Doppler radar. *J. Appl. Meteor.,* **7,** 105-113.

Bryan, G. H., J. C. Wyngaard, and J. M. Fritsch, 2003: Resolution requirements for the simulation of deep moist convection. *Mon. Wea. Rev.*, **131,** 2394-2416.

Chang, E. M., S. Lee, and K. L. Swanson, 2002: Storm track dynamics. *J. Climate,* **15,** 2163-2183.

Charlevoix, D. J., 2008: Improving teaching and learning through classroom research. *Bull. Amer. Meteor. Soc.*, **89,** 1660-1664.

Corfidi, S. F., J. H. Merritt, and J. M. Fritsch, 1996: Predicting the movement of mesoscale convective complexes. *Wea. Forecasting*, **11,** 41-46.

Davis, C. A., and S. B. Trier, 2002: Cloud-resolving simulations of mesoscale vortex intensification and its effect on a serial mesoscale convective system. *Mon. Wea. Rev.*, **130,** 2839-2858.

Davis, C. A., and S. B. Trier, 2007: Mesoscale convective vortices observed during BAMEX. Part I: Kinematic and thermodynamic structure. *Mon. Wea. Rev.*, **135,** 2029-2049.

Done, J., C. A. Davis, and M. Weisman, 2004: The next generation of NWP: Explicit forecasts of convection using the Weather Research and Forecasting (WRF) Model. *Atmos. Sci. Lett.*, **5,** 110-117.

Eichler, T., and W. Higgins, 2006: Climatology and ENSO-related variability of North American extratropical cyclone activity. *J. Climate,* **19,** 2076-2093.

Frederick, K., and C. Schumacher, 2008: Anvil characteristics as seen by C-POL during the Tropical Warm Pool International Cloud Experiment (TWP-ICE). *Mon. Wea. Rev.*, **136,** 206-222.

Fritsch, J. M., and C. F. Chappell, 1980: Numerical prediction of convectively driven mesoscale pressure systems. Part I: Convective parameterization. *J. Atmos. Sci.*, **37,** 1722-1733.

Fritsch, J. M., and G. S. Forbes, 2001: Mesoscale convective systems. *Severe Convective Storms, Meteor. Monogr.,* No. 9, Amer. Meteor. Soc., 323-357.

Gamache, J. F., and R. A. Houze, Jr., 1982: Mesoscale air motions associated with a tropical squall line. *Mon. Wea. Rev.*, **110,** 118-135.

George, D., and P. Mallery, 2003: SPSS for Windows step by step: A simple guide and Reference. 11.0 update (4th ed.). Allyn & Bacon, 400 pp.

Gershunov, A., and T. P. Barnett, 1998: ENSO influence on intraseasonal extreme rainfall and temperature frequencies in the contiguous United States: Observations and model results. *J. Climate*, **11,** 1575-1586.

Gonzales-Espada, W. J., and D. S. LaDue, 2006: Evaluation of the impact of the NWC REU program compared with other undergraduate research experiences. *J. Geosci. Educ.*, **54,** 541-549.

Grell, G. A., 1993: Prognostic evaluation of assumptions used by cumulus parameterizations. *Mon. Wea. Rev.*, **121,** 764-787.

Grell, G. A., and D. Devenyi, 2002: A generalized approach to parameterizing convection combining ensemble and data assimilation techniques. *Geophys. Res. Lett.*, **29(14),** 1693, doi:10.1029/2002GL015311.

Halstead, J. A., 1997: Council on Undergraduate Research: A resource (and a community) for science educators. *J. Chemical Education*, **74,** 148-149.

Hartmann, D. L., H. H. Hendon, and R. A. Houze, Jr., 1984: Some implications of the mesoscale circulations in tropical cloud clusters for large-scale dynamics and climate. *J. Atmos. Sci.*, **41,** 113-121.

Hershfield, D. M., 1961: Rainfall frequency atlas of the United States for durations from 30 minutes to 24 hours and return periods from 10 to 100 years. U.S. Weather Bureau Tech. Paper 40, 61 pp.

Hopper, L. J., Jr., and C. Schumacher, 2009: Baroclinicity influences on storm divergence and stratiform rain: Subtropical upper-level disturbances. *Mon. Wea. Rev.,* **137,** 1338-1357.

Houze, R. A., Jr., 1982: Cloud clusters and large-scale vertical motions in the tropics. *J. Meteor. Soc. Japan,* **60,** 396-410.

Houze, R. A., Jr., 1989: Observed structure of mesoscale convective systems and implications for large-scale heating. *Quart. J. Roy. Meteor. Soc.*, **115,** 425-461.

Houze, R. A., Jr., 1997: Stratiform precipitation in regions of convection: A meteorological paradox? *Bull. Amer. Meteor. Soc.*, **78,** 2179-2196.

Houze, R. A., Jr., S. Brodzik, C. Schumacher, S. E. Yuter, and C. R. Williams, 2004: Uncertainties in oceanic radar rain maps at Kwajalein and implications for satellite validation. *J. Appl. Meteor.*, **43,** 1114-1132.

Iguchi, T., T. Kozu, R. Meneghini, J. Awaka, and K. Okamoto, 2000: Rain-profiling algorithm for the TRMM precipitation radar. *J. Appl. Meteor.,* **39,** 2038-2052.

Jakob, C., R. Pincus, C. Hannay, and K-M. Xu, 2004: Use of cloud radar observations for model evaluation: A probabilistic approach. *J. Geophys. Res.*, **109,** D03202, doi: 10.1029/2003JD003473.

Joss, J., and A. Waldvogel, 1967: Ein Spektograph für Niederschlagstopfen mit automatischer Auswertung. *Pure Appl. Geophys.*, **68,** 240-246.

Joss, J., and A. Waldvogel, 1969: Raindrop size distribution and sampling size errors. *J. Atmos. Sci.*, **26,** 566-569.

Kain, J. S., and J. M. Fritsch, 1990: A one-dimensional entraining/detraining plume model and its application in convective parameterization. *J. Atmos. Sci.*, **47,** 2784-2802.

Kain, J. S., 2004: The Kain-Fritsch convective parameterization: An update. *J. Appl. Meteor.*, **43,** 170-181.

Knox, J., 2008: Recent and future trends in U. S. undergraduate meteorology enrollments, degree recipients, and employment opportunities. *Bull. Amer. Meteor. Soc.*, **89,** 873-883.

Krishnamurti, T. N., S. Low-Nam, and R. J. Pasch, 1983: Cumulus parameterization and rainfall rates II. *Mon. Wea. Rev.*, **111,** 815-828.

Lang, S., W.-K. Tao, J. Simpson, and B. Ferrier, 2003: Modeling of convective-stratiform precipitation processes: Sensitivity to partitioning methods. *J. Appl. Meteor.*, **42,** 505-527.

Lang, S., W.-K. Tao, R. Cifelli, W. Olson, J. Halverson, S. Rutledge, and J. Simpson, 2007: Improving simulations of convective systems from TRMM LBA: Easterly and westerly regimes. *J. Atmos. Sci.*, **64,** 1141-1164.

Lent, R. W., S. D. Brown, and G. Hackett, 1994: Toward a unifying social cognitive theory of career and academic interest, choice, and performance. *J. Vocational Behavior*, **45,** 79-122.

Lenth, R. V., 1989: Quick and easy analysis of unreplicated factorials. *Technometrics*, **31,** 469-473.

Libarkin, J. C., and J. P. Kurdziel, 2001: Research methodologies in science education: Strategies for productive assessment. *J. Geosci. Educ.*, **49,** 300-304

Likert, R., 1931: A technique for the measurement of attitudes. *Archives of Psychology*. Columbia University Press, 55 pp.

Luo, Y., Y. Wang, H. Wang, Y. Zheng, and H. Morrison, 2010: Modeling convective-stratiform precipitation processes on a Mei-Yu front with the Weather Research and Forecasting model: Comparison with observations and sensitivity to cloud microphysics parameterizations. *J. Geophys. Res.*, **115,** D18117, doi: 10.1029/2010JD013873.

Maddox, R. A. , D. J. Perkey, and J. M. Fritsch, 1981: Evolution of upper tropospheric features during the development of a mesoscale convective complex. *J. Atmos. Sci.*, **39,** 1664-1674.

Mapes, B. E., 1993: Gregarious tropical convection. *J. Atmos. Sci.*, **50,** 2026-2037.

Mapes, B. E., and R. A. Houze, Jr., 1995: Diabatic divergence profiles in western Pacific mesoscale convective systems. *J. Atmos. Sci.,* **52,** 1807-1828.

Mapes, B. E., and J. Lin, 2005: Doppler radar observations of mesoscale wind divergence in regions of tropical convection. *Mon. Wea. Rev.,* **133,** 1808-1824.

Marshall, J. S., and W. McK. Palmer, 1948: The distribution of raindrops with size. *J. Meteor.*, **5,** 165-166.

Matejka, T. J., R. A. Houze, Jr., and P. V. Hobbs, 1980: Microphysics and dynamics of clouds associated with mesoscale rainbands in extratropical cyclones. *Quart. J. Roy. Meteor. Soc.*, **106,** 29-56.

May, P. T., and T. P. Lane, 2009: A method for using weather radar to test cloud resolving models. *Meteor. Appl.*, **16,** 425-432.

McFarquhar, G. M., and R. List, 1993: The effect of curve fits for the disdrometer calibration on raindrop spectra, rainfall rate, and radar reflectivity. *J. Appl. Meteor.*, **32,** 774-782.

Morrison, H., G. Thompson, and V. Tatarskii, 2009: Impact of cloud microphysics on the development of trailing stratiform precipitation in a simulated squall line: Comparison of one- and two-moment schemes. *Mon. Wea. Rev.*, **137,** 991-1007.

Myers, J. L, A. D. Wolf, and R. F. Lorch, 2010: *Research Design and Statistical Analysis*. Routledge, 809 pp.

Ninomiya, K., 1971a: Dynamical analysis of outflow from tornadic-producing thunderstorms as revealed by ATS III pictures. *J. Appl. Meteor.*, **10,** 275-294.

Ninomiya, K., 1971b: Mesoscale modifications of synoptic situations from thunderstorms development as revealed by ATS III and aerological data. *J. Appl. Meteor.*, **10,** 1103-1121.

Norman, G., 2010: Likert scales, levels of measurement, and the “laws” of statistics. *Advances In Health Sci. Education*, **15,** doi: 10.1007/s10459-010-9222-y.

Parker, M. D., and R. H. Johnson, 2000: Organizational modes of midlatitude mesoscale convective systems. *Mon. Wea. Rev.*, **128,** 3413-3436.

Reisner, J., R. Rasmussen, and R. T. Bruintjes, 1998: Explicit forecasting of supercooled liquid water in winter storms using the MM5 mesoscale model. *Quart. J. Roy. Meteor. Soc.*, **124,** 1071-1107.

Ropelewski, C. F., and M. S. Halpert, 1996: Quantifying Southern Oscillation-precipitation relationships. *J. Climate*, **9,** 1043-1059.

Russell, S. H., 2006: Evaluation of NSF support for undergraduate research opportunities (URO): Synthesis report. SRI International, 29 pp. [Available online at http://www.sri. com/policy/csted/reports].

Rutledge, S. A., and R. A. Houze, Jr., 1987: A diagnostic modeling study of the trailing stratiform region of a midlatitude squall line. *J. Atmos. Sci.*, **44,** 2640-2656.

Sadler, T. D., and L. McKinney, 2010: Scientific research for undergraduate students: A review of the literature. *J. College Science Teaching*, **39**(5), 68-74.

Sanders, F., 2005: Real front or baroclinic trough? *Wea. Forecasting*, **20,** 647-651.

Schaefer, J. T., 1974: The life cycle of the dryline. *J. Appl. Meteor.*, **13,** 444-449.

Schultz, D. M., 2004: Cold fronts with and without prefrontal wind shifts in the central United States. *Mon. Wea. Rev.*, **132,** 2040-2053.

Schumacher, C., and R. A. Houze Jr., 2000: Comparison of radar data from the TRMM satellite and Kwajalein oceanic validation site. *J. Appl. Meteor.,* **39,** 2151-2164.

Schumacher, C., and R. A. Houze Jr., 2003: Stratiform rain in the tropics as seen by the TRMM precipitation radar. *J. Climate,* **16,** 1739-1756.

Schumacher, C., and R. A. Houze, Jr., 2006: Stratiform precipitation production over sub-Saharan Africa and the tropical East Atlantic as observed by TRMM. *Quart. J. Roy. Meteor. Soc.,* **132,** 2235-2255.

Schumacher, C., R. A. Houze, Jr., and I. Kraucunas, 2004: The tropical dynamical response to latent heating estimates derived from the TRMM Precipitation Radar. *J. Atmos. Sci.,* **61,** 1341-1358.

Schumacher, R. S., and R. H. Johnson, 2005: Organization and environmental properties of extreme-rain-producing mesoscale convective systems. *Mon. Wea. Rev.*, **133,** 961-976.

Schumacher, R. S., and R. H. Johnson, 2009: Quasi-stationary, extreme-rain producing convective systems associated with midlevel cyclonic circulations. *Wea. Forecasting*, **24,** 555-575.

Silberstein, D. S., D. B. Wolff, D. A. Marks, D. Atlas, and J. L. Pippitt, 2008: Ground clutter as a monitor of radar stability at Kwajalein, RMI. *J. Atmos. Oceanic Technol.*, **25,** 2037-2045.

Skamarock, W. C., J. B. Klemp, J. Dudhia, D. O. Gill, D. M. Barker, M. G. Duda, X.-Y. Huang, W. Wang, and J. G. Powers, 2008: A description of the Advanced Research WRF version 3. NCAR/TN-475+STR, 113 pp. [Available online at http://www.mmm.ucar.edu/wrf/users/docs/arw_v3.pdf].

Steiner, M. and A. Waldvogel, 1987: Peaks in raindrop size distributions. *J. Atmos. Sci.*, **44,** 3127-3133.

Steiner, M., R. A. Houze, Jr., and S. E. Yuter, 1995: Climatological characterization of three-dimensional storm structure from operational radar and rain gauge data. *J. Appl. Meteor.,* **34,** 1978-2007.

Steiner, M., and J. A. Smith, 2000: Reflectivity, rain rate, and kinetic energy flux relationships based on raindrop spectra. *J. Appl. Meteor.*, **39,** 1923-1940.

Stensrud, D. J., 1996: Effects of persistent, midlatitude mesoscale regions of convection on the large-scale environment during the warm season. *J. Atmos. Sci.,* **53,** 3503-3527.

Stoelinga, 2005: Simulated equivalent reflectivity factor as currently formulated in RIP: Description and possible improvements. White paper, 5 pp. [Available online at http://www.atmos.washington.edu/~stoeling/].

Tao, W.-K., and J. Simpson, 1993: Goddard cumulus ensemble model. Part I: Model description. *Terr. Atmos. Oceanic Sci.,* **4,** 25-72.

Tao, W.-K., J. Simpson, and M. McCumber, 1989: An ice-water saturation adjustment. *Mon. Wea. Rev.,* **117,** 231-235.

Tao, W.-K., J. Simpson, C.-H. Sui, B. Ferrier, S. Lang, J. Scala, M.-D. Chou, and K. Pickering, 1993: Heating, moisture, and water budgets of tropical and midlatitude squall lines: Comparisons and sensitivity to longwave radiation. *J. Atmos. Sci.*, **50,** 673-690.

Thompson, G., R. M. Rasmussen, and K. Manning, 2004: Explicit forecasts of winter precipitation using an improved bulk microphysics scheme. Part I: Description and sensitivity analysis. *Mon. Wea. Rev.*, **132,** 519-542.

Tokay, A., and D. A. Short, 1996: Evidence from tropical raindrop spectra of the origin of rain from stratiform versus convective clouds. *J. Appl. Meteor.*, **35,** 355-371.

Tokay, A., D. B. Wolff, K. R. Wolff, and P. Bashor, 2003: Rain gauge and disdrometer measurements during the Keys Area Microphysics Project (KAMP). *J. Atmos. Oceanic Technol.*, **20,** 1460-1477.

Waldvogel, A., 1974: The N_o jump in raindrop spectra. *J. Atmos. Sci.,* **31,** 1067-1078.

Warner, T. T., and H.-M. Hsu, 2000: Nested-model simulation of moist convection: The impact of coarse-grid parameterized convection on fine-grid resolution convection. *Mon. Wea. Rev.*, **128,** 2211-2231.

White, M. A., M. Turner, L. Litizzette, and M. J. Taylor, 2008: University camp increases student interest in science. *Eos Trans. Amer. Geophys. Union,* **89**, 313-315. doi:10.1029/2008E0340002.

Winkler, J. A., B. R. Skeeter, and P. D. Yamamoto, 1988: Seasonal variations in the diurnal characteristics of heavy hourly precipitation across the United States. *Mon. Wea. Rev.*, **116,** 1641-1658.

WMO, 1974: Manual on codes. Vol. 1. WMO Publication 306, 348 pp.

Yanai, M., S. Esbensen, and J.-H. Chu, 1973: Determination of bulk properties of tropical cloud clusters from large-scale heat and moisture budgets. *J. Atmos. Sci.*, **30,** 611-627.

Yang, G.-Y., and J. Slingo, 2001: The diurnal cycle in the tropics. *Mon. Wea. Rev.*, **129,** 784-801.

Yang, M.-J., and R. A. Houze, Jr., 1995a: Multicell squall line structure as a manifestation of vertically trapped gravity waves. *Mon. Wea. Rev.*, **123,** 641-661.

Ye, K., and M. Hamada, 2000: Critical values of the Lenth method for unreplicated factorial designs. *J. Quality Technology*, **32,** 57-66.

Yuter, S. E., and R. A. Houze, Jr., 1997: Measurements of raindrop size distributions over the Pacific warm pool and implications for Z-R relations. *J. Appl. Meteor.*, **36,** 847-867.

Zhang, D.-L., and R. A. Anthes, 1982: A high-resolution model of the planetary boundary layer---Sensitivity tests and comparisons with SESAME-79 data. *J. Appl. Meteor.,* **21,** 1594-1609.

Zhang, D.-L., and J. M. Fritsch, 1986: Numerical simulation of the meso-β scale structure and evolution of the 1977 Johnstown flood. Part I: Model description and verification. *J. Atmos. Sci.,* **43,** 1913-1943.

Zhang, F., N. Bei, R. Rotunno, C. Snyder, and C. C. Epifanio, 2007: Mesoscale predictability of moist baroclinic waves: Convection-permitting experiments and multistage error growth dynamics. *J. Atmos. Sci.*, **64,** 3579-3594.

APPENDIX A

FIGURES

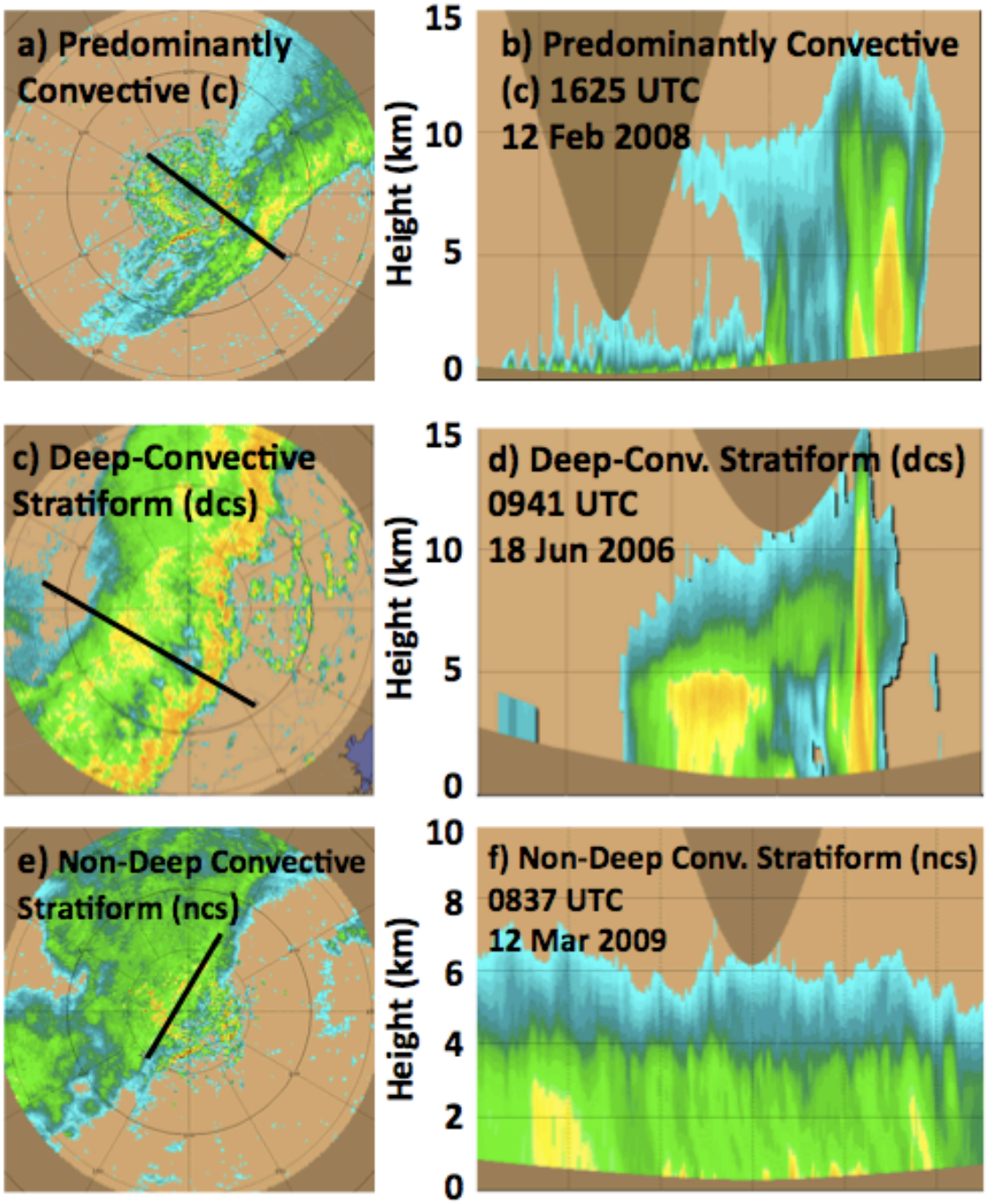

Figure A.1. Horizontal cross sections at 2 km MSL and vertical cross sections for example a) predominantly convective, b) deep-convective stratiform, and c) non-deep convective stratiform storm structures.

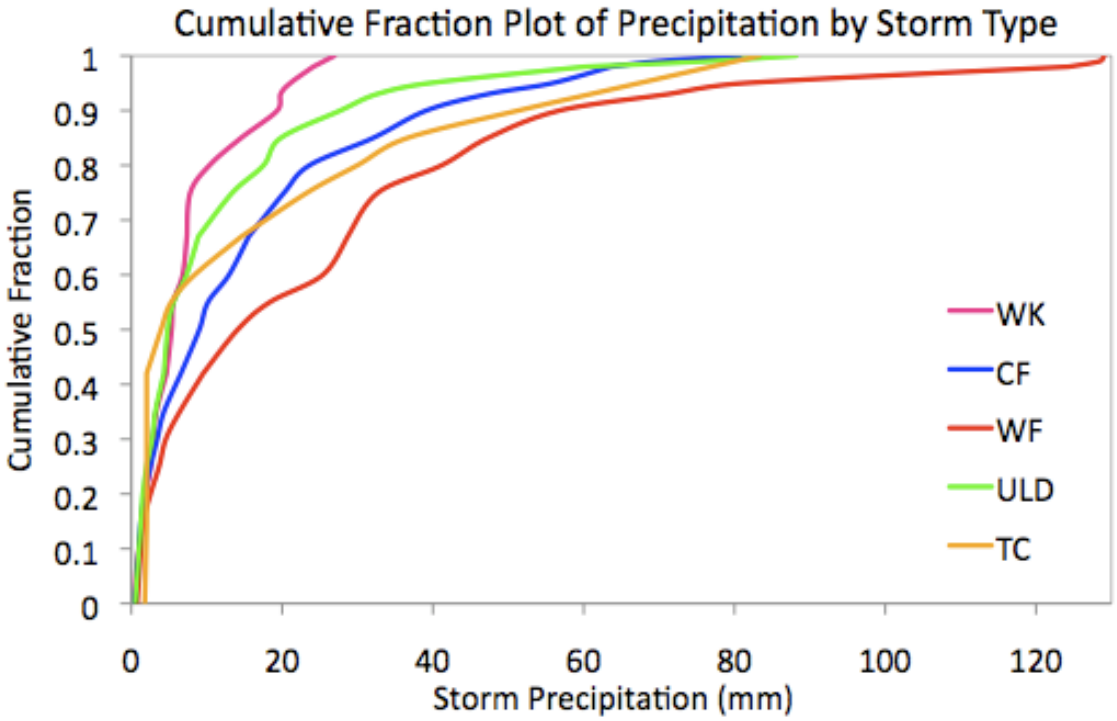

Figure A.2. Cumulative fraction plots of individual storm precipitation totals in College Station, TX for each storm type between March 2002-February 2010.

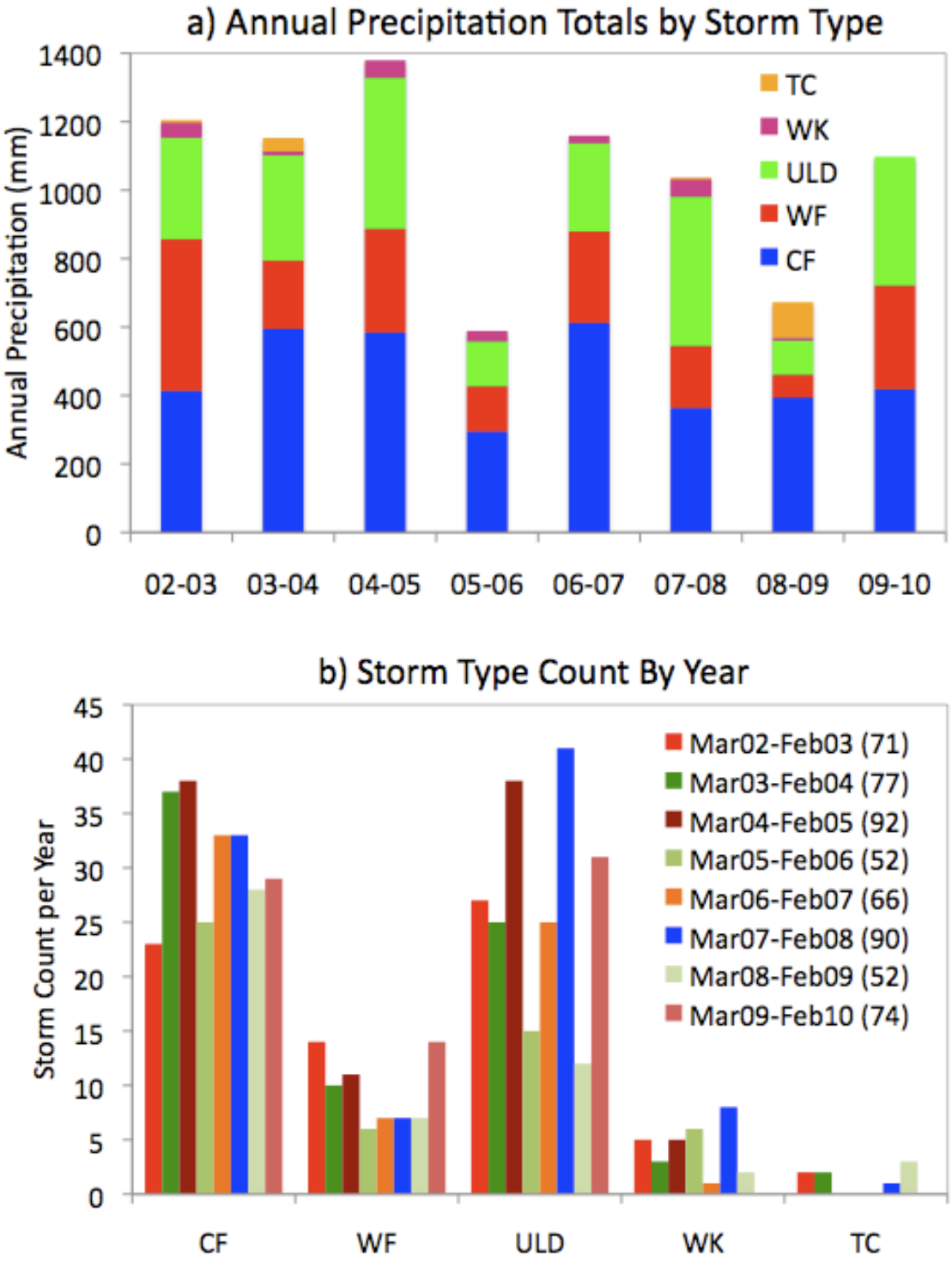

Figure A.3. Annual a) precipitation totals subdivided by storm type and b) occurrences of each storm type in College Station, TX between March 2002-February 2010.

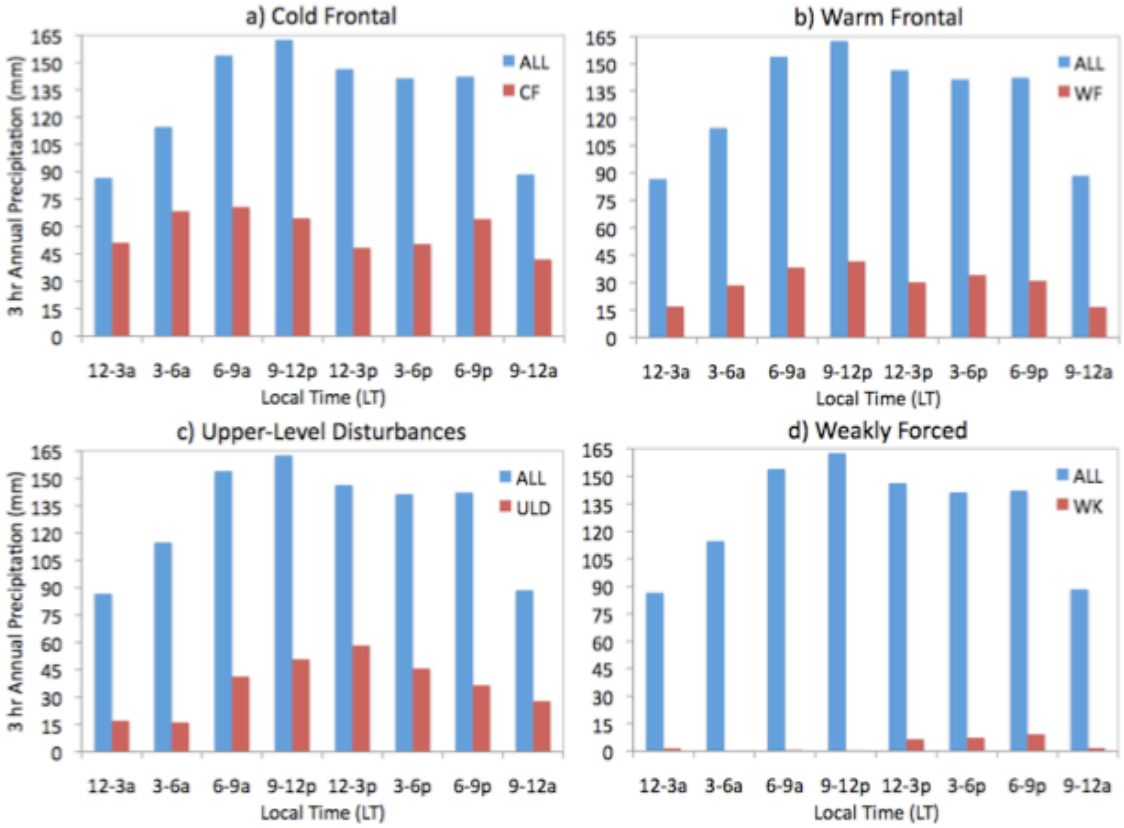

Figure A.4. Annual precipitation time series for a) cold frontal, b) warm frontal, c) upper-level disturbances, and d) weakly forced storms (all in red) relative to the annual diurnal cycle (in blue) for College Station, TX between March 2002-February 2010.

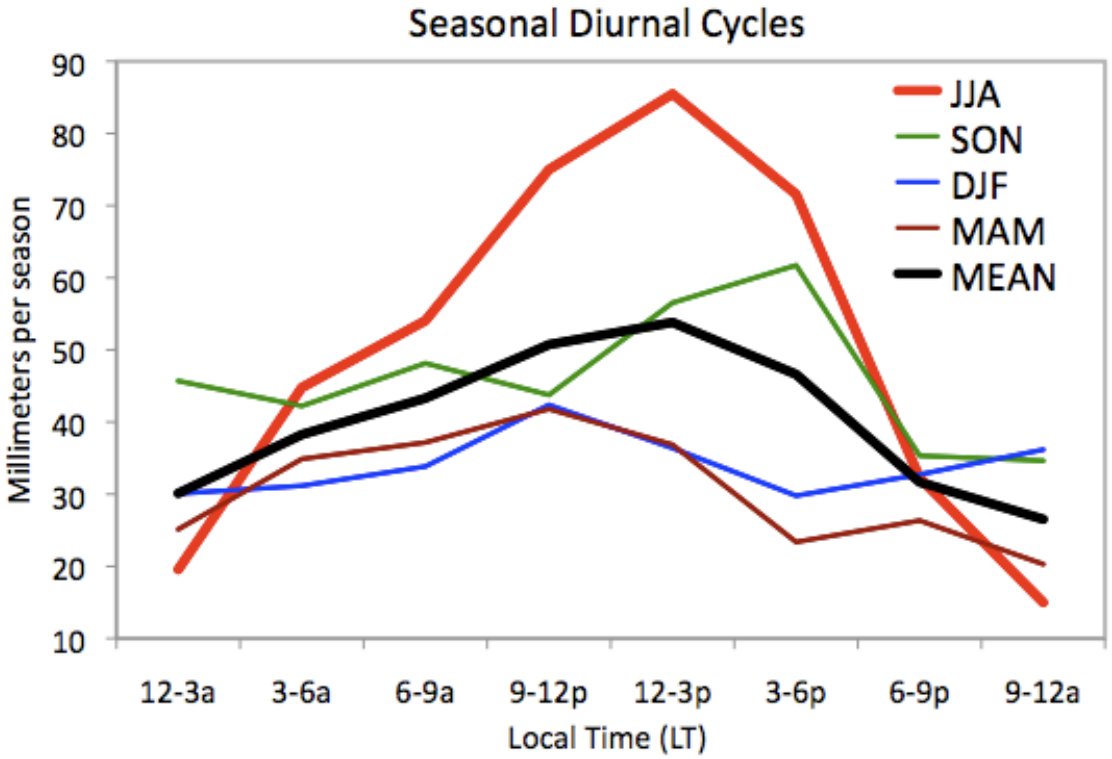

Figure A.5. Seasonal precipitation time series relative to the mean diurnal cycle (in black) for five sites (CLL, LFK, IAH, HOU, and BPT) in southeast Texas between 2002-2009.

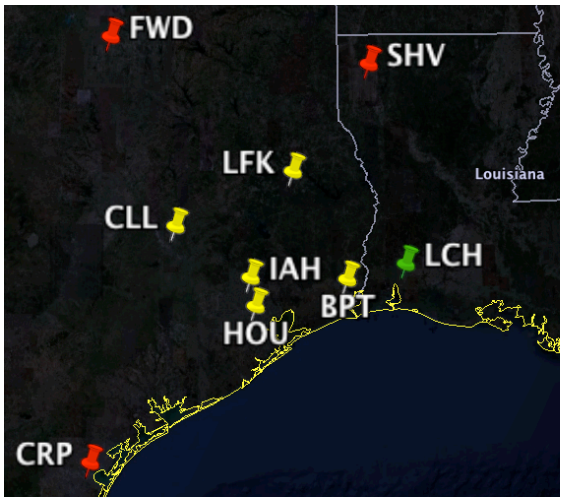

Figure A.6. National Center for Climatic Data (NCDC) Hourly Precipitation Dataset (HPD) tipping-bucket rain gauge locations (in yellow) analyzed during summer (JJA) 2002-2008 along with the location of the Lake Charles, LA sounding (in green) used for analysis instability at BPT and other local radiosonde launch locations (in red).

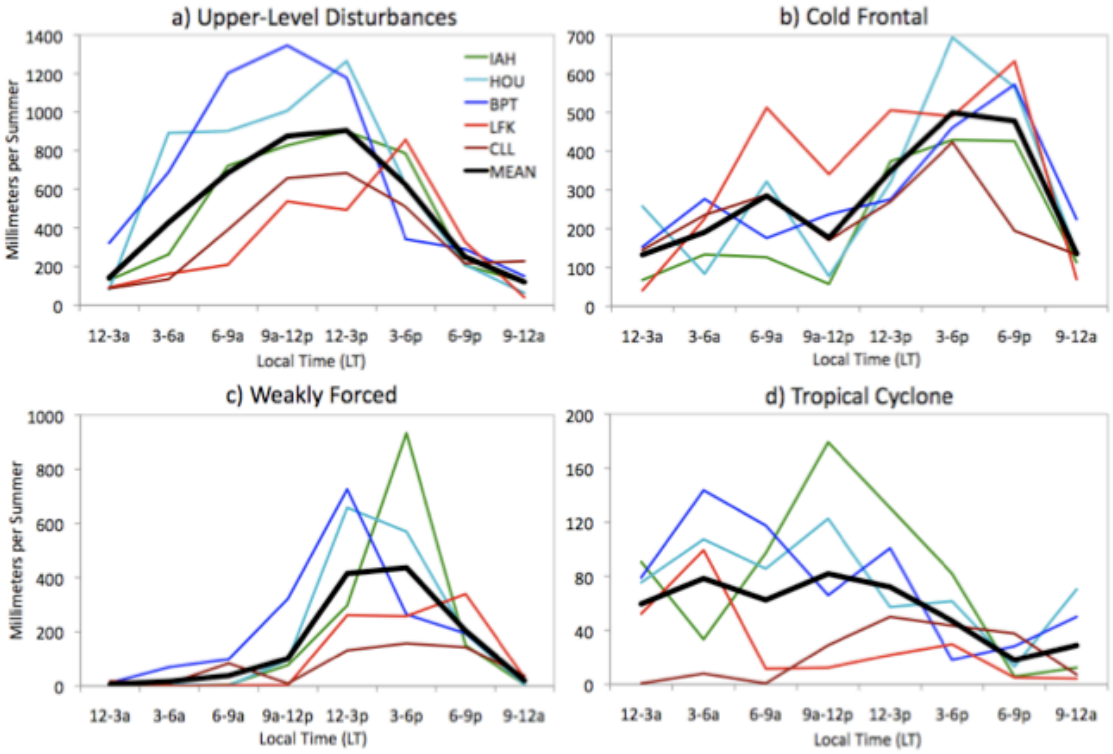

Figure A.7. Mean (solid black) summer (JJA) precipitation time series for a) upper-level disturbances, b) cold frontal storms, c) weakly forced storms, and d) tropical cyclones between 2002-2008 for five sites in southeast Texas (assorted colors).

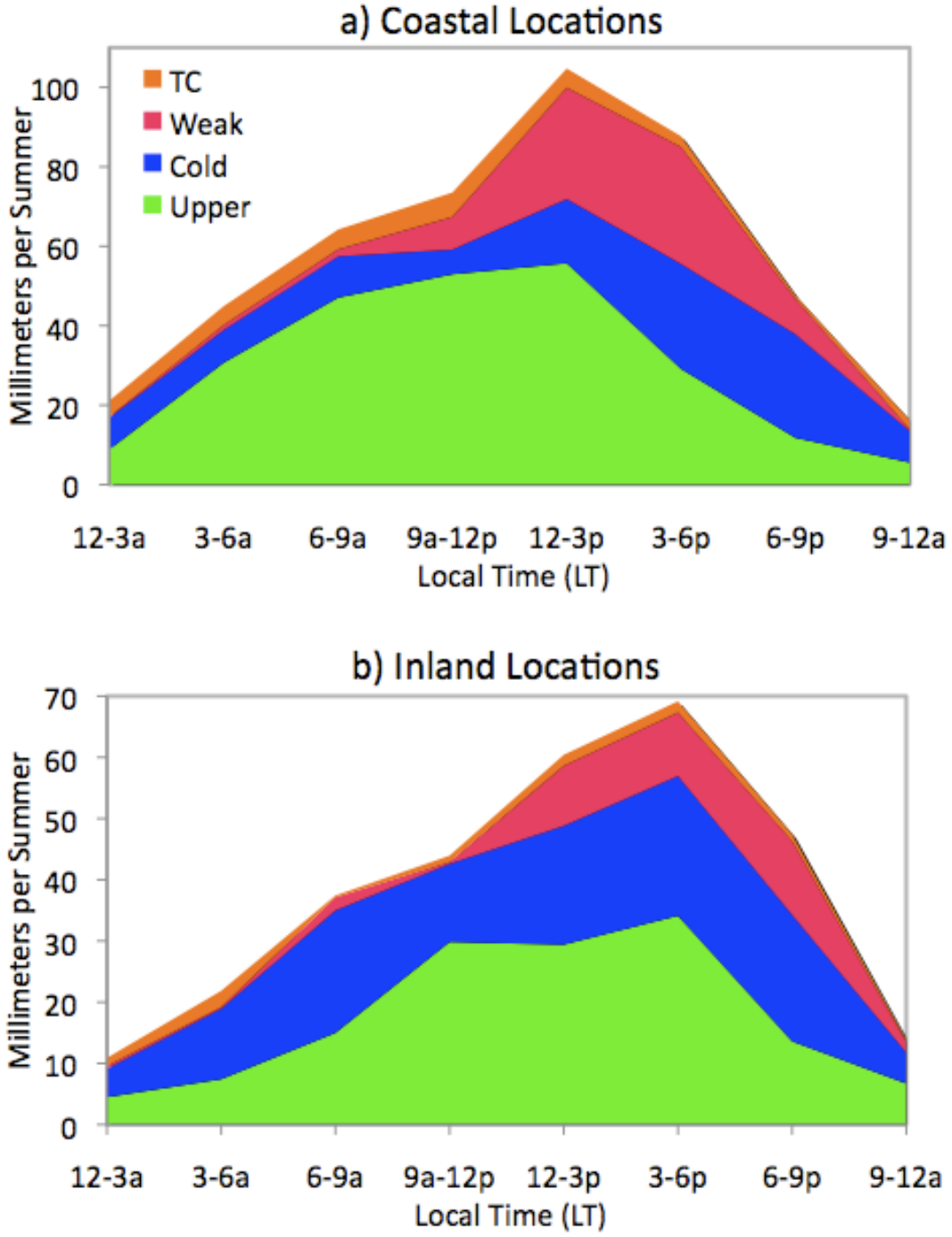

Figure A.8. Summer (JJA) precipitation time series subdivided by storm type for a) coastal locations (IAH, HOU, and BPT) and b) inland locations (CLL and LFK) between 2002-2008.

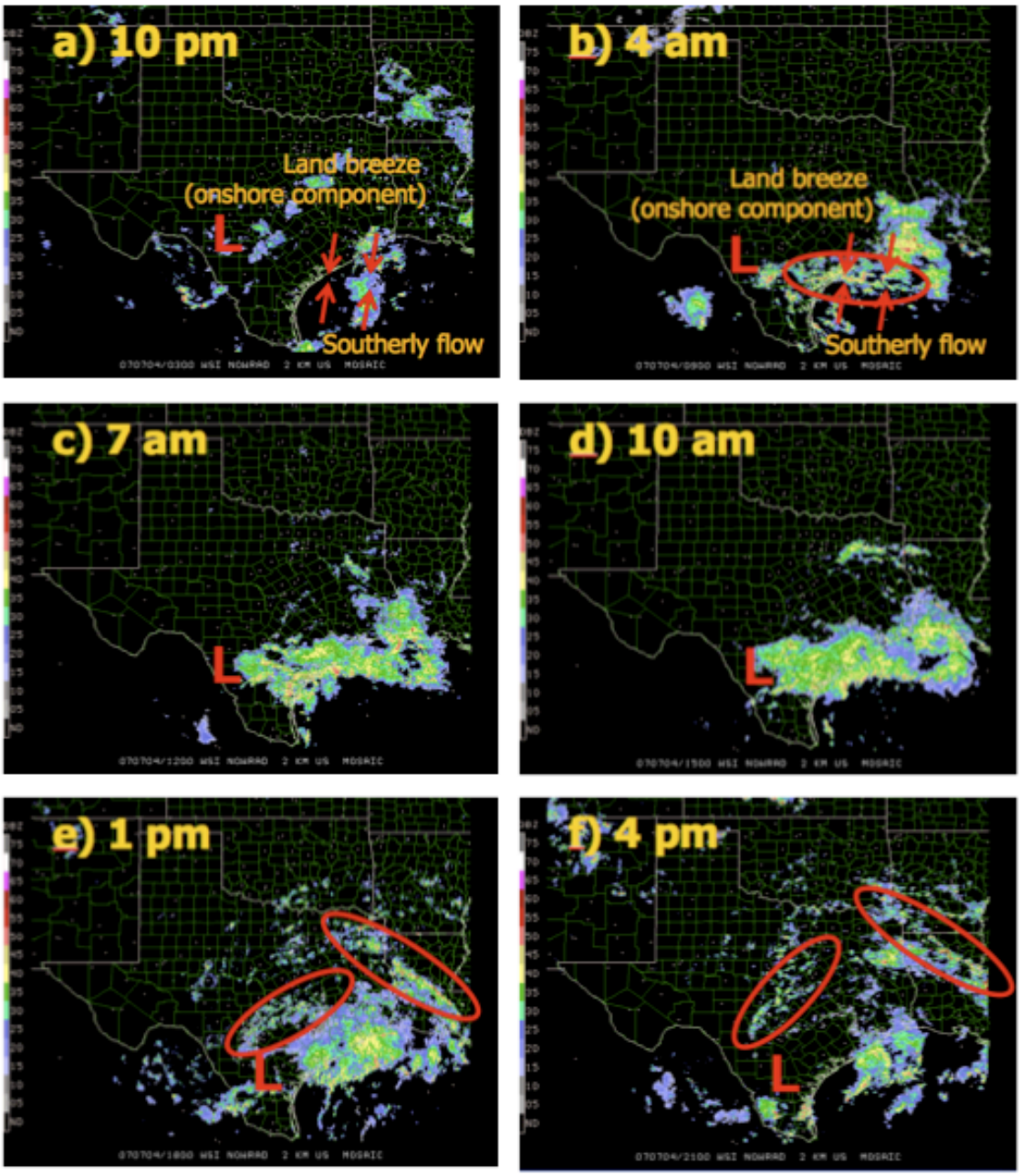

Figure A.9. Illustration of Winkler's (1988) hypothesis for the midday summertime precipitation peak in the context of upper-level disturbances located to the west of southeast Texas using a storm from 4 July 2007 (Images adapted from an online archive maintained by the Precipitation Diagnostics Group (PDG) in the Mesoscale and Microscale Meteorology Division of NCAR.)

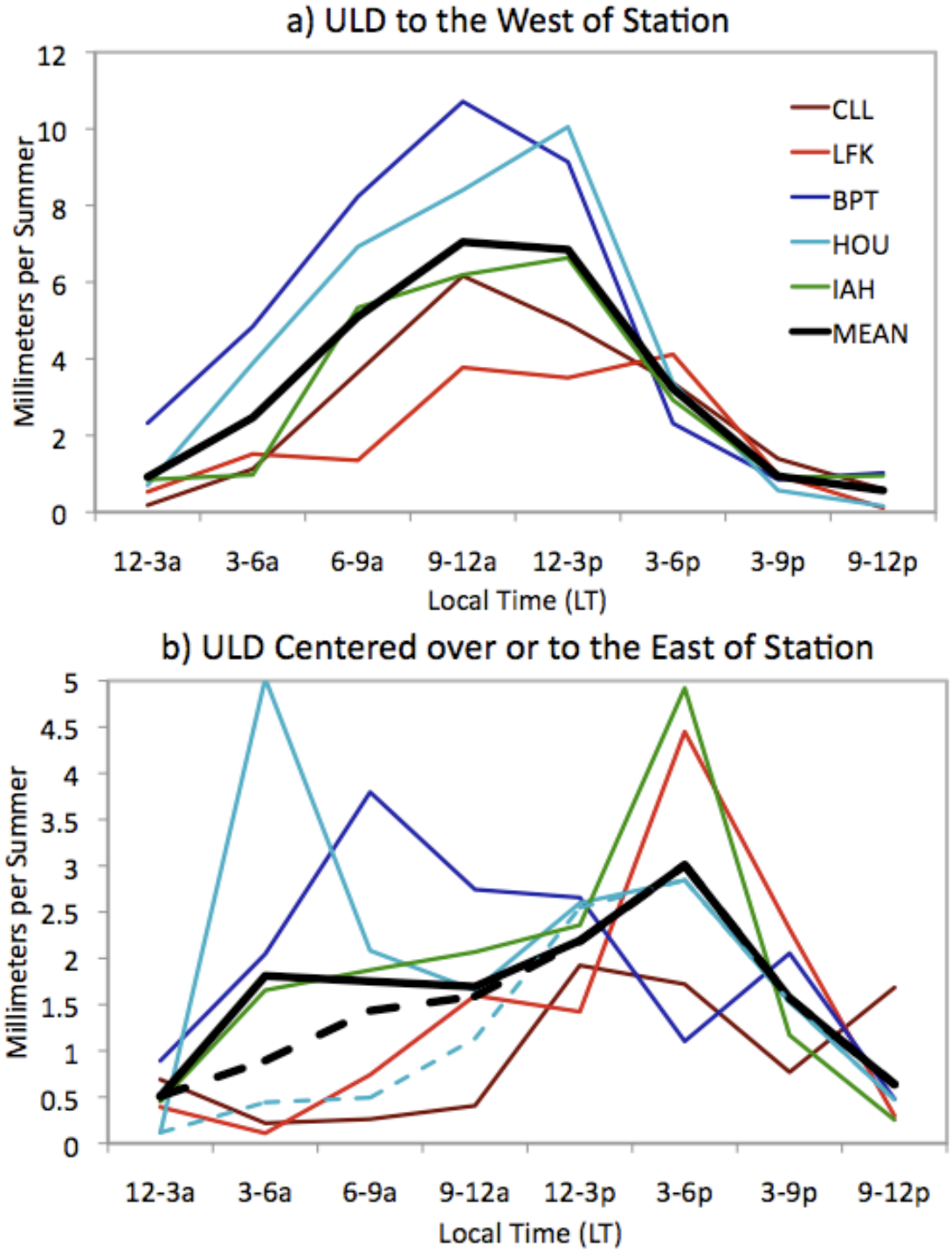

Figure A.10. Mean (solid black) summer (JJA) precipitation time series for upper-level disturbances located west of each of the five sites in southeast Texas analyzed (assorted colors) and b) centered over or east of each of the sites between 2002-2008.

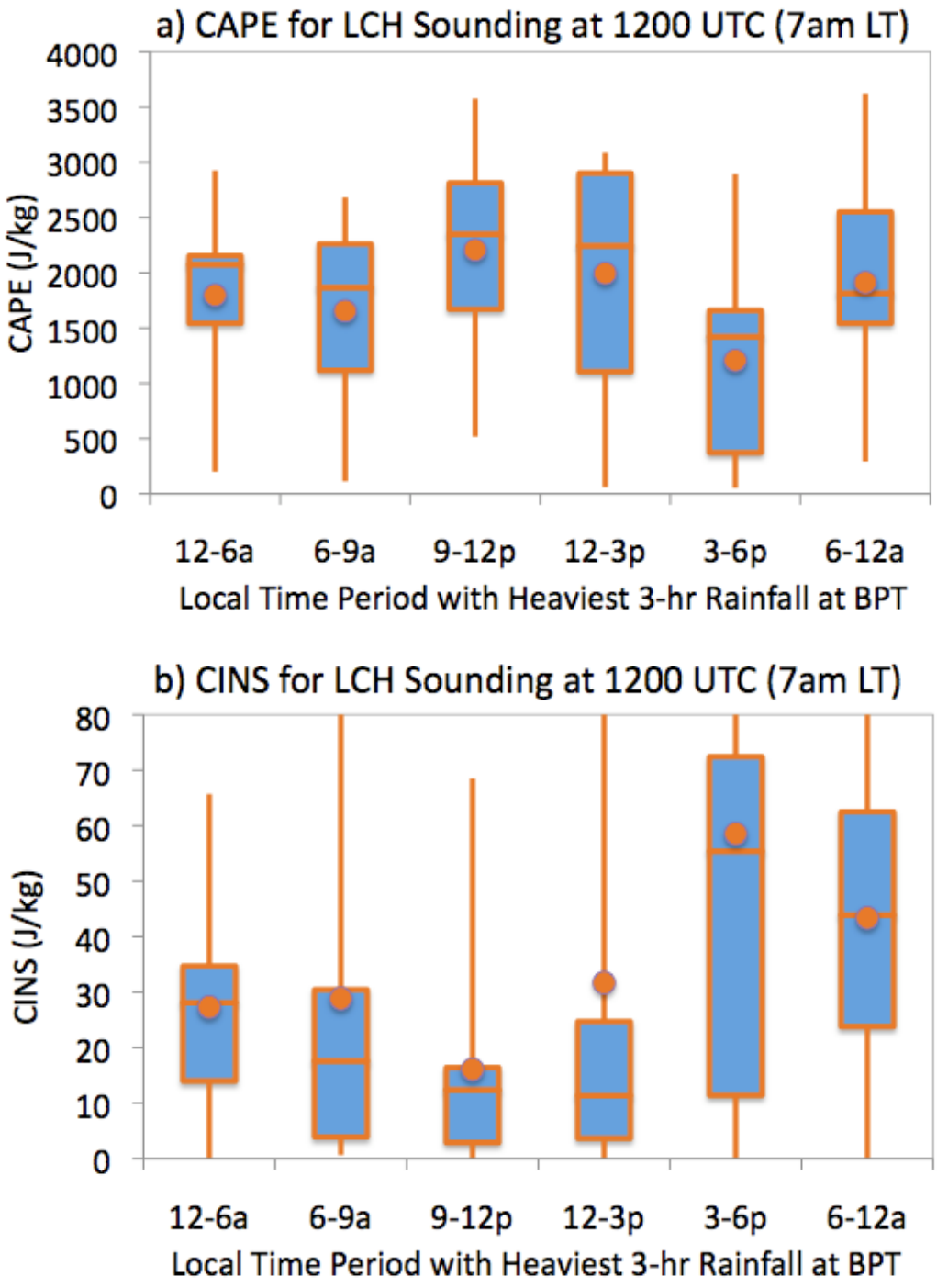

Figure A.11. Box plots and mean (orange dots) surface-based values of a) convective available potential energy and b) convective inhibition calculated from 1200 UTC Lake Charles, LA sounding observations separated by the local time period during which the heaviest 3-hr rainfall caused by upper-level disturbances in Beaumont, TX occurred. The 12-3am and 3-6am time periods along with the 6-9pm and 9-12pm time periods have been combined together due to small sample sizes (> 10 storms).

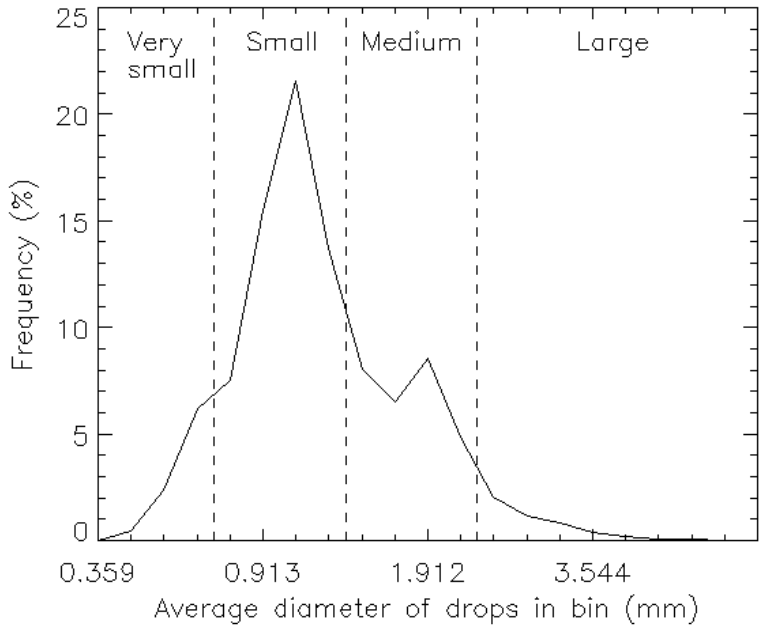

Figure A.12. Mean normalized climatological DSD observed between December 2004-September 2008 in College Station, TX. Raindrop-size modes of very small, small, medium, and large are identified on the figure.

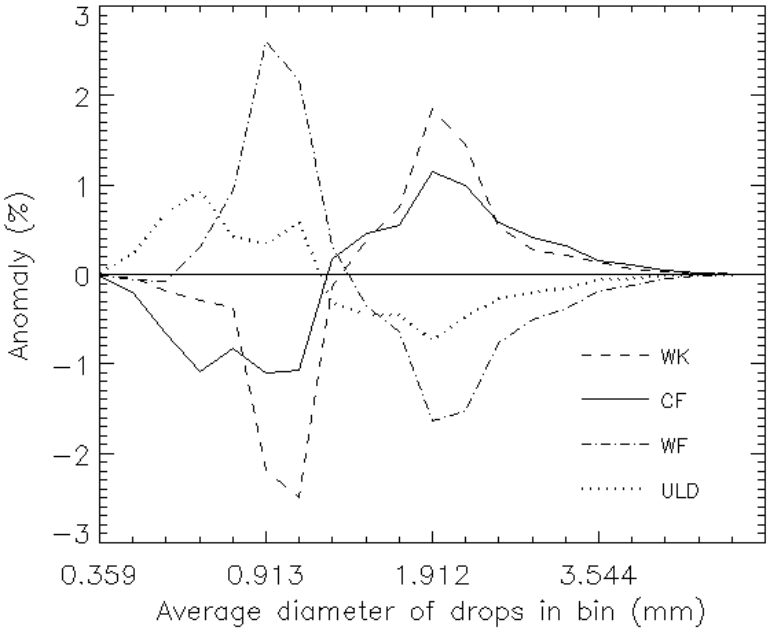

Figure A.13. Storm type DSD anomalies from the climatological DSD shown in Fig. A.12 for weakly forced (WK), cold frontal (CF), warm frontal (WF), and upper-level disturbance (ULD) storm types.

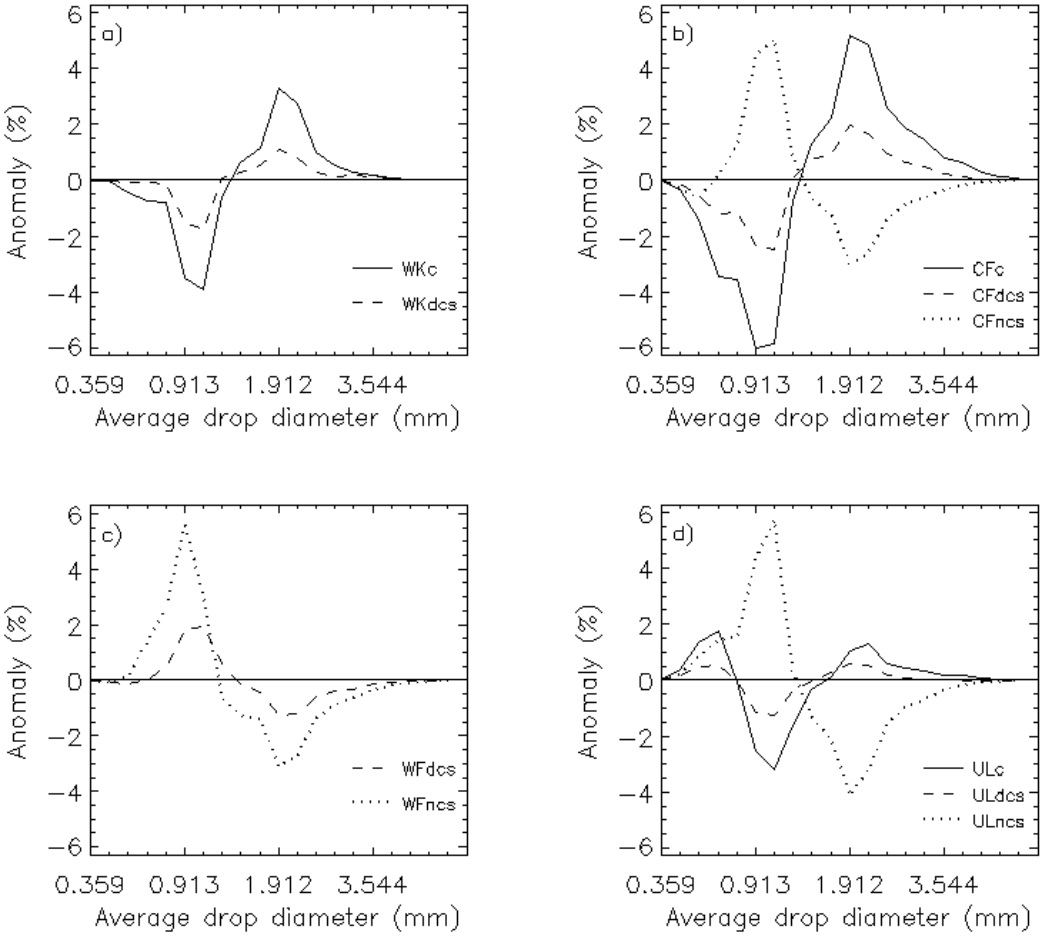

Figure A.14. Climatological DSD anomalies for predominantly convective (c; solid black), deep-convective stratiform (dcs; dashed black), and non-convective stratiform (ncs; dotted black) storm structures for a) weakly forced, b) cold frontal, c) warm frontal, d) and upper-level disturbance storm types from December 2004-September 2008.

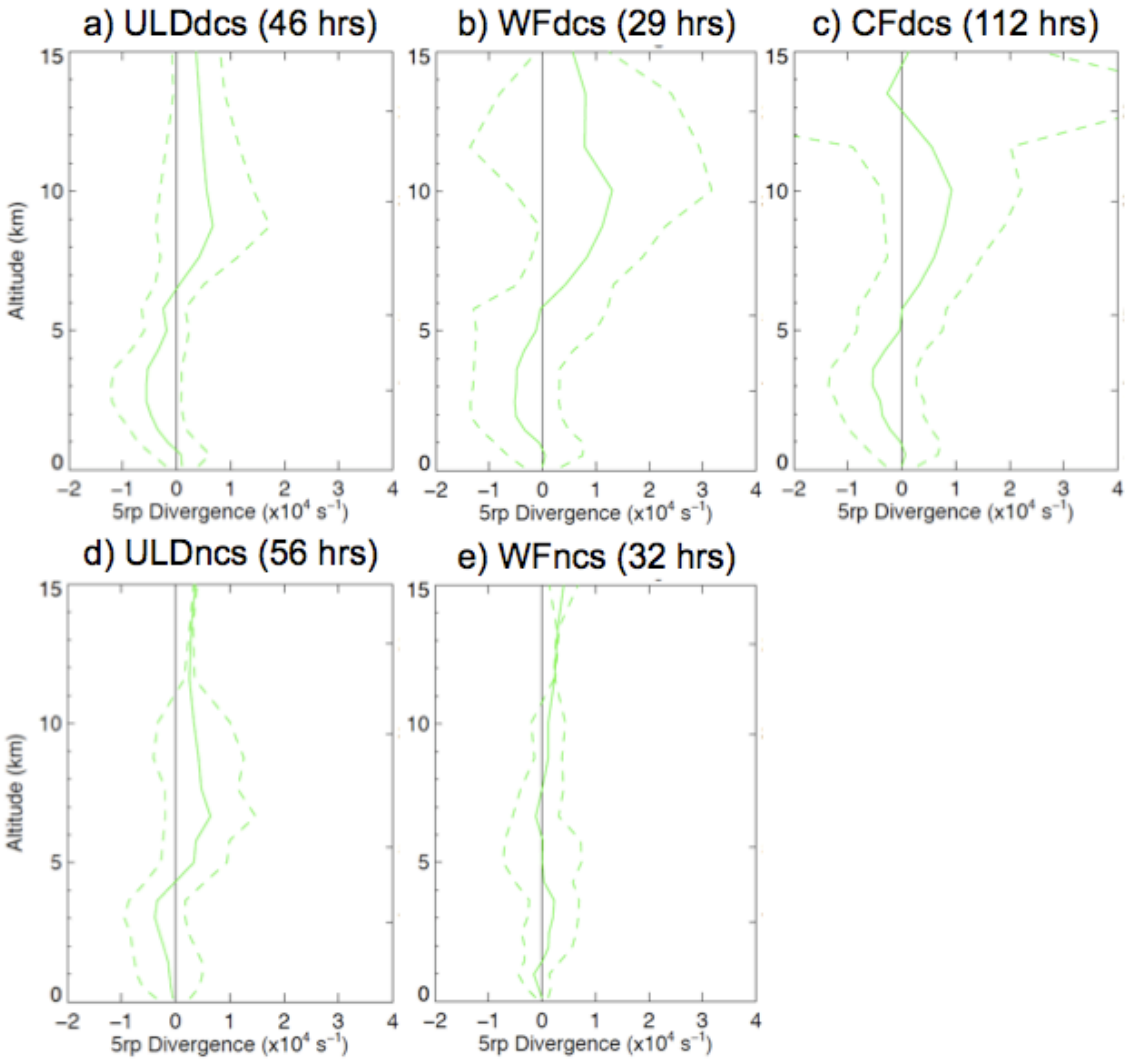

Figure A.15. Climatological VAD divergence profiles for deep-convective stratiform storm structures caused by a) upper-level disturbances, b) warm fronts, and c) cold frontal storms and non-convective stratiform storm structures caused by d) upper-level disturbances and e) warm fronts observed by ADRAD between June 2006-July 2010. Mean divergence profiles (solid green) and their standard deviations (dotted green) plotted for each storm type reflect five-range pooled data between 16-56 km centered about the 36 km annulus (Unpublished figure courtesy C. Homeyer).

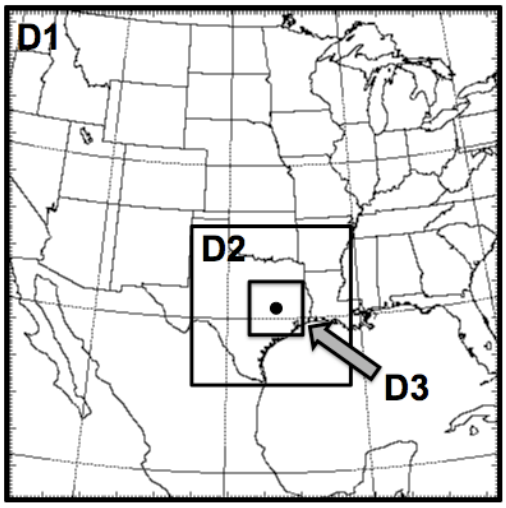

Figure A.16. The WRF-ARW model domains. The grid spacing of the outermost coarse domain (D1), intermediate domain (D2), and innermost analysis domain (D3) are 27, 9, and 3 km, respectively. ADRAD's position is indicated by the dot near the center of D3 (30.62^{o}N, 96.34^{o}W).

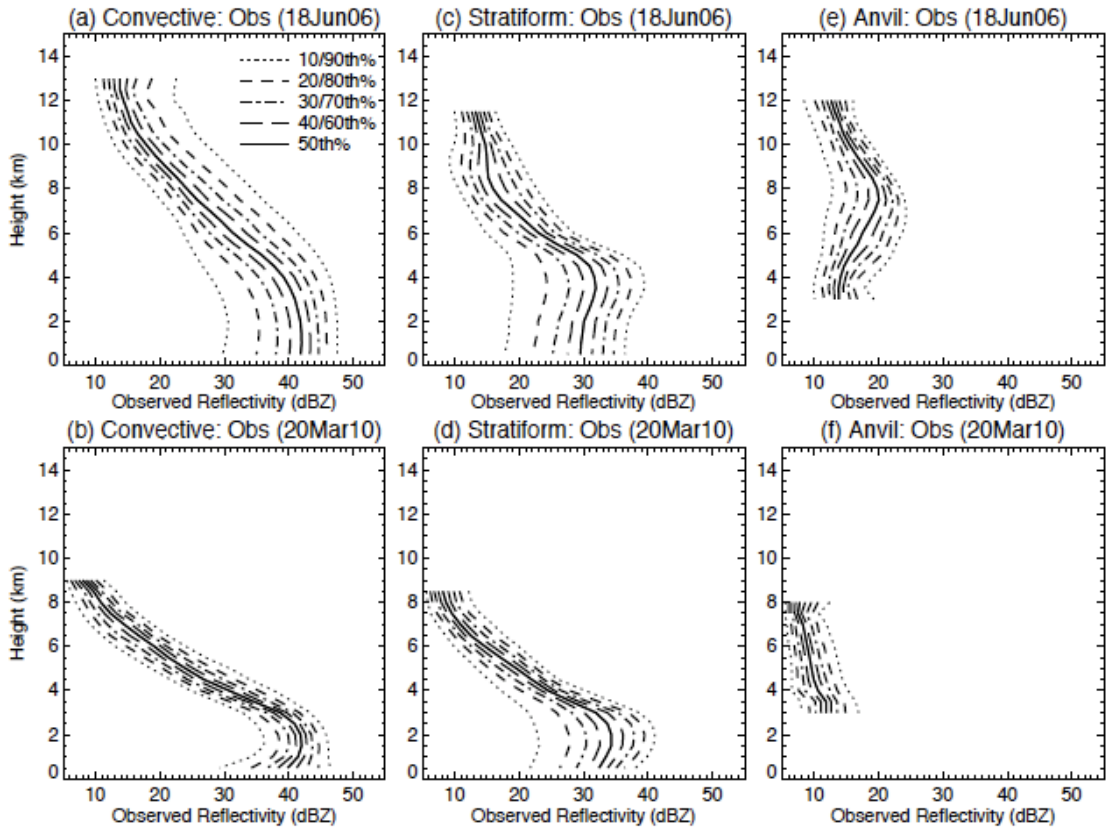

Figure A.17. Vertical distribution of radar reflectivity observed by ADRAD during the analysis times given in Table B.6 within (a),(b) convective, (c),(d) stratiform, (e),(f) and non-precipitating anvil regions for the (top panels) 18 Jun 2006 warm season and (bottom panels) 20 March 2010 strongly baroclinic LLTS-MCSs. Each line represents a 10% quantile from 10% to 90% with the median profile in solid black. Altitudes with less than 0.5% of the total count are not plotted.

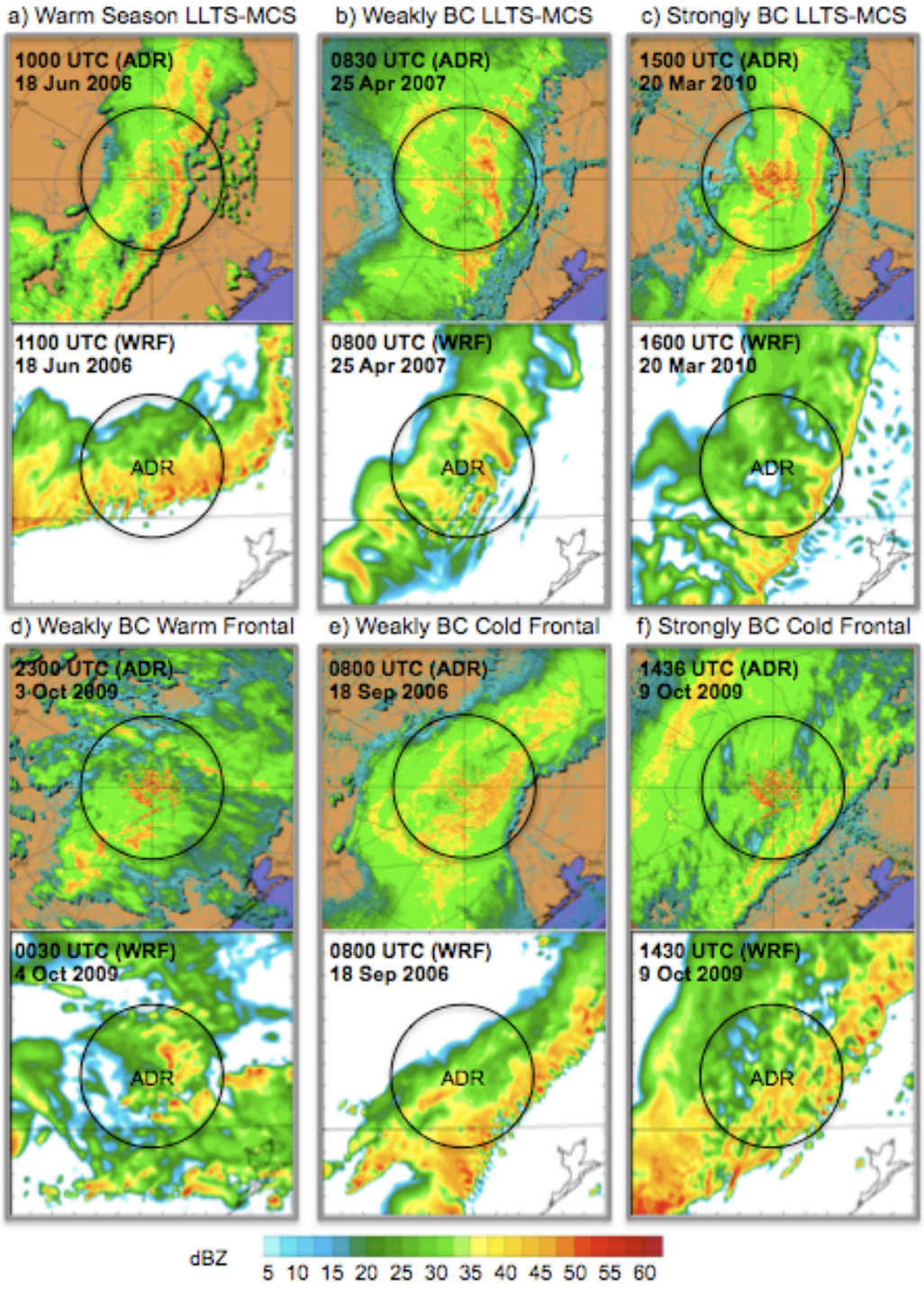

Figure A.18. Observed 0.5° or 1.0° surveillance scans from ADRAD (ADR; top panels) and simulated 2 km MSL horizontal cross sections (WRF; bottom panels) at similar points in the KFexpGod ensemble member (denoted in Table B.5) of each case presented in this study. The circles on each image denote the 96 km radius of the radar domain and 3 km WRF-ARW grid (D3) included in the analyses for each case.

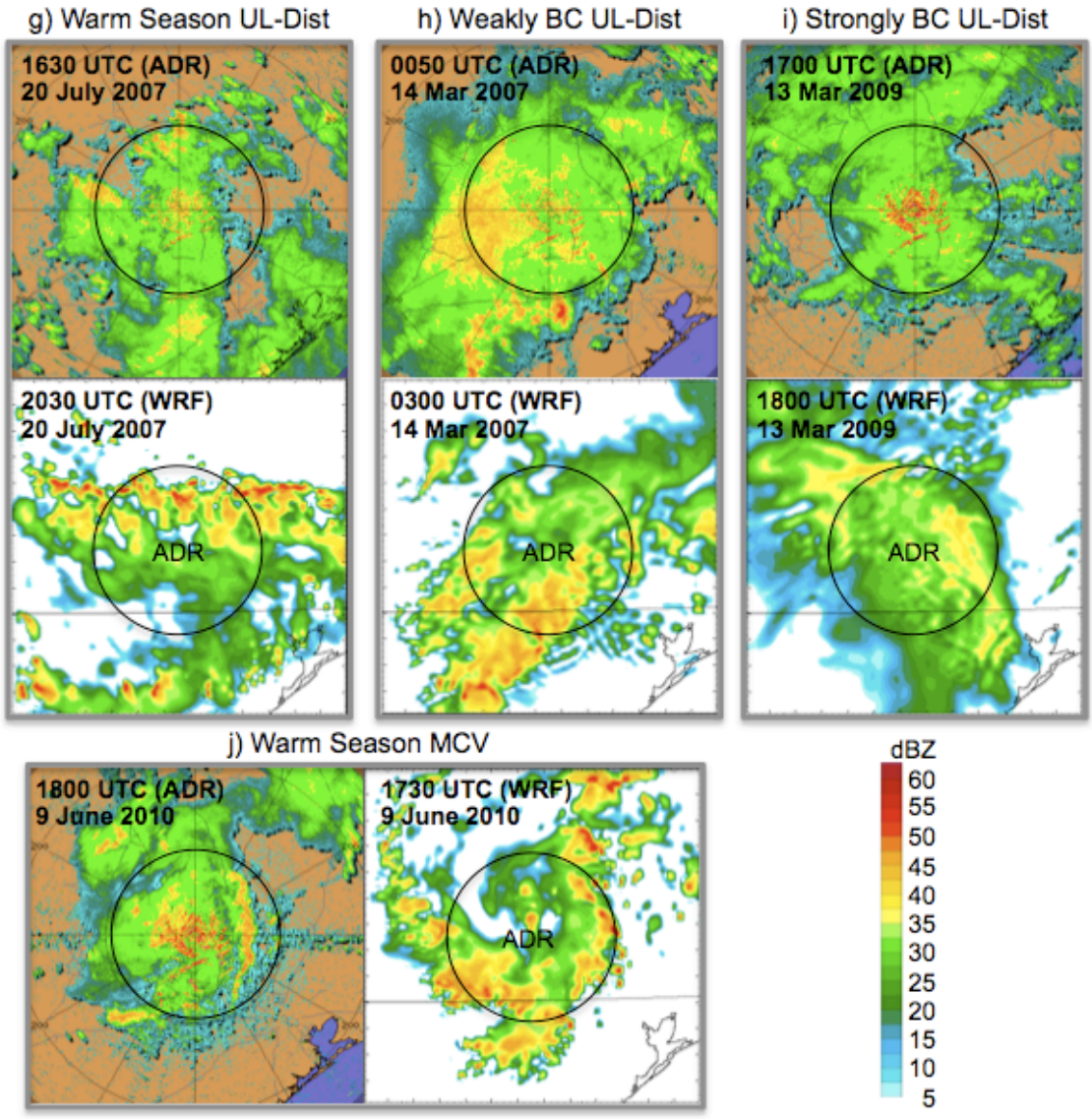

Figure A.18. Continued. Observed 0.5° or 1.0° surveillance scans from ADRAD (ADR; top panels) and simulated 2 km MSL horizontal cross sections (WRF; bottom panels) at similar points in the KFexpGod ensemble member (denoted in Table B.5) of each case presented in this study. The circles on each image denote the 96 km radius of the radar domain and 3 km WRF-ARW grid (D3) included in the analyses for each case.

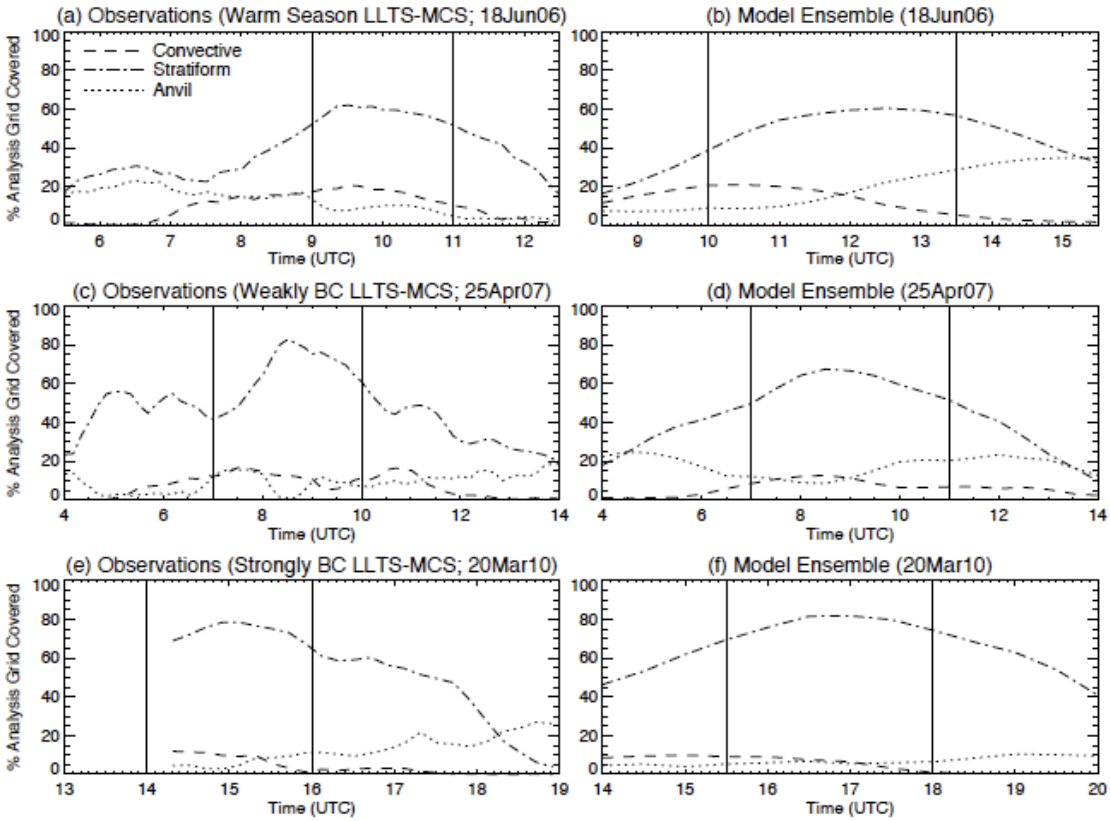

Figure A.19. Observed and modeled percentages of ADRAD's and WRF-ARW's analysis grids covered by convective rain (dashed), stratiform rain (dash-dot), and anvil (dotted) for the (a),(b) 18 June 2006 warm season, (c),(d) 25 April 2007 weakly baroclinic, and (e),(f) 20 March 2010 strongly baroclinic LLTS-MCS cases. The solid vertical lines indicate the beginning and end of the observed analysis periods and the range of time periods used in the model ensemble of the for each case.

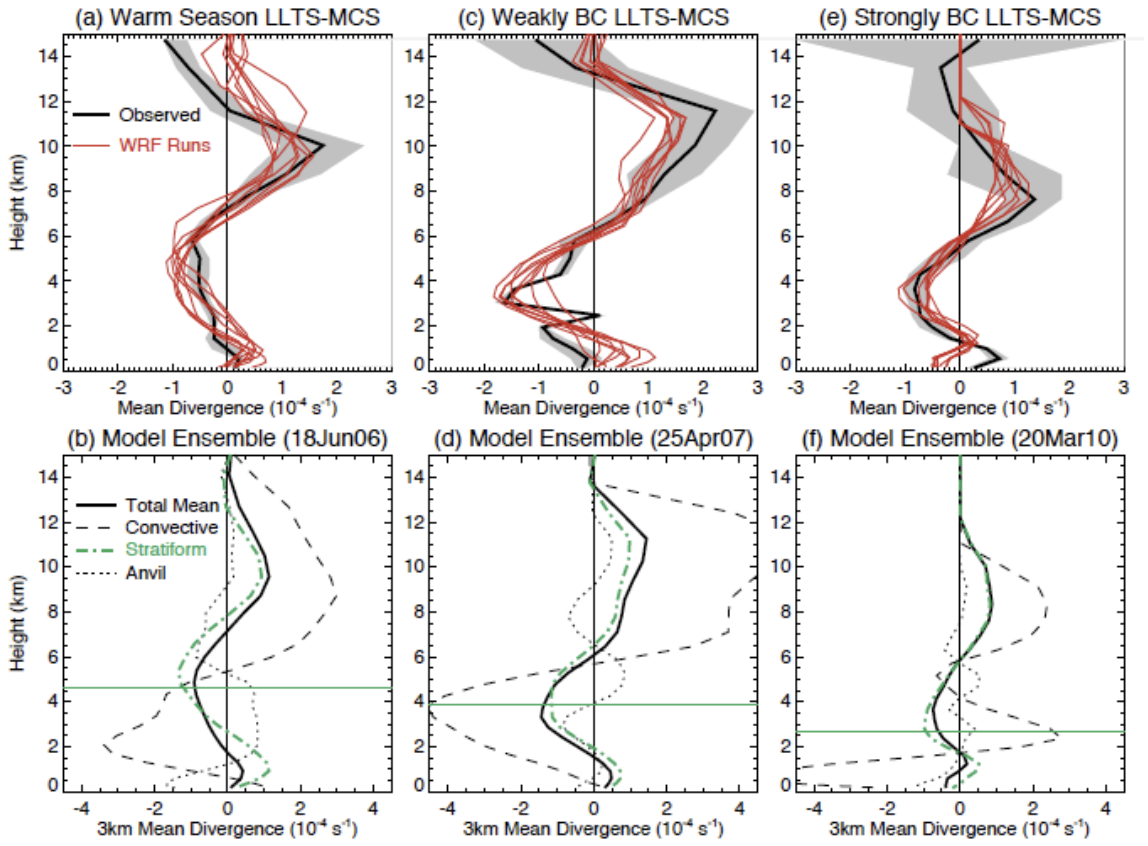

Figure A.20. Mean divergence profiles (top panels) observed by ADRAD (thick black) and simulated by each ensemble member (thin red) along with ensemble mean divergence profiles (bottom panels; dark solid) for convective (dashed), stratiform (green dash-dot), and anvil (dotted) regions as defined in section 2c. Hourly mean observed VAD divergence profiles (Mapes and Lin 2005) are averaged together during the time periods in Table B.6 to create the mean observed divergence profiles. Each hourly mean includes five-range pooled 40-km annulus segments using 8-km annuli centered about 20, 28, 36, 44, 52, 60, 68, and 76 km from ADRAD's center that are augmented by two adjacent 8-km annuli on both sides. Sampling variability in the observed VAD divergence profiles is shown by the light gray shading that displays +/- one standard deviation of the five-range pooled mean estimates. The horizontal lines plotted on the bottom figures indicate the 0^{o}C levels for each case. Divergence profiles are presented for the (a),(b) warm season, (c),(d) weakly baroclinic, and (e),(f) strongly baroclinic LLTS-MCS cases.

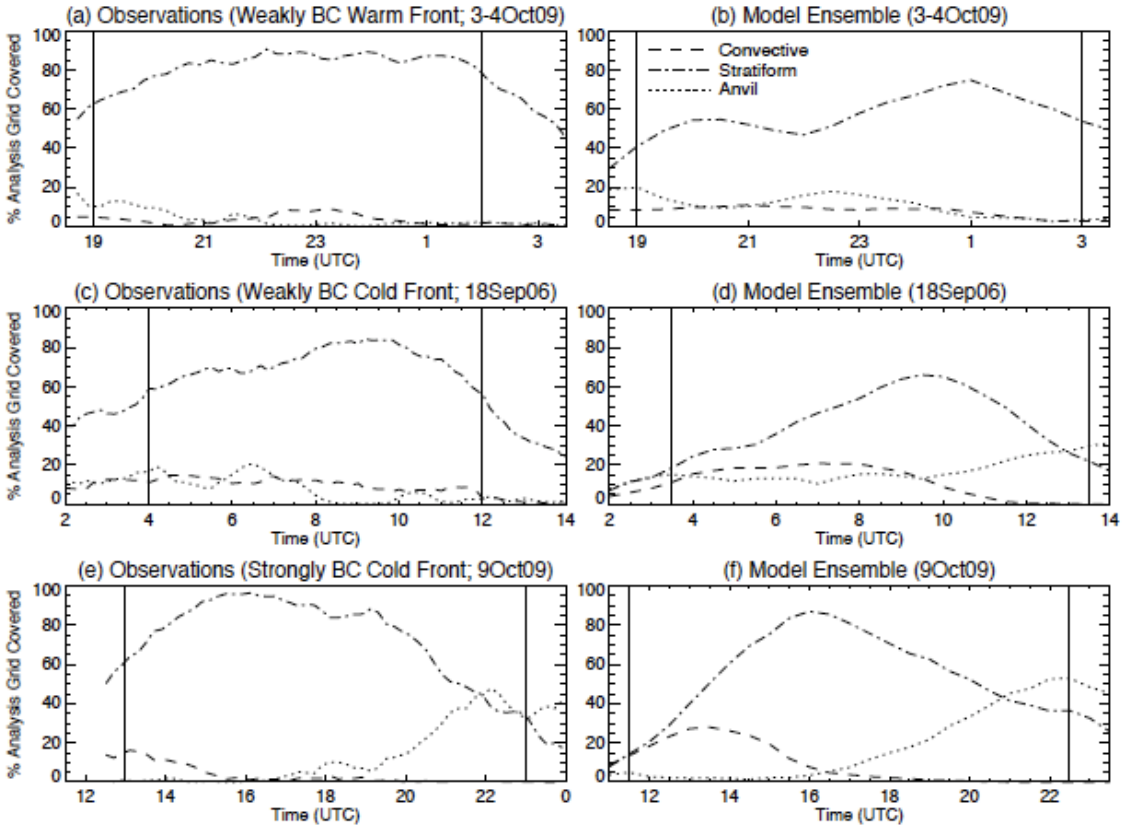

Figure A.21. Observed and modeled percentages of ADRAD's and WRF-ARW's analysis grids covered by convective rain, stratiform rain, and anvil for the (a),(b) 3-4 October 2009 weakly baroclinic warm frontal case, (c),(d) 18 September 2006 weakly baroclinic cold frontal case, and (e),(f) 9 October 2009 strongly baroclinic cold frontal case.

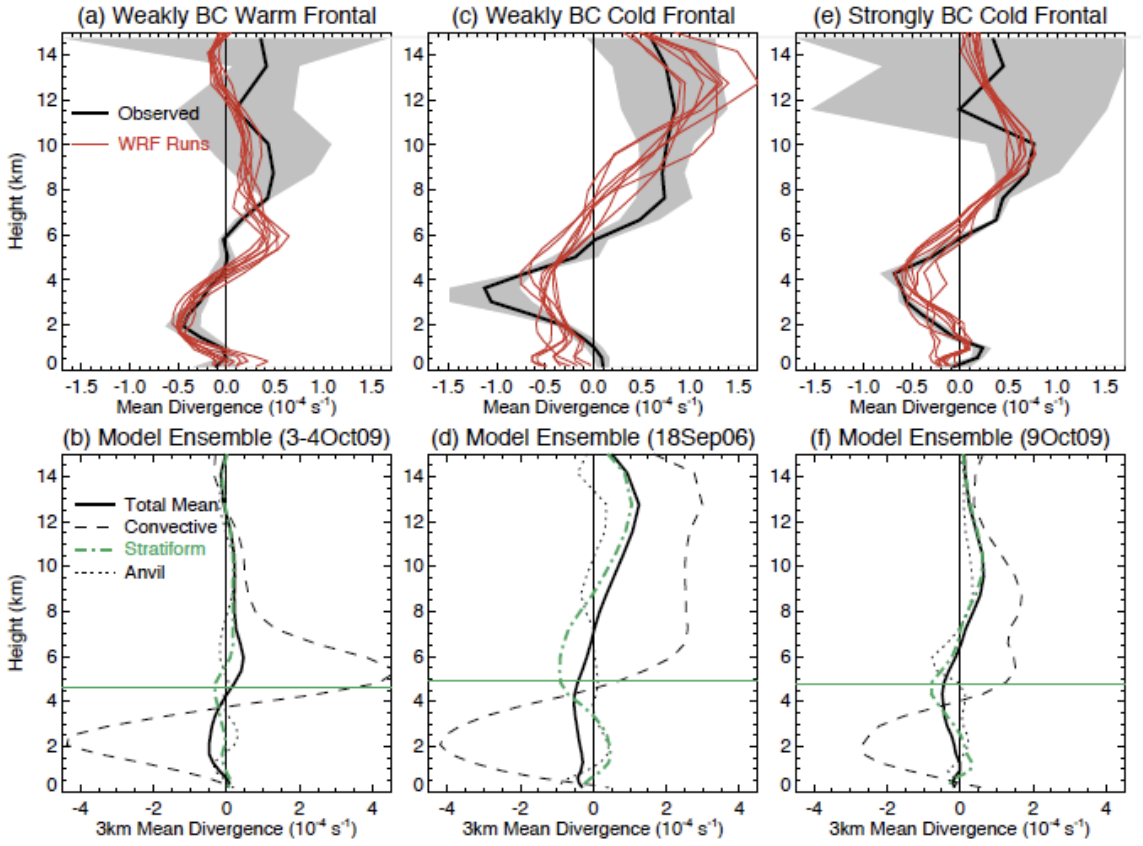

Figure A.22. Mean divergence profiles (top panels) observed by ADRAD and simulated by each ensemble member along with model ensemble mean divergence profiles (bottom panels) for convective, stratiform, and anvil regions following the plotting convection in Fig. A.20. Divergence profiles are presented for the (a),(b) weakly baroclinic warm frontal, (c),(d) weakly baroclinic cold frontal, and (e),(f) strongly baroclinic cold frontal cases.

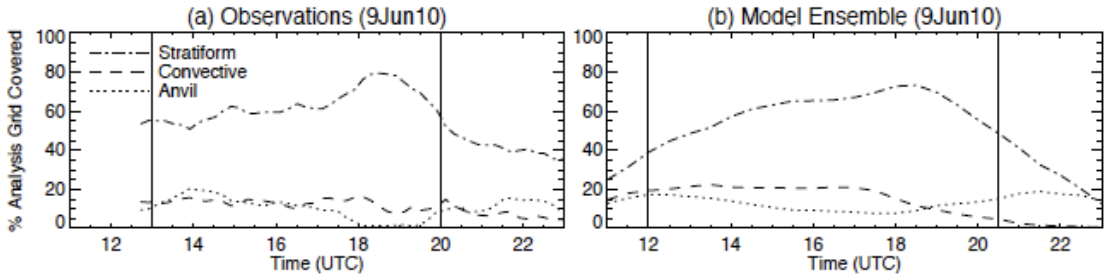

Figure A.23. (a) Observed and (b) modeled percentages of ADRAD's and WRF-ARW's analysis grids covered by convective rain, stratiform rain, and anvil for the 9 June 2010 warm season MCV.

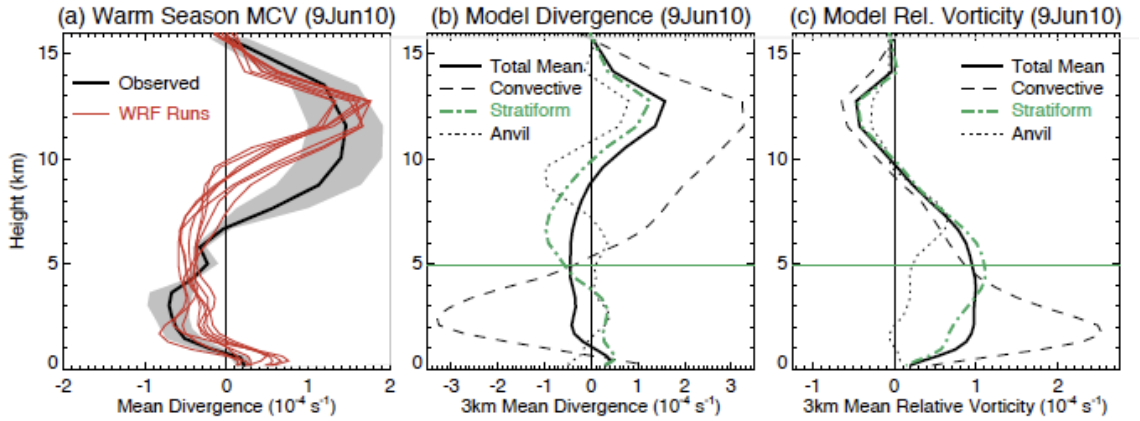

Figure A.24. Mean divergence profiles for the warm season MCV case (a) observed by ADRAD and simulated by each ensemble member and (b) model ensemble mean divergence profiles for convective, stratiform, and anvil regions following the plotting convention in Fig. A.20. (c) Mean model ensemble relative vorticity profiles (solid) are also presented for convective (dashed), stratiform (dash-dot), and anvil (dotted) regions.

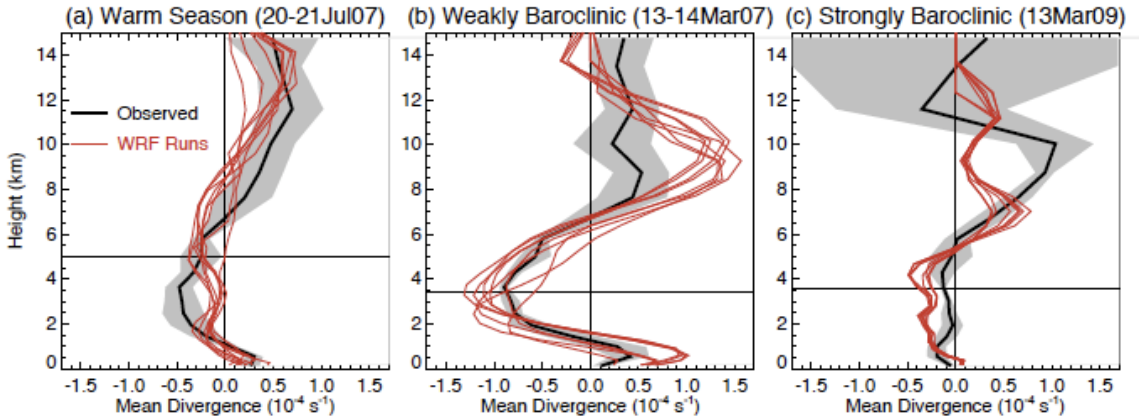

Figure A.25. Mean divergence profiles observed by ADRAD and simulated by each ensemble member for the (a) warm season, (b) weakly baroclinic, and (c) strongly baroclinic upper-level disturbance cases following the plotting convention in Fig. A.20.

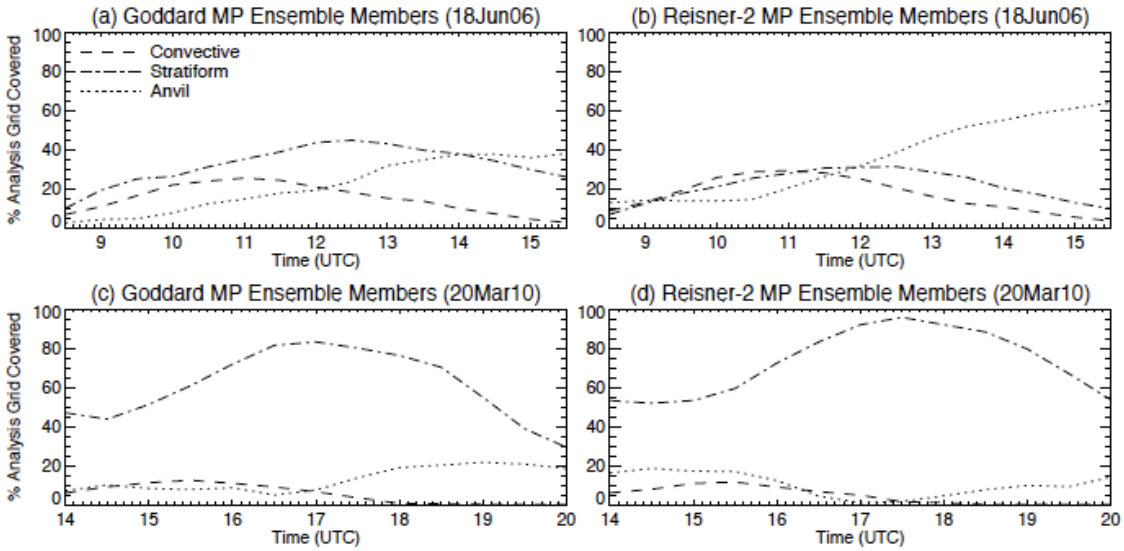

Figure A.26. Percentage of model analysis grid covered for the 18 June 2006 warm season LLTS-MCS (a) Goddard and (b) Reisner-2 MP ensemble members and for the 20 March 2010 strongly baroclinic LLTS-MCS (c) Goddard and (d) Reisner-2 MP model runs.

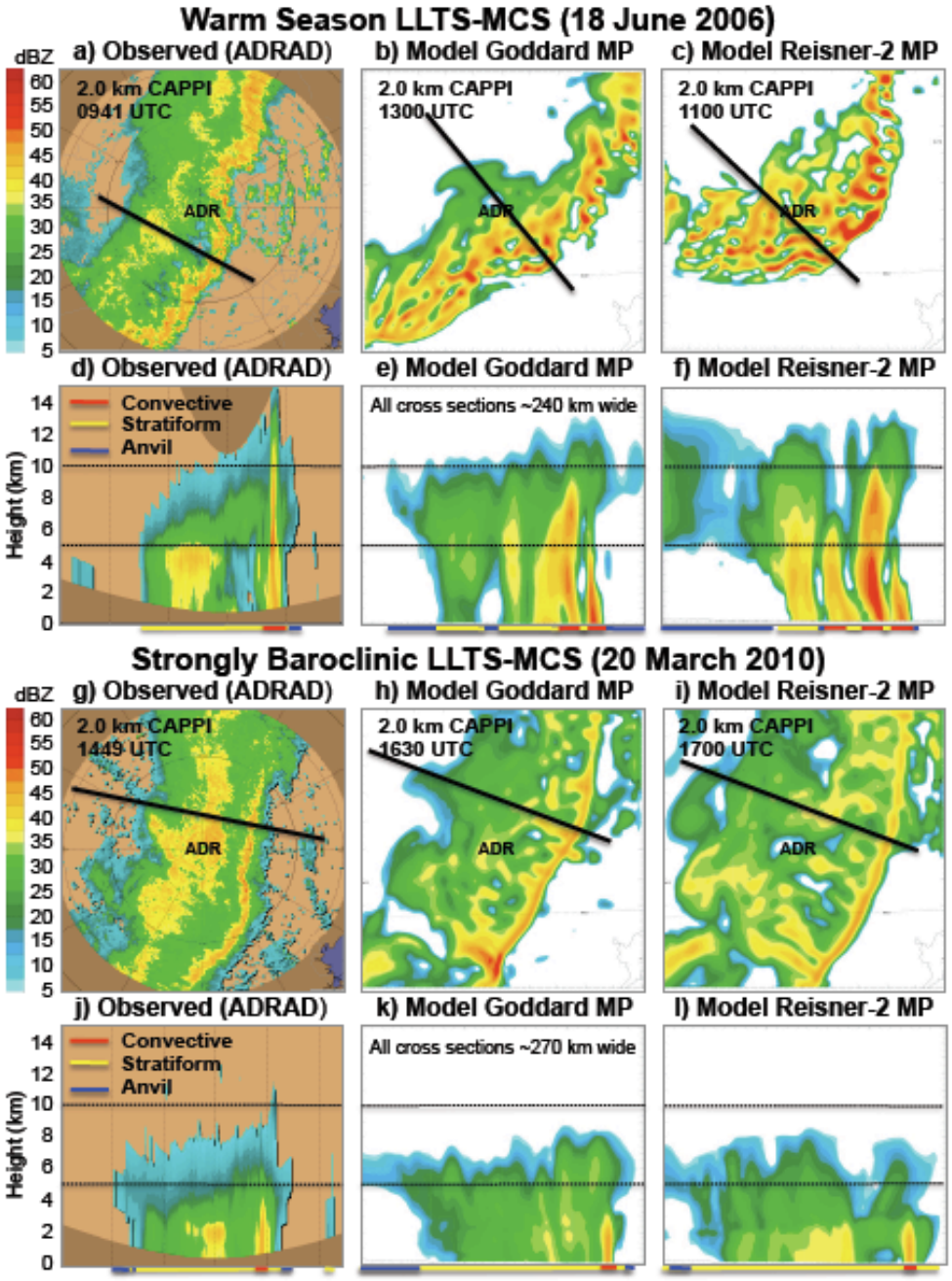

Figure A.27. Observed ADRAD (a) horizontal cross section at 2 km MSL and (d) vertical cross section on 0941 UTC 18 Jun 2006 and corresponding modeled (b), (c) horizontal cross sections and (e), (f) vertical cross sections for Kain-Fritsch CP model runs with explicit convection on D2 using the Goddard and Reisner-2 MPs at 1300 and 1100 UTC, respectively. Observed (g), (j) images on 1449 UTC 20 Mar 2010 and simulated images for the Goddard (h), (k) and Reisner-2 MPs (i), (l) at 1630 and 1700 UTC, respectively, are also presented using the same plotting conventions as the 18 Jun 2006 case.

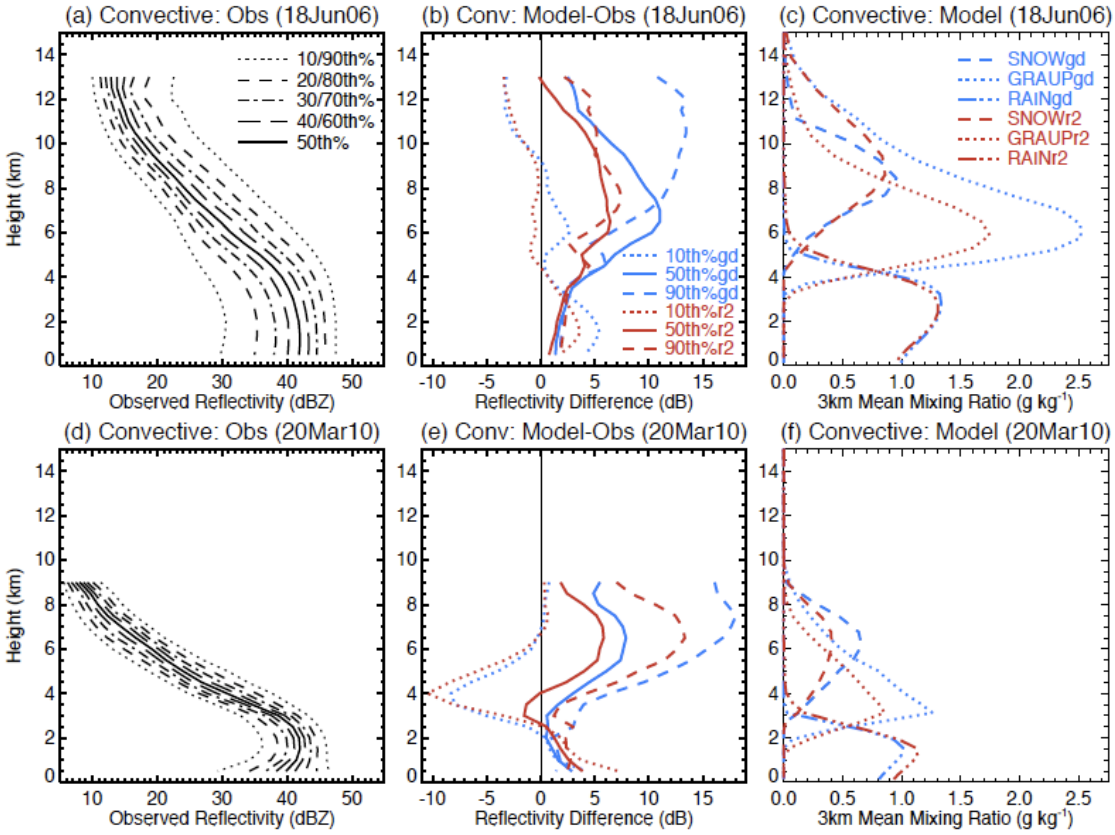

Figure A.28. (a) Vertical distribution of radar reflectivity observed by ADRAD within convective regions for the 18 Jun 2006 warm season LLTS-MCS case. Each line represents a 10% quantile from 10% to 90% with the median profile in solid black. In addition, (b) differences between the reflectivities modeled using the Goddard (blue) and Reisner-2 (red) MPs from those observed are presented for the 10%, 50%, and 90% quantiles along with (c) vertical profiles of mean mixing ratios simulated by both MPs for snow (dashed), graupel (dotted), and rain (dash-dot-dot-dot). The (d) vertical distribution of radar reflectivity observed by ADRAD, (e) differences between modeled and observed reflectivities, and (f) simulated hydrometeor mean mixing ratios within convective regions are also presented for the 20 Mar 2010 strongly baroclinic LLTS-MCS case.

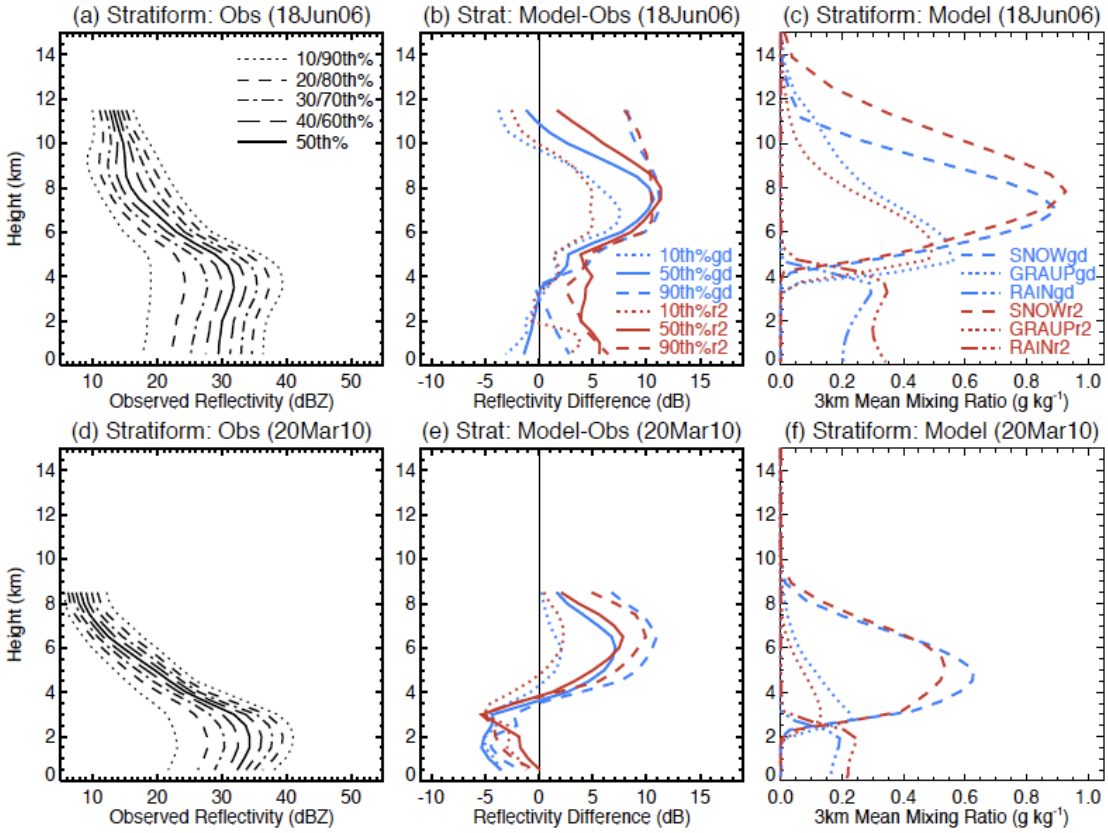

Figure A.29. The (a),(d) vertical distributions of radar reflectivity observed by ADRAD, (b),(e) differences between modeled and observed reflectivities, and (c),(f) simulated hydrometeor mean mixing ratios following the plotting convection in Fig. A.28 within stratiform regions for the (top figures) warm season and (bottom figures) strongly baroclinic LLTS-MCS cases.

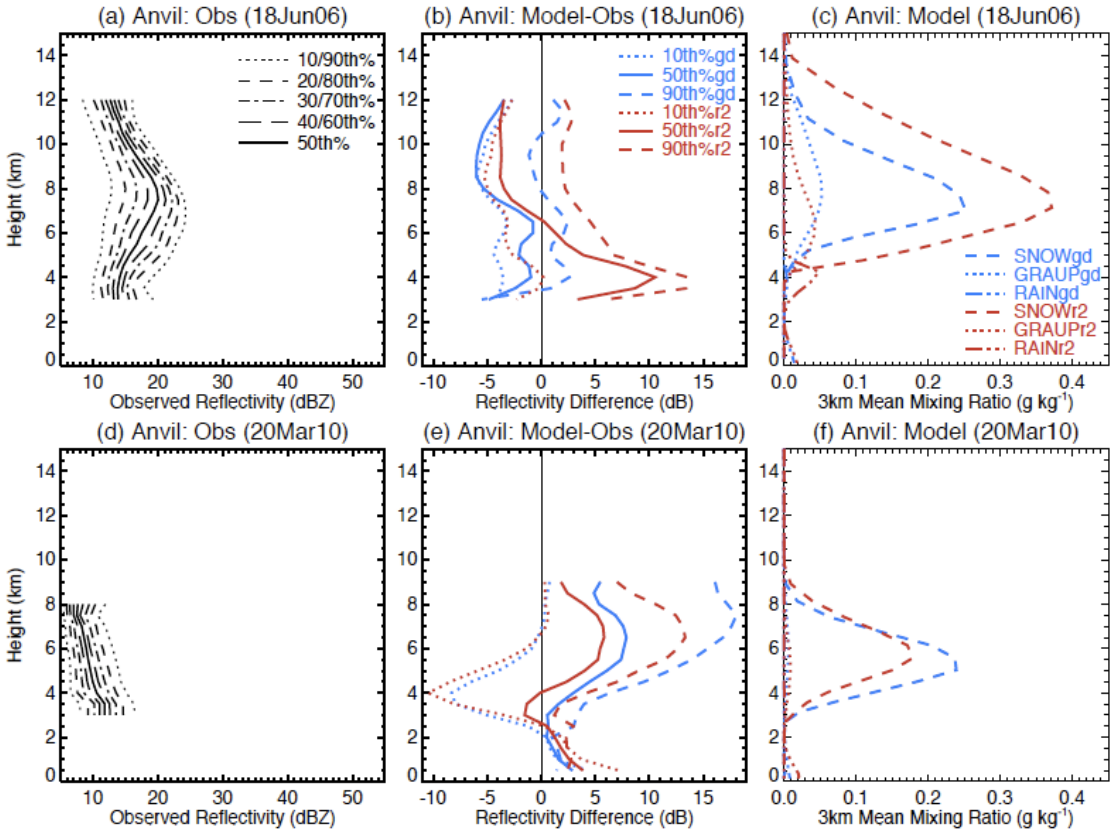

Figure A.30. The (a),(d) vertical distributions of radar reflectivity observed by ADRAD, (b),(e) differences between modeled and observed reflectivities, and (c),(f) simulated hydrometeor mean mixing ratios following the plotting convection in Figs. A.28 and A.29 within anvil regions for the (top figures) warm season and (bottom figures) strongly baroclinic LLTS-MCS cases.

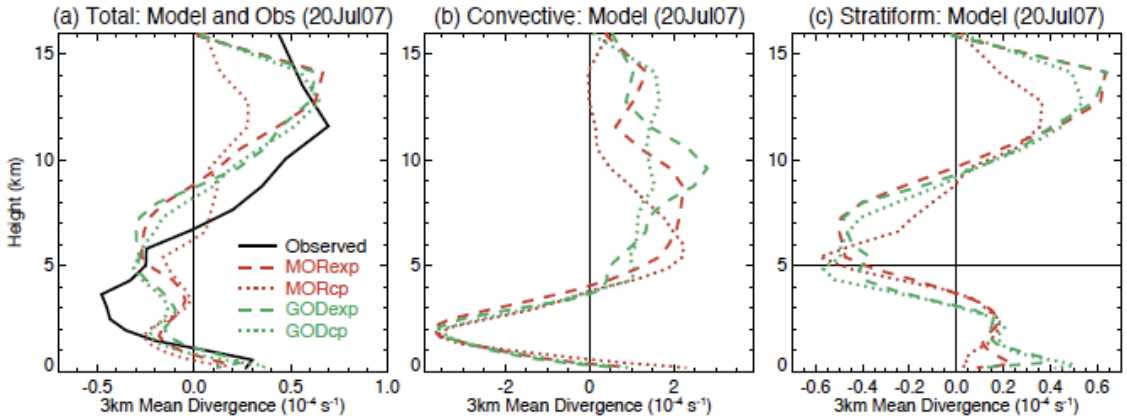

Figure A.31. Observed (solid black) and simulated (a) mean, (b) convective, and (c) stratiform divergence profiles for the 20 July 2007 warm season case when using the Morrison two-moment MP with explicit (dashed red; MORexp) and parameterized (dotted red; MORcp) convection on D2 and the Goddard one-moment MP with explicit (dashed green; GODexp) and parameterized (dotted green; GODcp) convection on D2. Each model ensemble set includes one corresponding Kain-Fritsch and Grell-Devenyi CP run.

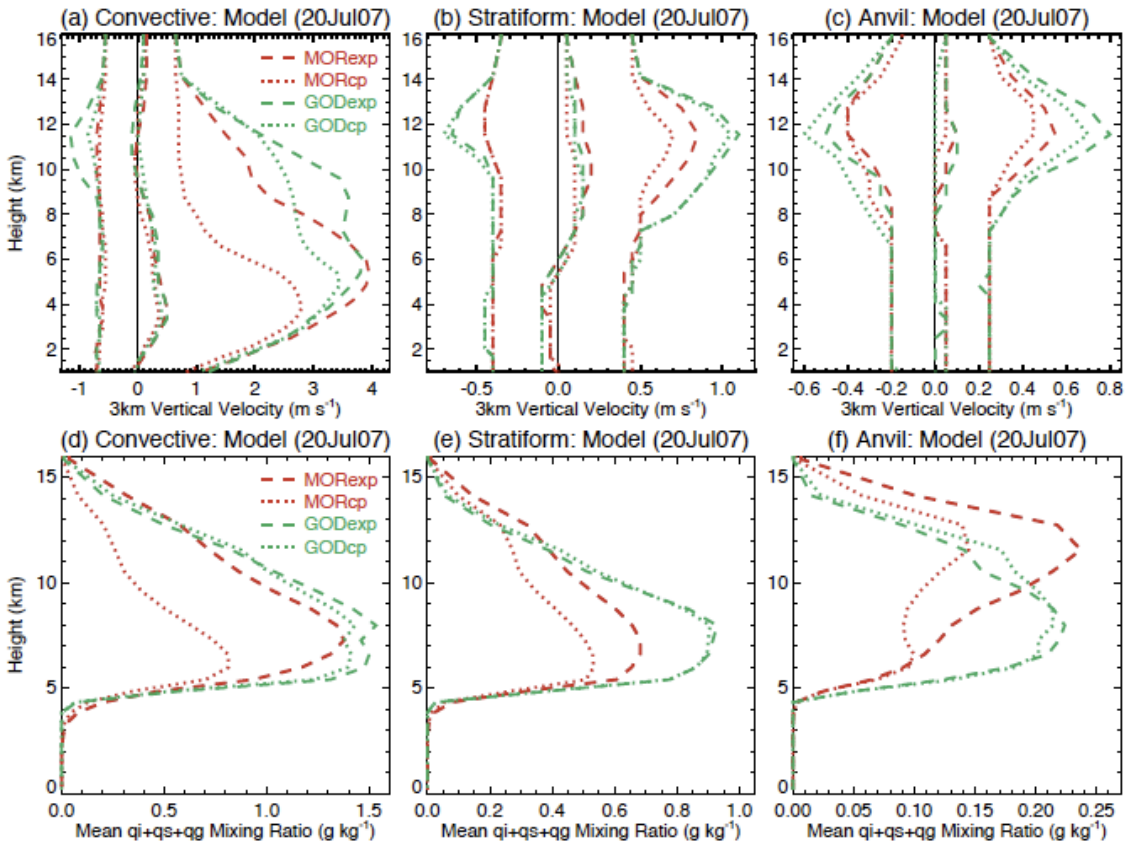

Figure A.32. Vertical distributions of vertical velocities simulated for the 20 July 2007 warm season upper-level disturbance case using different sets of ensemble members following the plotting convention in Fig. A.31 for (a) convective, (b) stratiform, and (c) anvil regions. Lines representing the 10% quantile (leftmost), median (middle), and 90% quantile (rightmost) are presented in each panel. In addition, simulated mean ice-phase hydrometeor mixing ratios (cloud ice, snow, and graupel) in (d) convective, (e) stratiform, and (f) anvil regions.

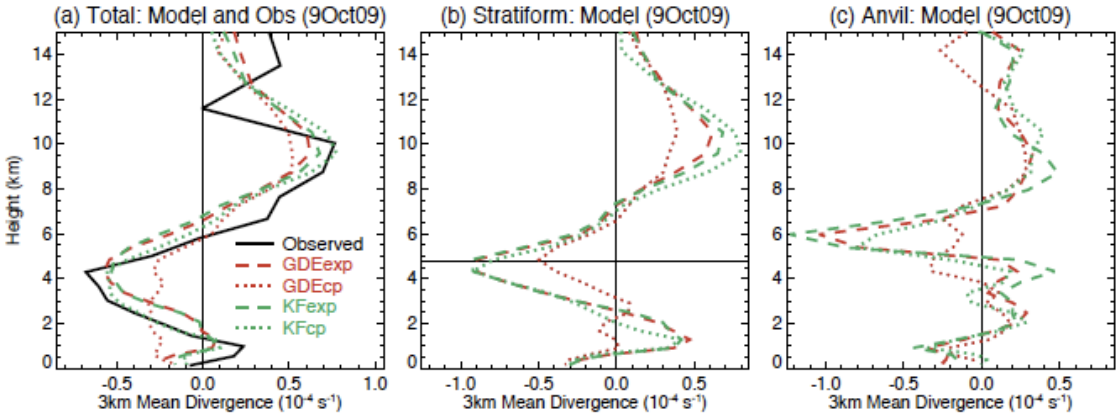

Figure A.33. Observed (solid black) and simulated (a) mean, (b) stratiform, and (c) anvil divergence profiles for the 9 October 2009 strongly baroclinic cold frontal MCS when using the Grell-Devenyi CP with explicit (dashed red; GDEexp) and parameterized (dotted red; GDEcp) convection on D2 and the Kain-Fritsch CP with explicit (dashed green; KFexp) and parameterized (dotted green; KFcp) convection on D2. Each model ensemble set includes one corresponding Morrison and Goddard MP run.

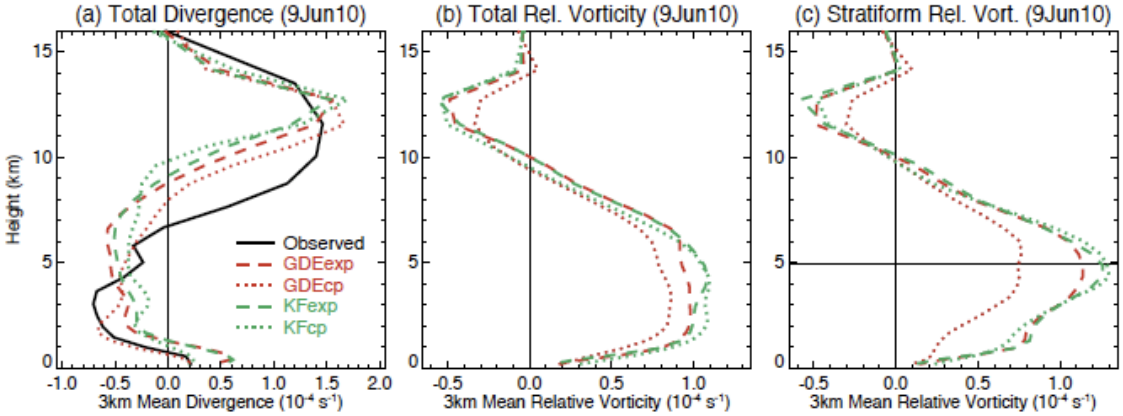

Figure A.34. (a) Mean observed (solid black) and simulated divergence profiles for the 9 June 2010 warm season MCV following the plotting convection in Fig. A.33 in addition to the mean simulated (b) total and (c) stratiform relative vorticity profiles.

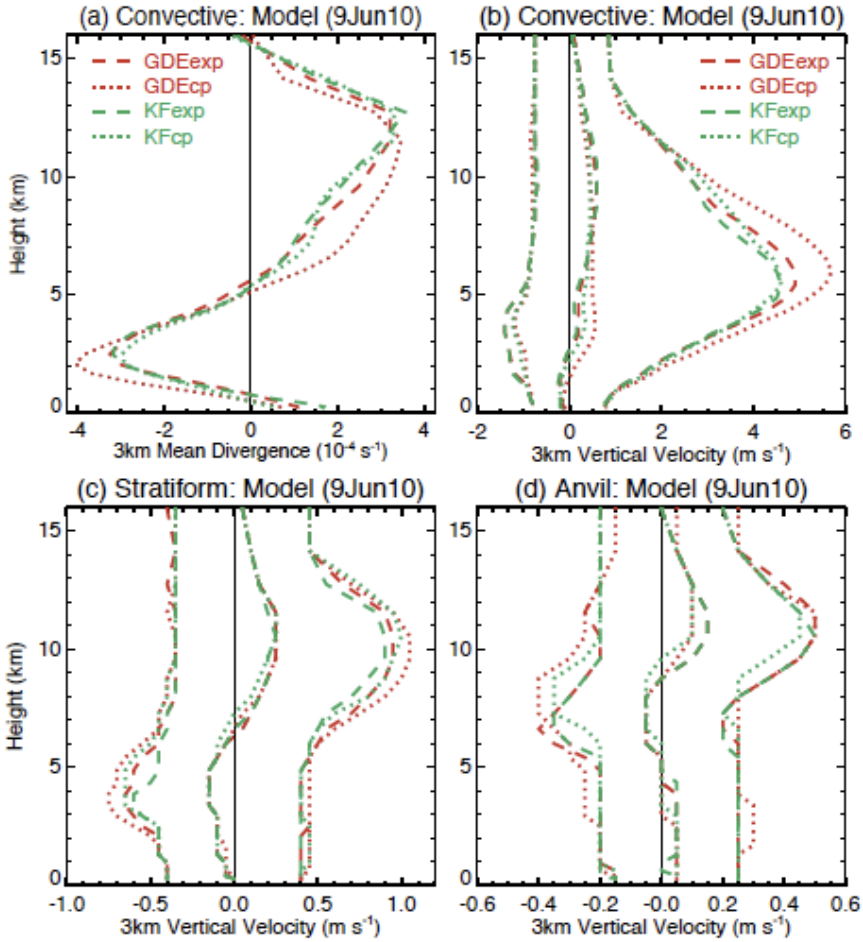

Figure A.35. (a) Convective divergence profiles for the 9 June 2010 warm season MCV case and vertical distributions of vertical velocities simulated for the warm season MCV case using different sets of ensemble members following the plotting convention in Fig. A.32 for (b) convective, (c) stratiform, and (d) anvil regions. Lines representing the 10% quantile (leftmost), median (middle), and 90% quantile (rightmost) are presented in each panel.

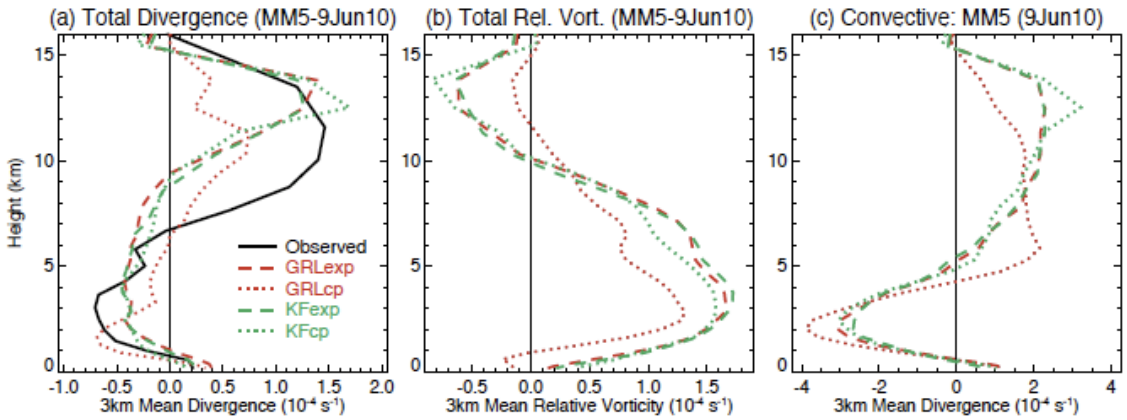

Figure A.36. Observed (solid black) and simulated mean (a) divergence and (b) relative vorticity profiles for the 9 June 2010 warm season MCV when using the Grell CP with explicit (dashed red; GRLexp) and parameterized (dotted red; GRLcp) convection on D2 and the Kain-Fritsch-2 CP with explicit (dashed green; KFexp) and parameterized (dotted green; KFcp) convection on D2 in MM5. (c) Convective divergence profiles are also presented following the same plotting convection. Each model ensemble set includes one corresponding Reisner-2 and Goddard MP run.

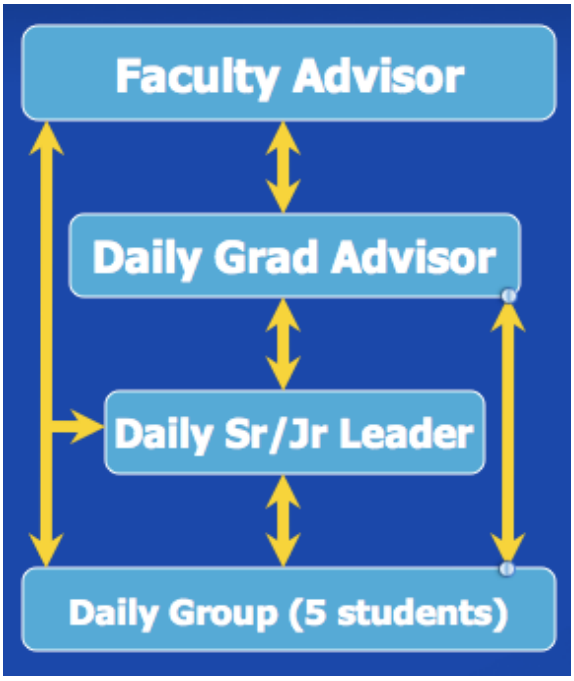

Figure A.37. Organizational structure of SOAP.

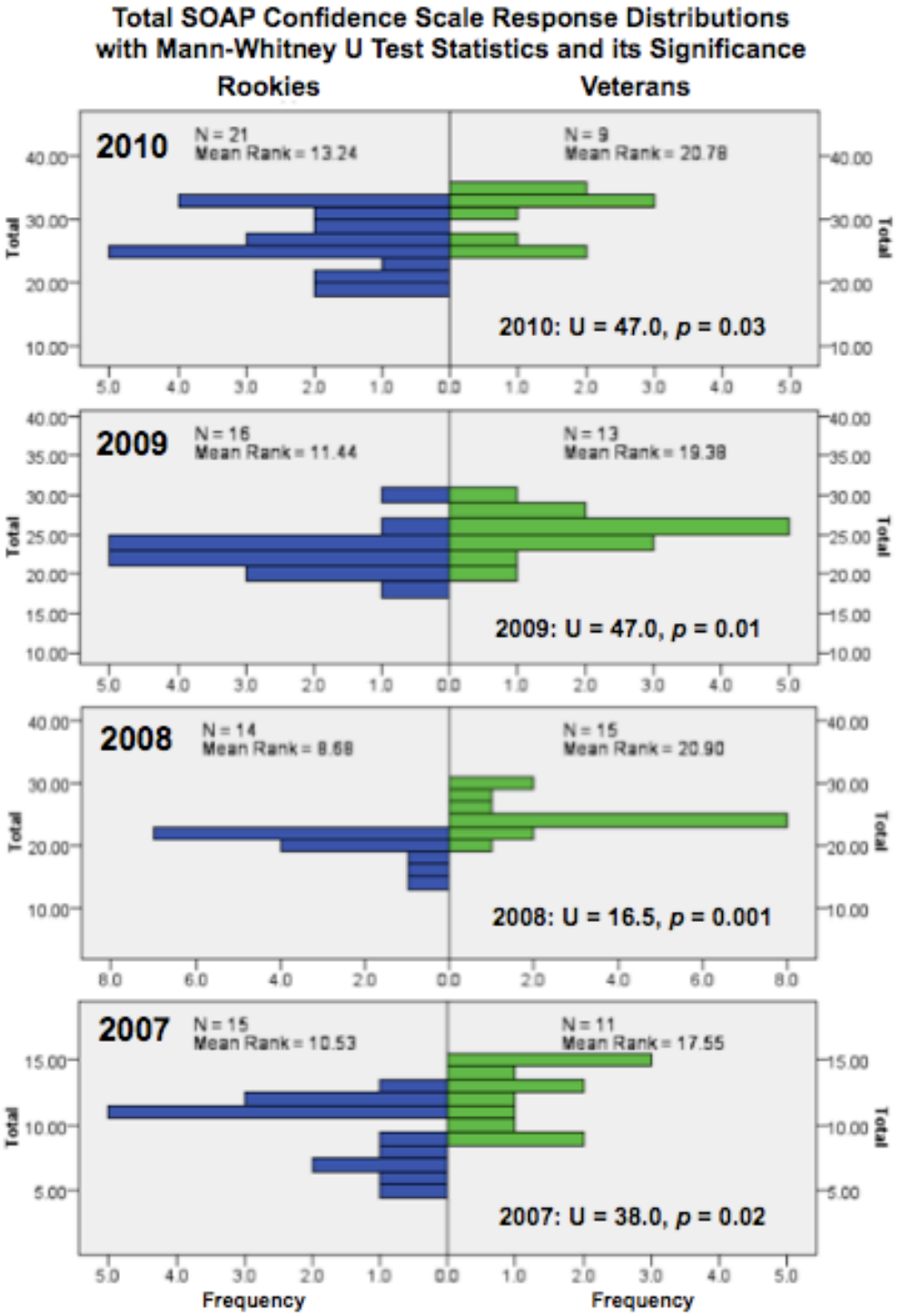

Figure A.38. Total confidence scale response distributions for first-year (Rookies; in blue) and multi-year (Veterans; in green) SOAP participants during 2007-2010 output from SPSS. Mann-Whitney U test statistics and their significance are also given for each year.

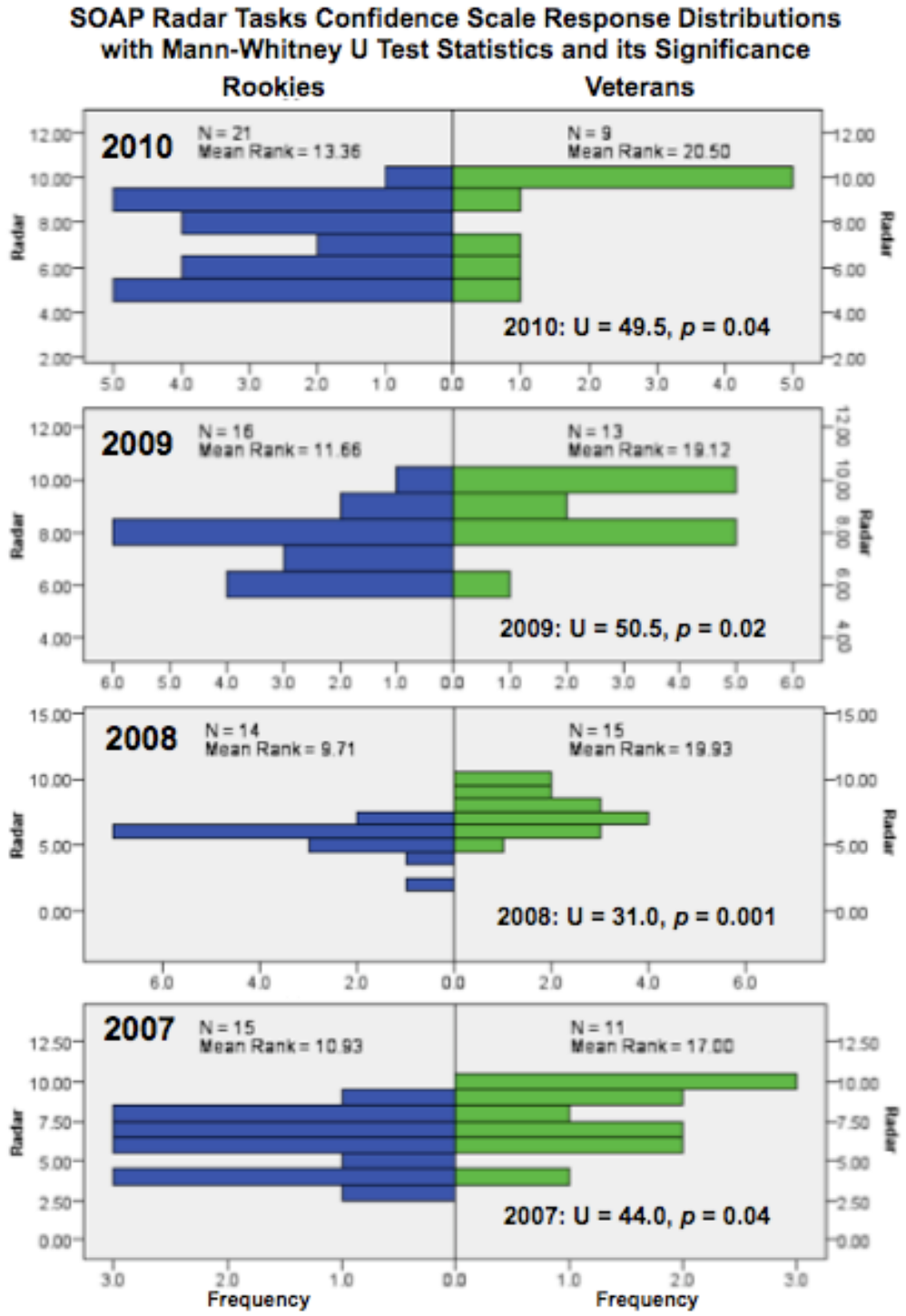

Figure A.39. Radar tasks confidence scale response distributions for first-year and multi-year SOAP participants during 2007-2010 following the plotting conventions in Fig. A.37. Mann-Whitney U test statistics and their significance are also given for each year.

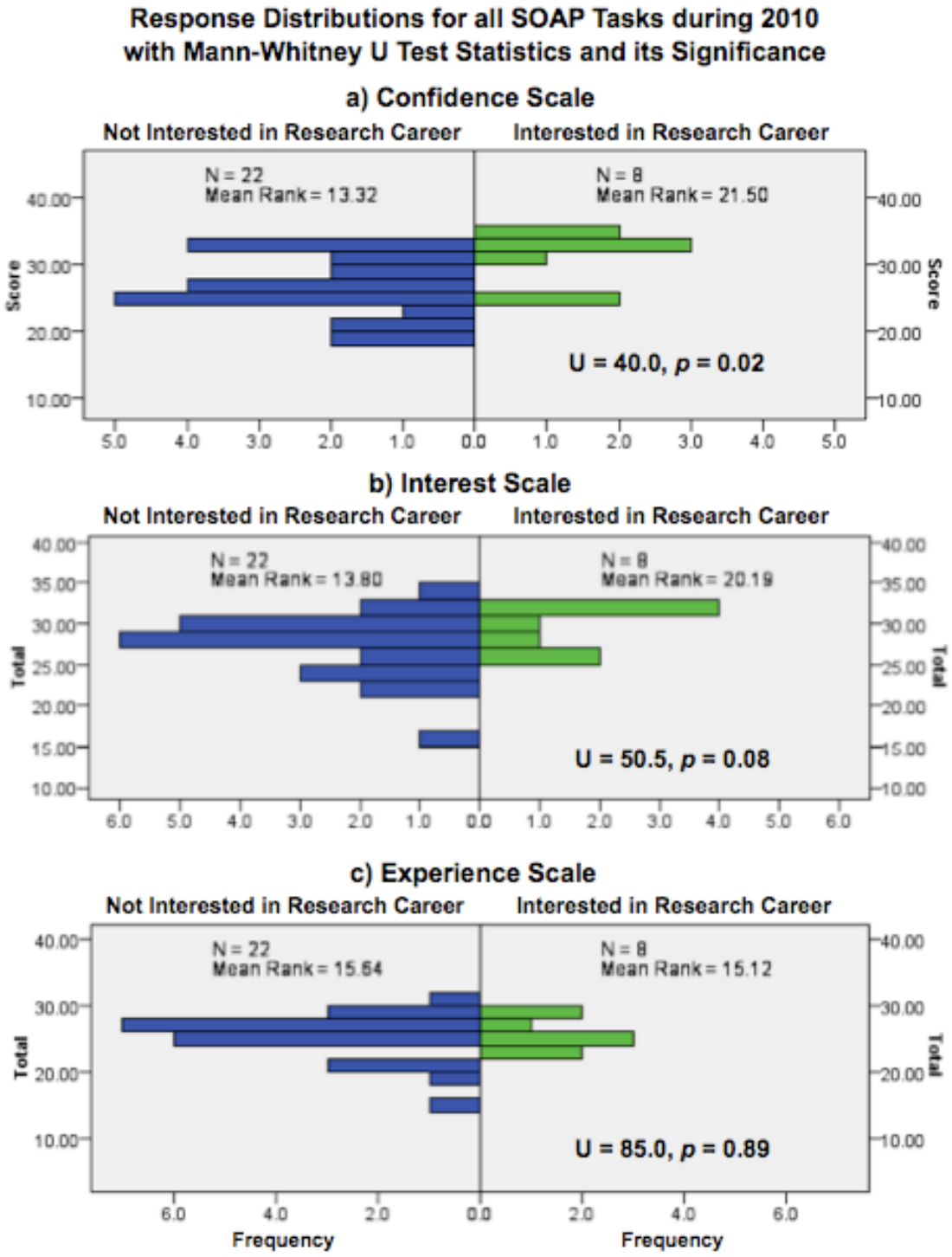

Figure A.40. Total (a) confidence, (b) interest, and (c) experience scale response distributions for first-year and multi-year SOAP participants during 2010 following the plotting convection in Fig. A.37. Mann-Whitney U test statistics and their significance are also given for each year.

APPENDIX B

TABLES

Table B.1. Number of events, total precipitation (in mm), and basic statistics for each storm type and structure between March 2002-February 2010 for Easterwood Airport in College Station, TX. Storm count and total precipitation fractions are also given in parentheses.

Storm Type or Structure	Count (%)	Total Precip; (mm; %)	Storm Mean (mm)	Storm 25th% (mm)	Storm 50th% (mm)	Storm 75th% (mm)	Storm Max (mm)
Cold Frontal (CF)	**246 (43)**	**3677 (44)**	**15.0**	**2.5**	**9.0**	**20.3**	**80.8**
CFc	90	624	6.9	1.0	3.3	8.8	50.8
CFdcs	120	2699	22.5	9.6	17.1	32.4	80.8
CFncs	36	354	9.8	1.3	4.2	10.8	66.0
Warm Frontal (WF)	**76 (13)**	**1895 (23)**	**24.9**	**3.7**	**14.1**	**32.7**	**129.0**
WFdcs	50	1687	33.7	9.1	27.6	45.1	129.0
WFncs	26	208	8.0	1.7	4.2	12.6	31.0
UL-Disturbance (ULD)	**214 (37)**	**2347 (28)**	**11.0**	**2.0**	**4.8**	**13.4**	**88.1**
ULDc	57	380	6.7	1.5	3.3	8.6	39.4
ULDdcs	80	1348	16.9	3.4	8.0	20.5	88.1
ULDncs	77	619	8.0	1.8	4.6	10.7	58.2
Weakly Forced (WK)	**30 (5)**	**219 (3)**	**7.3**	**2.5**	**5.3**	**7.8**	**26.9**
WKc	22	134	6.1	2.2	5.2	7.3	26.9
WKdcs	8	85	10.6	4.3	7.6	19.4	22.1
Tropical Cyclone (TC)	**8 (2)**	**153 (2)**	**19.2**	**2.0**	**3.9**	**23.3**	**83.3**
TCc	3	10	3.2	0.4	0.7	2.0	3.3
TCdcs	5	144	28.7	2.0	2.0	5.8	37.6
ALL STORMS	**574**	**8291**	**14.4**	**2.3**	**7.1**	**19.3**	**129.0**

Table B.2. Mean seasonal precipitation totals (in mm) and fractions (%; in parentheses) by storm type for College Station, TX from March 2002-February 2010.

Storm Type	MAM (mm; %)	JJA (mm; %)	SON (mm; %)	DJF (mm; %)
Cold Frontal (CF)	140.2 (60)	92.2 (37)	137.2 (43)	90.0 (39)
Warm Frontal (WF)	44.9 (19)	----	101.7 (32)	90.3 (39)
UL-Disturbance (ULD)	49.9 (21)	130.5 (52)	60.4 (19)	52.6 (22)
Weakly Forced (WK)	----	21.8 (9)	5.6 (2)	----
Tropical Cyclone (TC)	----	7.7 (3)	11.4 (4)	----
Mean Seasonal Precipitation	235.0	252.2	316.3	232.9

Table B.3. October-March precipitation totals (in mm) in College Station, TX for storm type by year. The Oceanic Niño Index (ONI) is given in parentheses below the heading for each year in addition whether each was designated as an El Niño (in red), La Niña (in blue) or neutral (in black) episode.

	02-03 (1.2) EL	03-04 (0.4) NEU	04-05 (0.7) EL	05-06 (-0.5) NEU	06-07 (0.7) EL	07-08 (-1.2) LA	08-09 (-0.5) NEU	09-10 (1.5) EL	EL NINO Mean	NEU/ NINA Mean
CF	274	229	351	232	281	284	120	257	**291 (41%)**	**216 (49%)**
WF	441	170	229	130	264	138	46	148	**270 (38%)**	**121 (27%)**
ULD	117	228	89	23	210	55	89	170	**146 (20%)**	**99 (23%)**
WK	20	----	----	----	----	15	3	----	**5 (1%)**	**4 (1%)**
All	852	627	669	385	755	492	258	575	**712**	**441**

Table B.4. Configurations and parameterizations (see Skamarock et al. 2008 for technical descriptions) used in each WRF-ARW, version 3.1.1, numerical model run that comprises the eight-member ensemble for each case. Multiple entries in the first three rows denote different configurations for domains 1-3.

Horizontal grid spacing	27 km, 9 km, 3 km
Domain size	133x133, 130x130, 130x130
Vertical levels	27, 27, 27
Longwave radiation	Rapid radiative transfer model
Shortwave radiation	Dudhia
Surface layer	MM5 similarity (Monin-Obukhov)
Land surface	Noah model
Boundary layer	Yonsei University
Turbulence	2D Smagorinsky
Cumulus convection	Variable (see Table B.5)
Microphysics	Variable (see Table B.5)

Table B.5. Summary of experiments used for each model run that comprises the eight-member ensemble for each case. The abbreviations in the experiment designations are as follows: "KF" is the Kain-Fritsch CP, "GDE" is the Grell-Devenyi CP, "exp" refers to the explicit representation of convection on the second domain, "cp" refers to the use of the same CP on D1 and D2, "God" is the Goddard MP, and "Mor" is the Morrison two-moment MP.

	Cumulus convection			**Microphysics**
Experiment	**D1 (Δx = 27 km)**	**D2 (Δx = 9 km)**	**D3 (Δx = 3 km)**	**All Grids**
KFexpGod	Kain-Fritsch	Explicit	Explicit	Goddard
KFexpMor	Kain-Fritsch	Explicit	Explicit	Morrison 2-M
KFcpGod	Kain-Fritsch	Kain-Fritsch	Explicit	Goddard
KFcpMor	Kain-Fritsch	Kain-Fritsch	Explicit	Morrison 2-M
GDEexpGod	Grell-Devenyi	Explicit	Explicit	Goddard
GDEexpMor	Grell-Devenyi	Explicit	Explicit	Morrison 2-M
GDEcpGod	Grell-Devenyi	Grell-Devenyi	Explicit	Goddard
GDEcpMor	Grell-Devenyi	Grell-Devenyi	Explicit	Morrison 2-M

Table B.6. List of storms with different primary forcings modeled in warm season (WS), weakly baroclinic (WB), and strongly baroclinic (SB) environments. Each of the eight ensemble members' initialization times and range of time periods over which calculations are performed for each case are given in addition to the times radar observations from ADRAD are analyzed for comparison. Model analysis time periods are of the same length as the observed analysis periods for each ensemble member, including data from the times each ensemble member's precipitating area fractions are the highest.

Storm/Model Run (Environment)	WRF Model Initiation Time	Range of WRF Analysis Periods	ADRAD Analysis Period
LLTS-MCSs			
18 Jun 2006 (WS; outflow boundary)	0000 UTC 18 Jun	1000-1330 UTC	0900-1100 UTC
25 Apr 2007 (WB; pre-frontal trough)	1200 UTC 24 Apr	0700-1100 UTC	0700-1000 UTC
20 Mar 2010 (SB; cold front)	0000 UTC 20 Mar	1530-1800 UTC	1400-1600 UTC
Large Frontal MCSs			
3-4 Oct 2009 (WB; warm front)	1200 UTC 3 Oct	1900-0300 UTC	1900-0200 UTC
18 Sep 2006 (WB; cold front)	1800 UTC 17 Sep	0330-1330 UTC	0400-1200 UTC
9 Oct 2009 (SB; cold front)	0000 UTC 9 Oct	1130-2230 UTC	1300-2300 UTC
Upper-Level Disturbances			
9 Jun 2010 (WS; MCV)	0000 UTC 9 Jun	1200-2030 UTC	1300-2000 UTC
20-21 Jul 2007 (WS; shortwave)	0600 UTC 20 Jul	1930-0130 UTC	1500-1900 UTC
13-14 Mar 2007 (WB; shortwave)	1200 UTC 13 Mar	2030-0930 UTC	2000-0400 UTC
13-14 Mar 2009 (SB; shortwave)	0000 UTC 13 Mar	1630-2230 UTC	1600-2200 UTC

Table B.7. Mean convective, stratiform, and anvil area fractions and levels of non-divergence (LNDs; in km) simulated by WRF-ARW and observed by ADRAD (in parentheses) over the analysis time periods given for each case in Table B.6. The 0°C level and convective, stratiform, and anvil LNDs generated by WRF-ARW are also given.

Storm/Model Run (Environment)	WRF (ADR) Conv Area	WRF (ADR) Strat Area	WRF (ADR) Anvil Area	WRF (ADR) LND (km)	WRF 0°C Lev (km)	WRF Conv LND (km)	WRF Strat LND (km)	WRF Anvil LND (km)
LLTS-MCSs								
18 Jun 2006 (WS)	17 (17)	58 (58)	14 (9)	7.2 (7.2)	4.6	5.4	7.9	9.2
25 Apr 2007 (WB)	10 (12)	62 (66)	13 (10)	6.1 (6.2)	3.9	5.7	6.5	9.2
20 Mar 2010 (SB)	7 (8)	77 (74)	6 (6)	5.9 (5.5)	2.7	1.7	5.8	7.5
Large Frontal MCSs								
3-4 Oct 2009 (WB)	8 (4)	60 (83)	10 (4)	4.3 (5.3)[1]	4.6	3.8	5.7	7.8
18 Sep 2006 (WB)	14 (11)	49 (73)	17 (8)	7.0 (5.7)	4.9	4.6	8.8	10.4
9-10 Oct 2009 (SB)	9 (3)	59 (76)	17 (13)	6.5 (5.8)	4.8	4.0	7.1	7.3
Upper-Level Dist.								
9 Jun 2010 (WSmcv)	18 (13)	63 (64)	11 (10)	8.9 (6.7)	4.9	5.4	9.9	10.8
20-21 Jul 2007 (WS)	9 (4)	71 (75)	11 (4)	8.4 (6.7)	5.0	3.8	9.3	11.3
13-14 Mar 2007 (WB)	14 (13)	62 (77)	9 (5)	6.5 (6.7)	3.4	5.1	7.1	8.1
13-14 Mar 2009 (SB)	1 (2)	76 (78)	6 (6)	5.4 (5.5)	3.6	5.5	5.4	8.8

[1]The LND for the warm frontal case is the mean of its two LNDs at 4.8 and 5.9 km.

Table B.8. Specified values of the raindrop size distribution intercept parameter N_o used in MM5 for hydrometeor species in the one-moment Goddard and Reisner-2 MP schemes.

Hydrometeor Species	Goddard MP Fixed N_o (m^{-4})	Reisner2 MP N_o (m^{-4}) Range
Rain	8×10^6	2×10^7 - 1×10^{10}*
Graupel	4×10^6	1×10^4 - 4×10^6**
Snow	2×10^7	2×10^6 - 2×10^8

* Lower-intercept limit has increased from 8×10^6 in Thompson et al. (2004) to 2×10^7.
** Upper-intercept limit has decreased from 5×10^7 in Thompson et al. (2004) to 4×10^6 to be consistent with replacing the gamma size distribution for graupel with an exponential distribution.

Table B.9. Mean convective, stratiform, and anvil area fractions and levels of non-divergence (LNDs; in km) simulated by MM5 and observed by ADRAD (in parentheses) over the analysis time periods given for each case in Table B.6.

Storm/Model Run (Environment)	MM5 (ADR) Conv Area	MM5 (ADR) Strat Area	MM5 (ADR) Anvil Area	MM5 (ADR) LND (km)
LLTS-MCSs				
18 Jun 2006 (WS)	24 (17)	36 (58)	23 (9)	7.3 (7.2)
25 Apr 2007 (WB)	18 (12)	57 (66)	8 (10)	5.9 (6.2)
20 Mar 2010 (SB)	6 (8)	83 (74)	7 (6)	5.8 (5.5)
Large Frontal MCSs				
3-4 Oct 2009 (WB)	10 (4)	56 (83)	17 (4)	4.6 (5.3)[1]
18 Sep 2006 (WB)	14 (11)	50 (73)	25 (8)	6.8 (5.7)
9-10 Oct 2009 (SB)	12 (3)	55 (76)	19(13)	6.9 (5.8)
Upper-Level Dist.				
9 Jun 2010 (WSmcv)	19 (13)	46 (64)	21 (10)	8.6 (6.7)
20-21 Jul 2007 (WS)	14 (4)	48 (75)	24 (4)	7.5 (6.7)
13-14 Mar 2007 (WB)	17 (13)	59 (77)	11 (5)	6.2 (6.7)
13-14 Mar 2009 (SB)	0.1 (2)	94 (78)	4 (6)	5.4 (5.5)

[1]The LND for the warm frontal case is the mean of its two LNDs at 4.8 and 5.9 km.

Table B.10. Mean convective, stratiform, and anvil coverage fractions observed by ADRAD (in bold) and simulated by WRF-ARW and MM5 for cases collated together by their background environments given in Tables B.6, B.7, and B.9.

Background Environment	Convective Area (%)			Stratiform Area (%)			Anvil Area (%)		
	ADR	WRF	MM5	**ADR**	WRF	MM5	**ADR**	WRF	MM5
Warm Season	**11**	15	19	**66**	64	43	**8**	12	23
Weakly Baroclinic	**10**	12	15	**75**	58	56	**7**	12	15
Strongly Baroclinic	**4**	6	6	**76**	71	77	**8**	10	9

Table B.11. Mean differences (i.e., main effects) in the area fractions simulated on D3 for MM5 between explicit and parameterized convection on D2 and using the Reisner-2 and Goddard MP treatments for cases collated together in different environments. Variations between both CPs and interaction effects between different combinations of parameterizations are not shown because they are generally smaller and insignificant for each case. Individual cases exhibiting statistically significant effects at the 95% confidence level ($p \leq 0.05$) are given in parentheses where "TS" refers to the LLTS-MCSs presented in section 3a, "WF" and "CF" refer to the warm and cold frontal storms shown in section 3b, and "UL" refers to the upper-level disturbances presented in section 3c of Chapter III.

	Reisner-2 – Goddard MP Mean Difference			Explicit – Parameterized D2 (9-km) CP Mean Difference		
Environment	**Conv**	**Strat**	**Anvil**	**Conv**	**Strat**	**Anvil**
Warm Season	+3.4	-16.1 (TS, UL)	+10.2 (TS, MCV)	+4.9	+9.2 (TS)	-5.0 (TS)
Weakly Baroclinic	+1.8	-14.1 (WF, CF)	+9.4 (WF, CF)	-1.5 (CF)	+3.0	+0.7
Strongly Baroclinic	0.0 (CF+, UL-)	-2.6 (CF)	+1.6 (TS-, CF+)	-1.0 (CF)	+1.7	-0.6

Table B.12. Mean differences (i.e., main effects) in area fractions simulated on D3 for WRF-ARW between explicit and parameterized convection on D2 and using the Morrison and Goddard MP treatments for cases collated together in different environments following the conventions in Table B.11. Individual cases exhibiting statistically significant effects at the 95% confidence level ($p \leq 0.05$) are given in parentheses.

	Morrison (2M) – Goddard (1M) MP Mean Difference			**Explicit – Parameterized D2 (9-km) CP Mean Difference**		
Environment	**Conv**	**Strat**	**Anvil**	**Conv**	**Strat**	**Anvil**
Warm Season	-0.7 (TS)	+0.9	-0.9	-1.4	+9.8 (ALL 3)	-2.8
Weakly Baroclinic	+3.1 (WF, UL)	-5.4 (WF, UL)	+1.2 (WF, CF)	+0.2 (WF-, CF+)	+14.4 (CF, UL)	-2.8 (CF, UL)
Strongly Baroclinic	+1.9 (TS, UL)	-5.5 (TS, UL)	+0.4	-0.4	+10.3 (TS, CF)	-4.4 (TS, CF)

Table B.13. Mean differences in LNDs for cases simulated in MM5 collated together for each environment (in km) associated with different parameterization treatments (main factor interactions) and between combinations of two parameterization treatments (two-factor interactions).

	Main Effect Differences (km)			**Two-Factor Interactions (km)**		
Environment (Mean LND; in km)	**9 km CP (Exp-CP)**	**CP (KF-GRL)**	**MP (Gd-R2)**	**9km*CP**	**9km*MP**	**CP*MP**
Warm Season (7.7)	0.3	1.0	0.4	-1.0	0.2	-0.3
Weakly Baroclinic (5.9)	0.0	-0.2	0.2	0.2	0.2	0.1
Strongly Baroclinic (6.0)	0.3	-0.2	-0.2	0.3	0.0	0.1

Table B.14. Mean differences in LNDs (in km) simulated for selected cases exhibiting a large ensemble spread associated with different parameterization treatments (main factor interactions) and between combinations of two parameterization treatments (two-factor interactions). Effects that are statistically significant at the 90% or 95% significance levels are indicated in bold.

	LND Main Effect Differences (km)			**Two-Factor Interactions (km)**		
Case (Mean LND; in km)	**9 km CP (exp-cp)**	**CP (KF-GDE)**	**MP (God-Mor)**	**9km*CP**	**9km*MP**	**CP*MP**
Warm Season MCV 9 Jun 2010 (8.9)	+0.1	**+1.1 ($p \leq 0.05$)**	+0.3	**-0.8 ($p \leq 0.1$)**	0.0	-0.4
Warm Season UL 20-21 Jul 2007 (8.4)	**+1.7 ($p \leq 0.05$)**	+0.5	+1.2	-0.4	**-1.3 ($p \leq 0.1$)**	-0.5
Weakly BC UL 13-14 Mar 2007 (6.5)	**+0.6 ($p \leq 0.05$)**	+0.1	+0.2	-0.1	-0.3	-0.1
Weakly BC CF 18 Sep 2006 (7.0)	+0.8	+0.9	+0.4	-0.5	+0.3	+0.3
Strongly BC CF 9-10 Oct 2009 (6.5)	**+0.7 ($p \leq 0.05$)**	**+0.4 ($p \leq 0.1$)**	-0.2	-0.2	+0.2	+0.1

Table B.15. Number of weeks out of 11 that students interacted with the faculty advisor or one of the graduate student mentors during SOAP.

Interactions with Faculty Advisor or Graduate Student Mentors	**2010 (n=30)**	**2009 (n=29)**	**2008 (n=29)**	**2007 (n=26)**
8+ interactions	67%	55%	62%	15%
5-7 interactions	27%	28%	21%	46%
2-4 interactions	6%	14%	17%	35%
0-1 interactions	---	3%	---	4%

Table B.16. Median and mode responses for Likert-type items comprising the confidence, interest, and experience Likert scales. Modes are given in parentheses when they differ from their respective medians. Items without values refer to activities not performed by students during that year's program.

CONFIDENCE SCALE: How CONFIDENT are you in performing the following activities?[1]	**2010 (n=30)**	**2009 (n=29)**	**2008 (n=29)**	**2007 (n=26)**
1) Operating the radar (ADRAD)	4	4	3	4.5 (5)
2) Analyzing radar data (cross-sections, precip summary)	4 (5)	4	3	4
3) Forecasting and writing the daily forecast discussion	5	4	4	4 (5)
4) Utilizing the FX-Net software to forecast	4	4 (5)	4	---
5) Creating a quantitative precipitation forecast (QPF)	3	3	---	---
6) Performing sounding launches	4.5 (5)	---	4	---
7) Learning modules for FX-Net and/or ADRAD	4	4	4 (3)	---
INTEREST SCALE: How much did you LIKE performing the following activities?[1]	**2010 (n=30)**	**2009 (n=29)**	**2008 (n=29)**	**2007 (n=26)**
1) Operating the radar	4	5	5	4.5 (5)
2) Analyzing radar data	4 (5)	4 (5)	4	4
3) Forecasting and writing discussion	4	4 (5)	4	4 (5)
4) Utilizing software to forecast	4	4	4	---
5) Creating a precipitation forecast	3	3	---	---
6) Performing sounding launches	5	---	5	---
7) Learning modules	4 (5)	4 (3)	3	---
EXPERIENCE SCALE: Approximately how many times/weeks (out of 11) did you perform each activity this semester?[2]	**2010 (n=30)**	**2009 (n=29)**	**2008 (n=29)**	**2007 (n=26)**
1) Operating the radar	3	3	3	3
2) Analyzing radar data	3 (4)	3	3	3
3) Forecasting and writing discussion	4 (5)	4	4	4 (3)
4) Utilizing software to forecast	4	4	4	---
5) Creating a precipitation forecast	3 (2)	3	---	---
6) Performing sounding launches	4	---	2	---
7) Learning modules	4	4	3	---

[1]Participants responded using a five point Likert format (1 = no confidence, 3 = neutral, and 5 = very confident; 1 = disliked, 3 = neutral, 5 = liked).

[2]Participants responded using a five point Likert format (1 = no experience and 5 = very experienced). Ranges of experience were used in the place of discrete values on the survey as follows: 1 = 0, 2 = 1, 3 = 2-4, 4 = 5-7, and 5 = 8+ for Items 1-4; and 1 = 0, 2 = 1, 3 = 2, 4 = 3, 5 = 4+ for Items 5-7.

Table B.17. Internal consistency of survey instrument for each year. Bolded Cronbach's alpha values are regarded as poor or unacceptable by George and Mallory (2003).

Likert Scale[1]	2010 α	2009 α	2008 α	2007 α
Cronbach's alpha for TOTAL CONFIDENCE scale	0.80	**0.51**	0.67	0.76
Cronbach's alpha for TOTAL INTEREST scale	0.72	0.61	0.71	**0.49**
Cronbach's alpha for TOTAL EXPERIENCE scale	**0.54**	0.64	0.67	**0.54**
Cronbach's alpha for RADAR CONFIDENCE subscale	0.74	0.71	0.72	0.84
Cronbach's alpha for RADAR INTEREST subscale	0.64	0.65	0.76	**0.53**
Cronbach's alpha for RADAR EXPERIENCE subscale	0.76	**0.58**	0.82	**0.57**

[1]Total scales use all items given in Table B.16, whereas the radar scales only use items 1 and 2.

Table B.18. Confidence correlation coefficients with experience and interest for SOAP participants during 2008-2010. Bolded values are statistically significant at the 95% confidence level ($p \leq 0.05$ for two-tailed test). Pearson's correlation coefficient between ranks is used to calculate Spearman's rank correlation coefficients presented above because there are tied ranks (Myers et al. 2010).

	Confidence and Experience			Confidence and Interest		
Activity/Scale	2010	2009	2008	2010	2009	2008
1) Operating the radar	0.33	0.09	**0.37**	**0.48**	**0.45**	**0.38**
2) Analyzing radar data	0.29	-0.29	**0.59**	**0.54**	0.06	0.35
3) Forecasting and writing discussion	0.20	0.27	**0.54**	**0.51**	**0.68**	**0.49**
4) Utilizing software to forecast	**0.39**	**0.52**	**0.72**	**0.42**	**0.60**	**0.54**
5) Creating a precipitation forecast	**0.46**	0.31	---	**0.59**	**0.73**	---
6) Performing sounding launches	**0.56**	---	**0.71**	**0.57**	---	**0.40**
7) Learning modules	**0.53**	0.33	**0.51**	**0.47**	**0.72**	**0.39**
TOTAL SCALE	0.34	0.05	**0.54**	**0.57**	**0.38**	**0.48**
RADAR SUBSCALE	0.27	-0.24	**0.52**	**0.54**	0.35	**0.44**

Table B.19. Stated career interests of SOAP participants between 2007-2010. Some multi-year participants are reflected in multiple categories depending on which year they took the survey. Students were also allowed to choose multiple careers or none of those listed. None of the differences between groups are statistically significant.

Career Interests of SOAP Participants/ Years Participation	1 Yr (n=66)	2 Yrs (n=36)	3-4 Yrs (n=12)	All (n=114)
Forecasting (Private Sector, NWS, Military)	68%	64%	67%	**67%**
Research (Graduate School)	36%	36%	50%	**38%**
Broadcast Meteorologist	35%	33%	23%	**33%**

Table B.20. Career outcomes of B.S. Meteorology degree recipients through Spring 2011 that participated in SOAP between 2007-2010. Ten 2006 SOAP graduates (five in research, two forecasting, one non-forecasting science, and two unknown) and three students that graduated with non-meteorology degrees are excluded in addition to two students that did not graduate. Degrees are still in progress for 21 SOAP participants.

Career Choices of SOAP Graduates/ Years Participation	1 Yr (n=27)	2 Yrs (n=20)	3-4 Yrs (n=12)	All (n=59)
Forecasting (Private Sector, NWS, Military)	26%	45%	50%	**37%**
Research (Graduate School)	22%	30%	42%	**29%**
Non-Forecasting Science (Analyst, Technician, Teacher)	15%	10%	---	**12%**
Broadcast Meteorologist	---	5%	8%	**3%**
Non-Science Occupations	18.5%	5%	---	**10%**
Unknown	18.5%	---	---	**9%**
METEOROLOGY/SCIENCE JOBS	**63%**	**95%**	**100%**	**81%**

APPENDIX C

LIST OF FALL SOAP PROJECTS

Fall SOAP 2009

*Haines, B, *R. Husted, J. Stachnik, and C. Schumacher, 2010: On the spatial variability of storms accumulations in southeast Texas. *Abstracts, 9th AMS Student Conference,* 16-17 Jan. 2010, Atlanta, GA.

*Reinhart, B. J., *C. McCaskill, L. J. Hopper, Jr., and C. Schumacher, 2010: Investigating the summertime midday precipitation peak in southeast Texas. *Abstracts, 9th AMS Student Conference*, 16-17 Jan. 2010, Atlanta, GA.

Fall SOAP 2008

*Cohen, M. D., *J. M. Stein, L. J. Hopper, Jr., and C. Schumacher, 2009: Precipitation distributions for storm types in southeast Texas. *Abstracts, 8th AMS Student Conference,* 10-11 Jan. 2009, Phoenix, AZ.

*Fanning, A., *B. Haines, J. Stachnik, and C. Schumacher, 2009: Does southeast Texas need an additional upper-air station? *Abstracts, 8th AMS Student Conference,* 10-11 Jan. 2009, Phoenix, AZ.

*Raper, M., C. Schumacher, K. E. Brugman, and L. J. Hopper, Jr., 2009: Drop-size distributions of storm types in southeast Texas. *Abstracts, 8th AMS Student Conference,* 10-11 Jan. 2009, Phoenix, AZ.

Fall SOAP 2007

*Boothby, D., *A. C. Ferrel, L. J. Hopper, Jr., and C. Schumacher, 2008: Variations in subtropical storm types and their contribution to rainfall in southeast Texas. *Abstracts, 7th AMS Student Conference,* 19-20 Jan. 2008, New Orleans, LA.

*Moore, J., *A. Fanning, J. Stachnik, and C. Schumacher, 2008: Changes in mesoscale divergence structures based on storm evolution. *Abstracts, 7th AMS Student Conference,* 19-20 Jan. 2008, New Orleans, LA.

*Wiley, A., *C. Homeyer, and C. Schumacher, 2008: Storm divergence from the Aggie Doppler Radar (ADRAD): Synoptic forcing and convective-stratiform variations. *Abstracts, 7th AMS Student Conference,* 19-20 Jan. 2008, New Orleans, LA.

*Indicates undergraduate student author

VITA

Name: Larry John Hopper, Jr.

Address: Department of Atmospheric Science, Earth Science, and Physics
University of Louisiana at Monroe
700 University Avenue, Monroe, LA 71209

Email Address: hopper@ulm.edu

Education: Ph.D., Atmospheric Sciences, Texas A&M University, 2011
M.S., Atmospheric Sciences, Texas A&M University, 2008
B.S., Meteorology, University of Oklahoma, 2005

Experience: Assistant Professor, January 2011-present
University of Louisiana at Monroe, Monroe, LA
Graduate Research Assistant, July 2005-January 2011
Texas A&M University, College Station, TX
Weather Intern, June 2002-May 2005
KOCO-TV (ABC), Oklahoma City, OK

Awards: TAMU Graduate Student Council Travel Award, Summer 2011
Buck Weirus Spririt Award, Texas A&M University, April 2010
Letzeiser Honor List, University of Oklahoma, April 2005

Publications: Hopper, L.J., Jr., and C. Schumacher, 2011: Modeled and observed variations in storm divergence and stratiform rain production in southeast Texas. *J. Atmos. Sci.*, conditionally accepted.
Hopper, L.J., Jr., and C. Schumacher, 2009: Baroclinicity influences on storm divergence and stratiform rain: Subtropical upper-level disturbances. *Mon. Wea. Rev.*, **137,** 1338-1357.
(for a full list of publications and presentations, see CV)

Service: Member, Weather Challenge Advisory Board (2011-present)
Member, AMS Committee on Mesoscale Processes (2009-2011)
Reviewer, Journal of Geophysical Research-Atmospheres
Texas A&M Student Service Fee Advisory Board (FY11 and FY12)
Vice President, Atmospheric Sciences Graduate Council (2008-2010)
College of Geosciences Senator, Texas A&M 61st Student Senate

Courses Taught: ATMO 203, *Weather Forecasting Lab*: Fall 2006, 2008, Spring 2010
ATMO 491, TA, *Advanced Undergraduate Research*: Fall 2007-2009
ATMO 291/491 TA, *Research (SOAP)*: Spring 2006-2010
ATMO 201 TA, *Introduction to Atmospheric Science*: Spring 2006